

AMERICAN UNIVERSITY OF BEIRUT

INTERACTION OF CURCUMIN WITH  
RHAMNOLIPIDS, DSPC LIPOSOMES AND  
CYCLODEXTRAN MOF; CURCUMIN AS A  
MOLECULAR PROBE TO INVESTIGATE  
HETEROGENEOUS SYSTEMS

by

Zeinab Hassan Moussa

A thesis

submitted in partial fulfillment of the requirements  
for the degree of Master of Science  
to the Department of Chemistry  
of the Faculty of Arts and Sciences  
at the American University of Beirut

Beirut, Lebanon

July 2016

AMERICAN UNIVERSITY OF BEIRUT

INTERACTION OF CURCUMIN WITH  
RHAMNOLIPIDS, DSPC LIPOSOMES AND  
CYCLODEXTRAN MOF; CURCUMIN AS A  
MOLECULAR PROBE TO INVESTIGATE  
HETEROGENEOUS SYSTEMS

by  
Zeinab Hassan Moussa

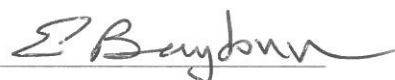
Approved by:



Dr. Digambara Patra, Associate Professor

Advisor

Chemistry



Dr. Elias Baydoun, Professor

Member of Committee

Biology



Dr. Mohammed Hmadeh, Assistant Professor

Member of Committee

Chemistry

Date of thesis defense: July 1, 2016

# AMERICAN UNIVERSITY OF BEIRUT

## THESIS RELEASE FORM

Student Name: Tloussa Skinala Hassan  
Last First Middle

Master's Thesis       Master's Project       Doctoral Dissertation

I authorize the American University of Beirut to: (a) reproduce hard or electronic copies of my thesis, dissertation, or project; (b) include such copies in the archives and digital repositories of the University; and (c) make freely available such copies to third parties for research or educational purposes.

I authorize the American University of Beirut, **three years after the date of submitting my thesis, dissertation, or project**, to: (a) reproduce hard or electronic copies of it; (b) include such copies in the archives and digital repositories of the University; and (c) make freely available such copies to third parties for research or educational purposes.

 July 19<sup>th</sup> 2016  
Signature Date

*To the ones who are silently working to change the course of history.*

# Acknowledgements

I would like to thank everyone who supported me, my family, colleagues and thesis committee especially my adviser Dr. Digambara Patra for his dedication, magnanimity and support. My deepest gratitude for both Dr. Mohammed Hmadeh and Dr. Elias Baydoun for their assistance and giving me the opportunity to conduct experimental work under their supervision.

I would like to thank my professors who made my learning experience, throughout the past four years, unique, Dr Haddadin, Dr Hasanayn, Dr Ghauch and Dr Karam. I am also grateful to the personnel in the Central Research Science Laboratory for their technical support and assistance.

Special thanks to Elsy El Khoury for her help and support in the lab when I first arrived.

I would like to thank my fellow grad students Christina, Antranik, Mazhar, Mahmoud, Maya, Leila who made this stay at AUB fruitful and enjoyable. I will never forget the moments, hours, we spent there talking about everything and “studying”.

I would like to thank my parents for all the efforts they did and the tough moments they lived to provide decent education to their children. My brothers and sisters for their patience and bearing my continuous complain.

To my friend Lara, whose presence in the past years was the reason for all happiness, love and serenity.

Finally I dedicate my work and success to my niece, Fatima, who left early before having the chance to fulfill her ambitions and big plans.

# An Abstract of the Thesis of

Zeinab Hassan Moussa for Master of Sciences  
Major: Chemistry

Title: Interaction of curcumin with rhamnolipids, DSPC liposomes and cyclodextran MOF; curcumin as a molecular probe to investigate heterogeneous systems.

Turmeric, extracted from the plant *Curcuma longa*, is a gold-colored spice commonly used for health care and for the preservation of food. Curcumin, the active ingredient in the turmeric herb has been shown to exhibit antioxidant, anti-inflammatory, antiviral, antibacterial, antifungal, and anticancer activities thus a therapeutic tool in various chronic illnesses. Rhamnolipids (RLs) are glycolipid biosurfactants produced mainly by *Pseudomonas aeruginosa* and can be described as glycosides that are composed, of a rhamnose moieties (that constitute the glycon part) and lipid part (that makes the aglycon part connected by an O-glycosidic bond). RLs are characterized by unique physiochemical properties namely surface activity, wetting ability, detergency, and other amphipathic- related qualities. For its applicability as a hydrophobic drug molecule and food spice, interaction of curcumin with rhamnolipids, a biosurfactant, bears importance. Here we have explored interaction of curcumin with rhamnolipids biosurfactant and its aggregation behavior. The impact of pH on critical micelle concentration (cmc) of rhamnolipids has been studied using fluorescence of curcumin and found that cmc of rhamnolipids increases with increase in pH of the medium.

Moreover, liposomes an efficient tool of intense application in various fields of science and technology because its biocompatibility along with the ability to lodge both hydrophobic and hydrophilic molecules, in addition to unique structural and functional properties. Curcumin has been applied as a molecular probe to investigate the properties of 1, 2-Dioctadecanoyl-sn-glycero-3-phosphocholine (DSPC) liposomes and study the effect of rhamnolipids on permeability and fluidity of the membranes. Here, we have explored new insight on intercalation of rhamnolipids with DSPC liposomes using curcumin and pyrene as external fluorescence probes. Intercalation of rhamnolipids exceptionally increases (~22-fold) partition of curcumin into solid gel phase of DSPC liposomes, whereas this increase is moderate (~1.9 fold) in liquid crystalline phase.

For both systems, the interaction between curcumin and rhamnolipids and the change in the properties of liposomes in the presence of the biosurfactant have been assessed by applying fluorescence quenching of both pyrene and curcumin by two different quencher molecules (one hydrophilic and other hydrophobic). Quenching data have established that the permeability and fluidity of the DSPC liposomes is enhanced in the presence of rhamnolipids. Membrane permeability and fluidity can be improved further by increase in percentage of rhamnolipids in DSPC liposomes. However, unlike pyrene, fluorescence quenching rate of curcumin by hydrophobic quencher decreases with percentage of rhamnolipids in DSPC liposomes, which is explained based on the fact that at higher percentage of rhamnolipids curcumin is buried into the deep hydrophobic layer of DSPC liposomes, thus, increasing the distance between head group of hydrophobic quencher molecule and curcumin. The phase transition temperature of DSPC liposomes decreases with increase in percentage of rhamnolipids in DSPC liposomes by encouraging fusion between solid gel and liquid crystalline phases. Similarly, fluorescence quenching by hydrophobic cetylpyridinium bromide confirms curcumin penetrates deep inside the hydrophobic pocket of rhamnolipid aggregates/micelle. Rhamnolipids suppress curcumin degradation and further boost the stability of curcumin in DSPC liposomes. Thus, mixing rhamnolipids with DSPC liposomes could potentially serve as a good candidate for drug delivery application. Curcumin has been successfully encapsulated in Cyclodextrin-Metal Organic Frameworks (CD-MOFs) without altering their crystallinity. The interaction between curcumin and CD-MOFs is strong through hydrogen bond type interaction between the OH group of cyclodextrin of CD-MOFs and the phenolic hydroxyl group of the curcumin. Interestingly, dissolving the curcumin loaded CD-MOFs crystals in water results in formation of a unique complex between curcumin, gamma cyclodextran and potassium cations. In fact, the initial interaction between curcumin and CD-MOF is crucial for the formation of the latter. This new complex formed in alkaline media at pH 11.5 has maximum absorbance at 520 nm and emittance at 600 nm. Most importantly, the stability of curcumin in this complex was enhanced by at least 3 order of magnitude compared to free curcumin and curcumin:gamma-CD at pH 11.5. These results suggest a promising benign system of CD-MOFs, which can be used to store and stabilize curcumin for food applications.

# Contents

<b>Acknowledgements</b>	<b>v</b>
<b>Abstract</b>	<b>vi</b>
<b>1 Introduction</b>	<b>1</b>
1.1 Curcumin . . . . .	1
1.1.1 Structural and Spectroscopic Characteristics of Curcumin . .	1
1.1.2 Biological Activity . . . . .	2
1.2 Biosurfactants . . . . .	3
1.2.1 What are Biosurfactants? . . . . .	3
1.2.2 What are rhamnolipids? (RLs) . . . . .	4
1.3 Liposomes . . . . .	7
1.3.1 What are liposomes? . . . . .	7
1.3.2 Classification of liposomes . . . . .	8
1.3.3 Methods of preparation . . . . .	9
1.3.4 Chemical Analysis and Characterization of Liposome Prepara- tions . . . . .	10
1.3.5 Applications of Liposomes . . . . .	10
1.4 Fluorescence . . . . .	12
1.4.1 Principles of fluorescence . . . . .	12
<b>2 Interaction of Curcumin with Biosurfactant Rhamnolipids: Controlling Tautomer for On-Off Ratiometric Fluorescence Temperature Sensing</b>	<b>16</b>
2.1 Introduction . . . . .	16
2.2 Materials and Methods . . . . .	17
2.2.1 Materials . . . . .	17
2.2.2 Spectroscopic measurements . . . . .	18
2.3 Results and discussion . . . . .	18
2.3.1 Interaction of Curcumin with Rhamnolipids . . . . .	18
2.3.2 Effect of pH on Micellization . . . . .	20
2.3.3 Accessibility of Probe Molecule in Rhamnolipids Micelle . .	23
2.3.4 Ratiometric Fluorescence Temperature Sensing . . . . .	26
2.3.5 Stability of Curcumin in Rhamnolipids . . . . .	29



<b>3</b>	<b>Intercalation of Rhamnolipids with 1, 2-Dioctadecanoyl-sn-glycero-3-phosphocholine Liposomes Enhances Membrane Fluidity, Permeability and Stability of Curcumin</b>	<b>32</b>
3.1	Introduction . . . . .	32
3.2	Materials And Methods . . . . .	34
3.2.1	Materials . . . . .	34
3.2.2	Preparation of liposomes . . . . .	35
3.2.3	Incorporation of RLs . . . . .	35
3.2.4	Spectroscopic measurements . . . . .	35
3.3	Results And Discussion . . . . .	35
3.3.1	Interaction and stabilization curcumin in DSPC liposomes . . . . .	35
3.3.2	Partition coefficient of curcumin in DSPC liposomes . . . . .	38
3.3.3	Determination of phase transition temperature of DSPC liposomes . . . . .	39
3.3.4	Fluorescence quenching study in DSPC liposomes . . . . .	42
3.3.5	Effect of rhamnolipids on stability of curcumin in DSPC liposomes . . . . .	44
3.3.6	Effect of rhamnolipids on partition coefficient of curcumin into DSPC liposomes . . . . .	44
3.3.7	Effect of RLs on fluidity of DSPC liposomes . . . . .	46
3.3.8	Effect of RLs on the phase transition of DSPC liposomes . . . . .	47
<b>4</b>	<b>Encapsulation of curcumin in cyclodextrin-metal organic frameworks: Dissociation of loaded CD-MOFs enhances stability of curcumin</b>	<b>51</b>
4.1	Introduction . . . . .	51
4.2	Materials And Methods . . . . .	53
4.2.1	Material . . . . .	53
4.2.2	Sample Preparation . . . . .	54
4.2.3	Spectroscopic measurement . . . . .	54
4.2.4	Surface area and pore volume measurements . . . . .	54
4.2.5	X-ray diffraction (XRD) . . . . .	55
4.3	Results And Discussion . . . . .	55
4.3.1	Inclusion of curcumin into CD-MOF pores . . . . .	55
4.3.2	Characterization of the loaded CD MOF crystals . . . . .	56
4.3.3	Spectroscopic study . . . . .	57
4.3.4	Dissociation of curcumin loaded CD-MOF crystals . . . . .	59
<b>5</b>	<b>Conclusion</b>	<b>64</b>

# List of Figures

1.1	3D structure of Curcumin . . . . .	1
1.2	Schematic diagram showing the photophysical and photochemical processes in curcumin . . . . .	2
1.3	Chemical structure of the first reported rhamnolipid $\alpha$ -L-rhamnopyranosyl- $\alpha$ -L-rhamnopyranosyl- $\beta$ -hydroxydecanoyl- $\beta$ -hydroxydecanoyl (Rha-Rha-C10-C10). . . . .	5
1.4	Schematic diagram of the essential self-assembly method from individual phospholipid molecules (a) to bilayer membrane leaflets (b), followed by conversion into liposomes (c). Each bilayer is around 5nm thick and contains well-arranged singular lipid molecules with their hydrophobic tails facing each other and their hydrophilic moieties directed towards the internal and external aqueous surrounding media (d) [1]. . . . .	8
1.5	Jablonski diagram . . . . .	13
2.1	(A) UV-visible absorption spectra of curcumin in difference concentration of rhamnolipids in neutral pH condition; (B) Plot of absorbance vs. rhamnolipid concentration. Arrow directs towards critical micelle concentration. . . . .	19
2.2	Fluorescence spectra of curcumin in difference concentration of rhamnolipids in neutral pH condition at $\lambda_{ex} = 425$ nm for $\beta$ -diketone form (A) and $\lambda_{ex} = 355$ nm for enol form (B); (C) Plot of fluorescence intensity vs. rhamnolipid concentration. Arrow directs towards critical micelle concentration. . . . .	20
2.3	UV-visible absorption spectra of curcumin in the absence (black) and presence (red) of rhamnolipids at pHs (A) 4; (B) 7; (C) 8 and (D) 13. Absorbance is normalized to maximum value. . . . .	21
2.4	Fluorescence spectra of curcumin in difference concentration of rhamnolipids in pH 4.0 condition at $\lambda_{ex} = 425$ nm for $\beta$ -diketone form (A) and $\lambda_{ex} = 355$ nm for enol form (B); Plot of fluorescence intensity vs. rhamnolipid concentration for pH 4 (C) and pH 8 (D). Arrow directs towards critical micelle concentration. . . . .	22

2.5	Fluorescence spectra of curcumin in difference concentration of rhamnolipids in pH 13.0 condition at $\lambda_{ex} = 425$ nm for $\beta$ -diketone form (A) and $\lambda_{ex} = 355$ nm for enol form (B); (C) Plot of fluorescence intensity vs. rhamnolipid concentration for pH 13. Arrow directs towards critical micelle concentration; (D) Plot of cmc vs. pH . . . . .	24
2.6	Fluorescence quenching of pyrene by CPB, corresponding Stern-Volmer plot is shown in (B); (C) Stern-Volmer plot for fluorescence quenching of curcumin by CPB; (D) Stern-Volmer plot for fluorescence quenching of pyrene by KI. . . . .	25
2.7	UV-visible absorption spectra of curcumin in neutral buffer at different temperature in the absence (A) and presence of rhamnolipids; (C) Plot absorbance ratio ( $A_{355}/A_{425}$ ) vs. temperature. . . . .	27
2.8	Fluorescence spectra of curcumin in difference temperature without rhamnolipids at $\lambda_{ex} = 425$ nm for $\beta$ -diketone form (A) and $\lambda_{ex} = 355$ nm for enol form (B); (C) Plot of fluorescence intensity ratio ( $F_{430}/F_{530}$ ) vs. temperature. . . . .	28
2.9	Fluorescence spectra of curcumin in difference temperature in the presence of rhamnolipids at $\lambda_{ex} = 425$ nm for $\beta$ -diketone form (A) and $\lambda_{ex} = 355$ nm for enol form (B); (C) Plot of fluorescence intensity ratio ( $F_{430}/F_{530}$ ) vs. temperature. . . . .	29
2.10	Stability of curcumin measured by UV-visible spectrophotometer at $\lambda_{abs}^{max}$ of curcumin at pHs (A) 4; (B) 7; (C) 8 and (D) 13. . . . .	30
3.1	Structure of (A) Pyrene; (B) Curcumin; (C) CPB; (D) DSPC; (E) Rhamnolipids . . . . .	33
3.2	(A) UV-visible absorption spectra of curcumin in DSPC liposomes at pH 7.0 buffer solution during different time interval; (B) Rate of degradation of curcumin at pH 7.0 buffer solution in the absence and presence of DSPC liposomes. . . . .	36
3.3	Normalized UV-visible absorption spectra of curcumin in the absence and presence of DSPC liposomes at (A) pH 7.0; (B) 4.0 and (C) 13.0 buffer solution. . . . .	37
3.4	Fluorescence emission spectra of curcumin in various concentrations of DSPC liposomes in (A) solid gel phase and (B) liquid crystalline phase. Plot of $1/F$ vs $1/[DSPC]$ in solid gel phase (C) and liquid crystalline phase (D). Fluorescence intensity was measured at excitation wavelength 425 nm and emission wavelength 492 nm. . . . .	38
3.5	Fluorescence emission spectra of $5 \mu M$ (A) and $100 \mu M$ (B) curcumin in DSPC liposomes ( $100 \mu M$ ); (C) Profile of fluorescence intensity of curcumin vs. temperature at various concentration of curcumin concentration in DSPC liposomes; (D) Variation in phase transition temperature of DSPC liposomes with curcumin concentration. . . . .	41

3.6	(A) Fluorescence spectra of pyrene in DSPC liposomes with different concentration of KI; (B) Stern-Volmer plot for fluorescence quenching of pyrene by KI (0 to 20 mM) in DSPC liposomes, inset shown the same plot for KI 0 to 5 M; (C) Fluorescence spectra of curcumin in DSPC liposomes with different concentration of KI. . . . .	42
3.7	UV-visible absorption spectra of curcumin in 10 % of RLs in DSPC liposomes at pH 7.0 (A) and pH 13. 0 (C) buffer solution during different time interval; Rate of degradation of curcumin at pH 7.0 (B) and pH 13.0 (D) buffer solution in the absence and presence of different % of RLs in DSPC liposomes. . . . .	45
3.8	(A) Fluorescence emission spectra of curcumin in various concentrations of DSPC liposomes in the presence of 10 % RLs in liquid crystalline phase; (B) Plot of $1/F$ vs. $1/[DSPC]$ in the presence of 10 % RLs in liquid crystalline phase. Fluorescence intensity was measured at excitation wavelength 425 nm and emission wavelength 492 nm. . .	46
3.9	(A) Stern-Volmer plots for fluorescence quenching of pyrene by KI (0 to 20 mM) in DSPC liposomes in the presence of different amount of RLs; (B) Plot of $K_{sv}$ vs. % of RLs in DSPC liposomes during fluorescence quenching of pyrene by KI; (C) Fluorescence spectra of pyrene in DSPC liposomes with different concentration of CPB; (D) Plot of $K_{sv}$ vs. % of RLs in DSPC liposomes during fluorescence quenching of pyrene by CPB. . . . .	48
3.10	(A) Plot of $K_{sv}$ vs. % of RLs in DSPC liposomes during fluorescence quenching of curcumin by KI; (B) Fluorescence spectra of curcumin in DSPC liposomes with different concentration of CPB; (C) Stern-Volmer plots for fluorescence quenching of pyrene by CPB (0 to 100 $\mu M$ ) in DSPC liposomes in the presence of different amount of RLs; (D) Plot of $K_{sv}$ vs. % of RLs in DSPC liposomes during fluorescence quenching of curcumin by CPB. . . . .	49
3.11	Illustration of contact between curcumin and CPB in DSPC liposomes in the absence and presence of rhamnolipids. . . . .	49
3.12	: (A) Fluorescence emission spectra of 5 $\mu M$ curcumin in 10 % of RLs in DSPC liposomes (100 $\mu M$ ); (B) Profile of fluorescence intensity of curcumin vs. temperature at various % of RLs in DSPC liposomes; (C) Variation in phase transition temperature of DSPC liposomes with % of RLs in DSPC liposomes. . . . .	50
4.1	Interaction between CD-MOF and curcumin . . . . .	52
4.2	FT-IR spectra of curcumin, free CD MOF and the curcumin loaded CD-MOFs. . . . .	56
4.3	Powder X-ray diffraction patterns for free CD-MOFs crystals washed by methanol (in black) and loaded CD-MOFs crystals with curcumin (in red) compared to the calculated pattern of CD-MOFs (blue). . . .	57

4.4	N <sub>2</sub> adsorption isotherms, for activated samples of free CD-MOFs and curcumin loaded CD-MOFs. Filled and open symbols represent adsorption and desorption branches, respectively. Connecting traces are for guidance only. . . . .	58
4.5	(A) UV-visible absorption spectra of the free curcumin in water (in black), methanol (in red), in $\gamma$ -cyclodextrin (in blue) and curcumin encapsulated CD-MOFs crystals in methanol (in green); (B) Fluorescence emission spectra of free curcumin in methanol (red), in curcumin encapsulated CD-MOFs crystals (in green) and that of curcumin in methanol (in black), both excited at 425 nm. Curcumin: $\gamma$ -CD = 1:10. . . . .	59
4.6	(A) UV-vis absorption spectrum of the dissolved loaded CD-MOF crystals (red) with curcumin in water and that of curcumin alone in water (black); (B) UV-vis absorption spectrum of curcumin (25 $\mu$ M) in the presence of different concentrations of $\gamma$ -cyclodextrin in water; (C) UV-vis absorption spectrum of curcumin (25 $\mu$ M) in different concentrations of KOH in water; (D). UV-vis absorption spectrum of curcumin (25 $\mu$ M) in different concentration of ( $\gamma$ -CD: KOH) complex in water. . . . .	60

# List of Tables

2.1	Add caption . . . . .	26
3.1	Partition Coefficients of Curcumin into DMPC Liposomes . . . . .	50

# Chapter 1

## Introduction

### 1.1 Curcumin

Curcumin [1, 7-bis-(4-hydroxy-3-methoxyphenyl)-1,6-heptadiene-3,5-dione] or simply diferuloylmethane is a polyphenolic phytochemical substance [2]. Curcumin is extracted from the roots of the perennial herb *Curcuma longa* Linn [3]. Curcumin was chemically characterized for the first time in 1910 and has been the focus of hundreds of research papers for the past three decades, investigating the anti-inflammatory, antioxidant and anti-cancer effects [4].

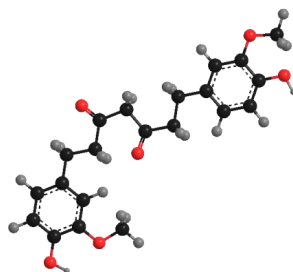


Figure 1.1: 3D structure of Curcumin

#### 1.1.1 Structural and Spectroscopic Characteristics of Curcumin

As implied, curcumin is a bis- $\alpha,\beta$ -unsaturated  $\beta$ -diketone. Hence it is found in equilibrium with the enol tautomer. At low pHs (acidic medium), neutral media and in the cell membrane, the bis-keto form dominates [5]. At the low pHs from 3 to 7 curcumin is known to be a strong H-atom donor [6]. However, above pH 8, the enolate form of curcumin is the major component. In alkaline media, curcumin serves as an electron donor [6]. Regarding solubility, curcumin dissolves poorly in water but it exhibits a

high solubility in organic solvents, such as ethanol, methanol, acetone and di-methylsulphoxide (DMSO) [7]. Moreover, the stability of curcumin at basic pH is very low and it undergoes hydrolytic degradation within half an hour. The degradation products are ferulic acid, vanillin and ferloylmethane [8]. Curcumin exhibits a higher stability in acidic media where 20% of total curcumin concentration degrades in an hour [5]. Theoretical and experimental studies have determined three acidity constants for curcumin. By pH-dependent degradation of curcumin, three pKa values of 7.75, 8.55 and 9.05 belonging to the ionization of enolic and the two phenolic OH protons are known [9].

Curcumin is a fluorescent molecule; its photo physical properties are greatly reliant on the polarity of the environment and the pH of the medium [10]. The absorption maximum of curcumin is at 420 nm in the largest part of the polar solvents, yet in hydrogen bond acceptor and donor solvents, it is shifted to 430-434 nm, excluding methanol where it is around 423-428 nm. In acidic media, the absorption maximum of curcumin is at 422 nm, however, at pH greater than 7, the yellow color of curcumin turns bright red, with the absorption maximum shifting to 463 nm caused by the ionization of phenolic OH group [10].

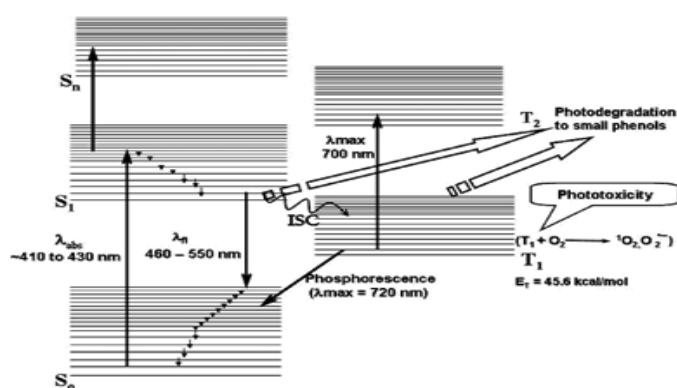


Fig. 8. Schematic diagram showing the photophysical and photochemical processes in curcumin.

Figure 1.2: Schematic diagram showing the photophysical and photochemical processes in curcumin

### 1.1.2 Biological Activity

Curcumin is well known for its wide range of biological activities. Within the past 10 years, research has shown that curcumin has a potent effect against several diseases both, malignant and benign [11]. Curcumin is effective against many inflammatory diseases, such as pancreatitis arthritis [12], colitis [13], allergy and inflammatory bowel



disease (IBD) [14]. This impact is mainly due to the down-regulation of inflammatory molecules. The potential of curcumin against different autoimmune disease has been reported as well, including multiple sclerosis and diabetes [15, 16]. Those effects are a result of curcumin regulation of pro-inflammatory signals. Curcumin has been shown to be effective against diabetes mellitus type II, where the patient shows resistance to insulin [16].

Moreover curcumin has a major anti-cancer effect supported by many reports and studies. This effect is mediated through the following possible mechanisms.

1. Down-regulation of anti-apoptotic proteins along with the activation of apoptotic molecules as caspases and increasing the expression of tumor suppressor genes as p53 [17, 18].
2. Inhibition of tumor invasion and metastasis by suppressing the expression of cell surface adhesion proteins and matrix metallo proteinases (MMPs) [19, 20].
3. Suppression of tumor angiogenesis by down-regulation of angiogenic cytokines [21, 22].
4. Inhibition of major inflammatory pathways mainly by targeting pro inflammatory molecules as TNF and NF $\kappa$ B [18, 19].

## 1.2 Biosurfactants

### 1.2.1 What are Biosurfactants?

Surfactants are chemical compounds that exhibit surface activity. Surfactants show tendency for interfaces of unlike polarities (liquid-liquid or liquid-air) and are soluble in both organic and aqueous solvents. This property is a result of their amphiphilic structures, which contain both a hydrophilic head and a hydrophobic tail [23].

Biosurfactants are surface-active biomolecules of microbial origin. The hydrophilic part is mostly made of amino acids, sugars, or polar groups such as carboxylic acids. The hydrophobic moiety is an aliphatic hydrocarbon chain of  $\beta$ -hydroxy fatty acids [24].

Based on their molecular structure, biosurfactants can be classified as glycolipids (e.g., rhamnolipids (RLs)), lipopeptides (e.g., surfactin), polymeric biosurfactants (e.g., emulsan), fatty acids (e.g. alkanolic acids (HAAs)), and phospholipids (e.g., phosphatidylethanolamine) [23, 24].

Biosurfactants have advanced since first bio-surfactant “surfactin” was isolated and characterized by Arima et al. (1968) [25]. They represent natural alternatives compared

to their synthetic counterparts; they are characterized by lower toxicity, stability at extremes thermal conditions, ionic strength and pH. In addition to their diversity in terms of structure, they are biodegradable, thus green chemicals [26].

### 1.2.2 What are rhamnolipids? (RLs)

Rhamnolipids, the glycolipid biosurfactants produced mainly by *Pseudomonas aeruginosa*, are the most intensively investigated biosurfactants. They were first described in 1949 particularly when grown on water immiscible C-sources [27].

#### Structure of rhamnolipids

Regarding their structure, RLs can be described as glycosides that are composed, of a rhamnose moieties that constitute the glycon part and lipid part that makes the aglycon part connected by a O-glycosidic bond. The glycon part is composed of one (for mono-RLs) or two (for di-RLs) rhamnose moieties linked to each other through a-1,2-glycosidic linkage. Rhamnolipids can be either mono-RLs with a single rhamnose part or di-RLs with two rhamnose moieties bonded by an  $\alpha$ -1,2-glycosidic linkage [28].

The aglycon part is usually composed one or two and rarely three  $\beta$ -hydroxy fatty acid chains [29]. These fatty acids are mostly saturated and in some cases mono- or polyunsaturated. The chain length varies from C8 to C16 [30]. They are linked by an ester bond formed between the  $\beta$ -hydroxyl group of the distal (relative the glycosidic bond) chain with the carboxyl group of the proximal chain [31]. (Fig1) The carboxyl group of the distal chain remains free. Still, a small number of RLs have this group esterified with an alkyl group [31].

#### Methods of RLs detection

RLs can be qualitatively or quantitatively detected and analyzed.

**Qualitative methods** Cetyltrimethyl ammonium bromide (CTAB) agar test is the most applied method for qualitative, screening of RL producing bacterial strains [32]. Simply, the anionic RLs form an insoluble complex with the cationic bromide salt and the complex is revealed using methylene blue present in the agar. The dark blue halo surrounding the RL producing colony is positive test for presence of RLs [33]. Other approaches can be the drop collapsing test, the oil spreading test and the measurement of surface tension of culture broths using duNouy-type tensiometer [34].

**Quantitative methods** Different strategies can be applied for quantifying RLs.

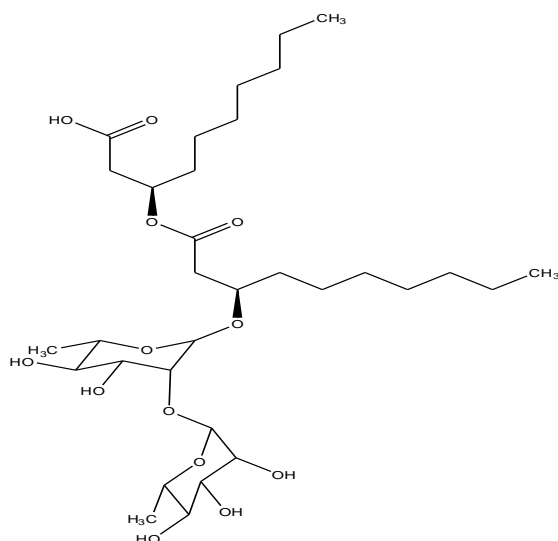


Figure 1.3: Chemical structure of the first reported rhamnolipid  $\alpha$ -L-rhamnopyranosyl- $\alpha$ -L-rhamnopyranosyl- $\beta$ -hydroxydecanoyl- $\beta$ -hydroxydecanoyl (Rha-Rha-C10-C10).

A common quantitative methods used are the spectrophotometric ones especially the Orcinol Test. Where extracts of the culture supernatant are heated in the presence of sulfur and 1,3-dihydroxy-5-methylbenzene (orcinol) [35]. A blue green color resulting from the interaction between the hydrolyzed rhamnose groups and orcinol is measured spectrophotometrically at 421 nm [36].

Taking into consideration the fact that RLs can be purified by simple extraction methods, due to their acidic nature and thus they can be retained in the aqueous phase in basic medium, during extraction by slightly non-polar solvents such as ethyl ether after acidification of the aqueous solution [36]. After extraction, more sensitive chromatographic measurements can be done to quantify RLs. These include thin layer chromatography [37], Gas chromatography [38], Liquid chromatography [39], and Liquid Chromatography Coupled to Mass Spectrometry [40].

In addition to other spectroscopic methods such as Infrared that is used for the quantification of complex RL mixtures [41]. Nuclear Magnetic Resonance (NMR) has been used mainly for the structural analysis of purified congeners rather than quantification of RL mixtures [42].

### Biosynthesis and regulation

The first step in the synthesis involves dimerization of two  $\beta$ -hydroxydecanoic acid chains. The formed dimer undergoes in order two rhamnosylation reactions with two

different rhamnosyltransferases: rhamnosyltransferase 1 (Rt-1) and rhamnosyltransferase 2 (Rt-2) [43].

Details of RLs biosynthesis pathway have been in large part elucidated. It can be divided into three sections: biosynthesis of the lipid moiety, biosynthesis of the sugar moiety, finally the enzymatic dimerization and the rhamnosyl transfers, thus yielding the product [43].

**Biosynthesis of the Lipid Moiety of Rhamnolipids** Several studies show that the biosynthesis of the lipid components follows the classical pathway of fatty acid synthesis starting with 2 carbon units [44].

The lipid part can go through post synthetic modifications. These modifications include a biosynthetic Link with PHA (poly (3-hydroxyalkanoates)) in addition to association with quorum sensing signal molecules [44].

**Biosynthesis of Rhamnose Moiety of Rhamnolipids** Investigations on the catabolic pathway of rhamnose using radioactive carbon sources showed that the carbons of rhamnose are derivatives of glycerol rather than acetate.

In 1958 Hauser and Karnovsky suggested the two-three carbons of glycerol condense preserving the carbon-carbon bond into glucose [45]. This hypothesis was confirmed by Glaser and Kornfeld where they used labeled glycerol to follow the biosynthetic pathway [46]. Later the conversion of glucose into Rhamnose in *P. aeruginosa* was shown to take place without randomization of the carbon chain and the carbon at position 1 in glucose maintains its position Rhamnose [47].

**Three Last Enzymatic Reactions in Rhamnolipids Biosynthesis** The final steps of RL biosynthesis in *P. aeruginosa* are governed by 3 enzymatic reactions [48]. (1) synthesis of the fatty acid dimers (HAAs) by RhlA (2) synthesis of mono RLs starting by an HAA and dTDP-L-Rhamnose as precursors by the membrane-bound RhlB; (3) production of di RLs mediated by RhlC starting from dTDP-L-Rhamnose and mono RLs [49, 50, 51].

**Regulation of Rhamnolipids Biosynthesis** Production of RLs is a complicated procedure for it is affected by many factors including genetic control and environmental conditions.

Regulation of RLs biosynthesis can be summarized as following:

1. Genetic regulation that can target the Rhamnosyltransferases involved in the biosynthesis as well as regulation of the sugar moiety production [52, 53].

2. Environmental effect on Rhamnolipid Production. Bacteria can adjust gene expression through quorum sensing in response to changes in growth factors [49, 54].

### **Diversity of physiological functions and roles**

RLs are characterized by unique physiochemical properties namely surface activity, wetting ability, detergency, and other amphiphilic-related qualities. These properties render RLs physiological functions that are highly important for the producing organism as well as several applications in industry.

Physiological roles can be summarized into:

- RLs endorse the uptake and biodegradation of poorly soluble substrates [55, 56].
- RLs as immune modulators and virulence elements [57, 58].
- RLs as antimicrobials [59].
- RLs in surface motility [54].
- RLs in biofilm development [54].

Industrial application includes:

- Bioremediation and enhanced oil recovery (EOR) [60].
- Pharmaceuticals and therapeutics [61].
- Cosmetics [62].
- Detergents and cleaners [63].
- Agriculture: for soil remediation and plant pathogen elimination [64].

## **1.3 Liposomes**

### **1.3.1 What are liposomes?**

Liposomes are small artificial spherical vesicles made of curved lipid bilayers that include portion of the surrounding solvent into their inside. Liposomes are formed by dissolving lipid molecules mainly phospholipids, which are amphiphilic molecules having a hydrophilic head section and hydrophobic tail (Fig. 1.4). This self-sealing of the dissolved lipid molecules where the hydrophobic tails face each other and the hydrophilic heads are directed toward the interior and exterior of the aqueous medium is driven by

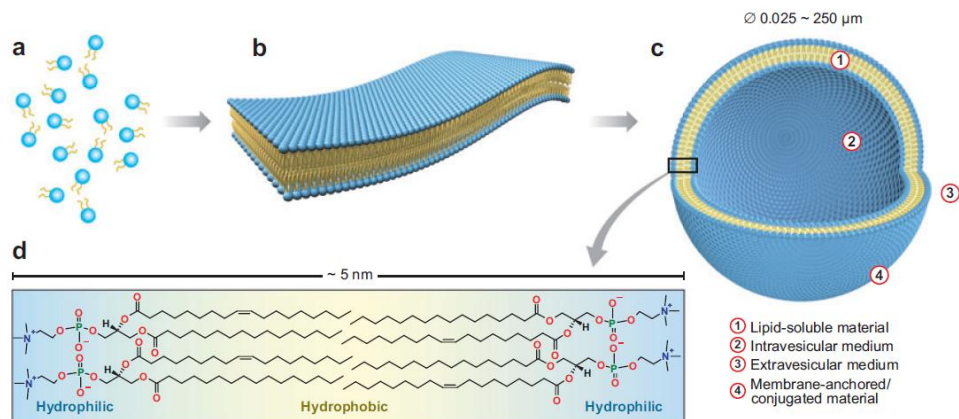


Figure 1.4: Schematic diagram of the essential self-assembly method from individual phospholipid molecules (a) to bilayer membrane leaflets (b), followed by conversion into liposomes (c). Each bilayer is around 5nm thick and contains well-arranged singular lipid molecules with their hydrophobic tails facing each other and their hydrophilic moieties directed towards the internal and external aqueous surrounding media (d) [1].

the decrease of their water solubility [65].

The most used lipids are phospholipids especially the neutral phosphatidylcholine and the several negatively charged ones that differ by the fatty acid chain in the hydrophobic moiety of the molecule, these include phosphatidylethanolamine, phosphatidylglycerol, phosphatidylserine and phosphatidic acid. Beside the charge, the nature of the fatty acid chain in the lipid molecule especially the degree of un-saturation affects the basic bilayers properties namely elasticity and phase behavior [1].

A major advantage of liposome is that it can trap and release two compounds of different solubility, a lipid soluble material and a water soluble one. Moreover due to their biocompatibility and low toxicity; food and pharmaceutical industries have extensively investigated liposomal systems and their applications [66].

### 1.3.2 Classification of liposomes

Liposomes are classified based on several criteria, lipid composition, vesicle size, lamellarity and preparation method. From a morphological viewpoint, liposomes are defined by the size and number of bilayers.)

#### According to size

- Unilamellar vesicles (ULV) are liposomes with a single bilayers membrane. ULVs can be further subdivided based on size into small ones (SUV), which is less than 100 nm, and large ones (LUV) that are above 100 nm [67].

- Liposomes that contain concentric lipid bilayers are multilamellar vesicles (MLV). Multivesicular vesicles (MVs) are made of non-concentric vesicles embedded within single bilayers [67].

### **Liposome based carrier system**

- Immunoliposomes: A class prepared for targeting bioactive agents inside the body [68].
- Lipotubes: Flexible membrane conduits of ~100 nm diameter and length that can be several hundred micrometers [69].
- Vesicular phospholipid gels (VPGs): These are of semisolid uniformity, highly concentrated aqueous phospholipid dispersions [70].
- Archaeosomes: These liposomes composed of polar ether lipids of bacterial origin precisely Archaea bacteria [71].
- Stealth Liposomes: These are produced after coating the surface with hydrophilic chains as poly ethylene glycol (PEG) [72].

### **1.3.3 Methods of preparation**

**Preparation of liposomes includes four main stages[67]:**

1. Evaporating the organic solvent in which the lipids are dissolved.
2. Re-suspension of the lipids in an aqueous solvent.
3. Purification of the obtained liposome.
4. Analysis and characterization of the final product.

### **Method of liposome preparation and drug loading**

Drug loading can be either passive or active.

1. Passive loading where the drug is encapsulated while preparing the liposome and it includes three different procedures:[73]
  - Solvent dispersion.
  - Mechanical dispersion.
  - Detergent removal of non-incorporated material [74].
2. Active loading, where the drug is added following the liposome preparation. Mainly water-soluble drugs with have protonizable amine functions are loaded actively [67].

### 1.3.4 Chemical Analysis and Characterization of Liposome Preparations

In liposome characterization, studies focus on five major aspects: size, lamellarity, encapsulation efficiency, analyzing the lipids quantitatively and quality assurance with respect to the industry [75]. The most new used methods for liposome characterizations include the following:

- Flow field-flow fractionation coupled to multiangle light scattering, gel exclusion chromatography, or Transmission electron microscopy performed at cryogenic temperature (cryo-TEM), for particle mean size and size distribution [76].
- Electron microscopy or spectroscopic techniques including Nuclear magnetic resonance for determination of lamellarity [1].
- Single molecule detection for encapsulation efficiency [77].

### 1.3.5 Applications of Liposomes

Liposomes biocompatibility along with the ability to lodge both hydrophobic and hydrophilic molecules, in addition to unique structural and functional properties made liposomes an efficient tool of intense application in various fields of science and technology. Some of the major applications of liposomes are listed below:

#### 1. Applications of Liposomes in Food Science

Lipid vesicles and liposomes are used to construct novel food packaging supplies with enhanced barrier and anti-microbial effect. Moreover, liposomes are implicated in developing nano-sensors for checking the food quality during transport and storage [78]. Liposomes are applied in food sciences to ameliorate and change the texture of food ingredients in addition to improving the absorption of nutraceutical supplements [79]. The first reported application of liposomes in food industry was in cheese production where proteinases encapsulated in liposomes were added to the cheese serving to enhance the quality and cost of cheese ripening [80].

#### 2. Applications of Liposomes in Cosmetics

Due to the similarity between the liposome bilayer structure and that of natural membranes, liposomes are widely used in skin treatments and cosmetic industry [81].

Several liposome forms such as creams, gels and lotions are used to carry compounds through stratum corneum [82].

Liposomes are reported to enhance the elimination of toxic pyrimidine dimers produced after exposing the skin to ultraviolet radiation [83].

Moreover delivery of antioxidants, anti-inflammatory agents by liposomes aid in the treatment of age spots, wrinkles and several skin-aging features [84].



### 3. Clinical applications

Liposome clinical applications can be either diagnostic or therapeutic.

#### (a) Diagnostic applications

Imaging agents are delivered to the liver and spleen via large liposomes. This can be achieved since large liposomes are quickly cleared by the phagocytic cells of the reticulo-endothelial system [85]. Aqueous contrast-enhancing molecules encapsulated in large liposomes can be targeted to specific organs, and we can distinguish between cancerous tissues and normal ones by applying computed tomography [86].

Moreover, liposomes that entrap gas are also applied in diagnosis; these systems are mostly used for ultrasound and magnetic resonance imaging [87].

#### (b) Therapeutic applications

##### i. Treatment of parasitic diseases and infections

Encapsulating antibiotics into liposomes is done in the case of very strong and toxic antibiotics which are delivered parenterally. Such a preparation is quite sensitive where the high ratio of drug-to-lipid is not easily established due to the interaction between the drugs and the lipid bilayers along with the high density of the surrounding aqueous medium which pushes the liposomes to float as a layer on the top of the tube [85].

Knowing that liposomes accumulate in the same infected cell population of known parasitic macrophages infection such as Leishmaniasis and Malaria, liposomes constitute an ideal drug delivery mean. An example is the treatment of mycobacterial infections can be highly improved by encapsulating the aminoglycosides antibiotics into liposomes [88].

##### ii. Treatment of respiratory disorders

Aerosolised liposomes are utilized in inhalation therapy and it is effective for bronchial constriction in asthma. An example is illustrated in treatment of adult respiratory distress syndrome with liposomal prostaglandin E1 (Lip-PGE1) introduced intravenously, where it resulted in a decrease of lung leak and lung lavage neutrophil buildup in rat models [89].

##### iii. Liposomes in anticancer therapy

Different liposome formulations encapsulating anti-cancer drugs have been prepared and found to be less toxic than the free agent. Moreover, the circulation time and efficiency of the drugs has been enhanced upon encapsulation into liposomes [90]. The drug effect has improved as reported in the case of ovarian cancer treatment by Muggia et al where liposomal doxorubicin had significant activity against refractory ovar-

ian cancer [91]. Anthracyclines, a well reported anti-cancer drug that cease the growth of dividing cells have side effects that include acute toxicities, especially cardio toxicity [92]. Upon liposome encapsulation, the drug toxicity has been reduced about 50% due to the fact that liposome encapsulation limits the delivery of the agent to normal cells [92]. In the case of systemic lymphoma, the consequence of liposome encapsulation has been an improvement in the drug effect caused by the sustained release effect [93].

## 1.4 Fluorescence

The emission of light from a substance is known as luminescence, and happens from electronically excited states. Based on the type of the excited state it can be termed as either fluorescence or phosphorescence. The latter being an emission of a photon from triplet excited states, where the excited electron has the same spin as the one in the ground state. However, fluorescence originates largely from aromatic molecules, where the electrons in the excited states, possess a spin opposite to that in the ground state. Hence the return to the ground state is spin allowed and happens fast with a photon emission at a rate of  $10^8 \text{ s}^{-1}$  thus fluorescence lifetime is generally around 10 ns ( $10 \times 10^{-9} \text{ s}$ ).]Fluorophores are encountered in daily lives such as quinine in tonic water, fluorescein or rhodamine in antifreeze, in addition to anthracene and perylene whose fluorescence is used to measure and monitor oil pollution [94].

The last couple of decades witnessed a notable growth in applying fluorescence in the biological sciences. Now it is considered a major tool for biochemical and biophysical research. It is dominant in the fields of biotechnology, DNA sensing and sequencing, diagnosis, and cellular imaging, to name a few. Fluorescence is very sensitive that it allows detection at the single molecule level in addition to revealing and measuring intracellular molecules.

### 1.4.1 Principles of fluorescence

The principles of luminescence can be described and discussed by the Jablonski diagram shown in Fig 1.5 [95].

After absorbing light, a fluorophore is excited to a higher vibrational level of either  $S_1$  or  $S_2$ . However molecules quickly relax within  $10^{-12}$  s or less to the lowest vibrational level of  $S$  via a process called internal conversion. Fluorescence emission has a life time of  $10^{-8}$  s thus it follows internal conversion taking place from a thermally equilibrated excited state corresponding to the lowest energy vibrational state of  $S_1$  [94].

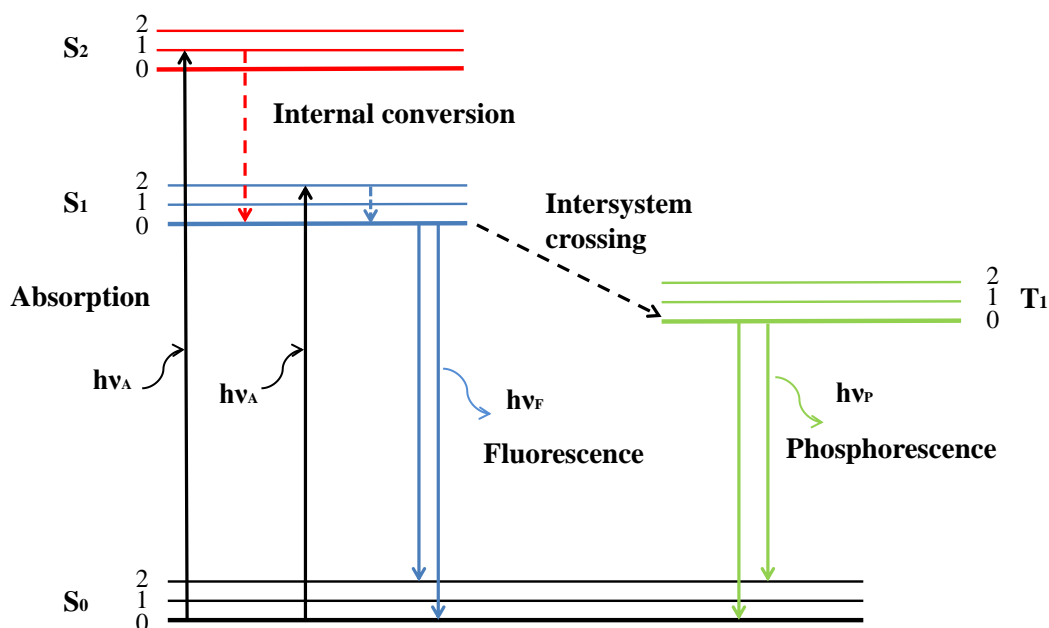


Figure 1.5: Jablonski diagram

Another process beside fluorescence that takes place is phosphorescence, which is a result of emission from the first triplet state  $T_1$ . Phosphorescence follows intersystem crossing after spin conversion from  $S_1$  to  $T_1$ . Such a transition from  $T_1$  to the singlet ground state is forbidden, thus it is a slow process (few milliseconds to seconds). Heavy atoms ease intersystem crossing thus improve phosphorescence quantum yields [94].

## Characteristics of Fluorescence

### 1. The Stokes Shift

Jablonski diagram reveals that the energy emitted by the fluorophore is less than that absorbed. This difference in the energy results in a red shift in the emission spectrum compared to that of the excitation spectrum, a shift referred to as Stokes shift. This energy loss is mainly caused by internal conversion, excited state reactions along with complex formation, energy transfer and solvent effects. Thus Stokes shift reflects the interaction between the fluorescent molecule and its surrounding environment [94].

### 2. Kasha's Rule

Another principle of fluorescence is that the emission spectrum is independent of the excitation wavelength. This aspect is named Kasha's rule for Michael Kasha explained that fluorescence occurs only from the lowest vibrational state of  $S_1$  whereby the excess of energy gained through absorption is dissipated through non radiant processes as internal conversions [96].

### 3. Quantum Yields

Quantum yield is indicated by the ratio of the number of photons emitted by the fluorescent molecule to that absorbed. Quantum yield is represented by

$$Q = \Gamma / (\Gamma + K_{nr}) \quad (1.1)$$

Where  $\Gamma$  and  $K_{nr}$  are the rate of radiative decay and non-radiative decay respectively.

Quantum yields are an indication regarding the fluorescent ability of the molecule. Moreover, it indicates the suitable environment for the fluorophore to get the best fluorescence, for instance a molecule of low quantum yield in water is expected to show an enhanced emission in a hydrophobic surrounding [94].

### 4. Fluorescence Lifetime

Lifetime  $\tau$  is the time the fluorophore remains in the excited state before emitting light and relaxing to the ground state; it is given by

$$\tau = 1 / (\Gamma + K_{nr}) \quad (1.2)$$

Quantum yield and life time are dependent on the rate constants  $\Gamma$  and  $K_{nr}$ , thus internal conversion rates affecting the latter can render a molecule non-fluorescent [94].

### 5. Fluorescence Quenching

Quenching is defined as the decrease in the fluorescence intensity. Quenching can be either collisional or static.

Collisional quenching is caused by deactivation of the fluorophore at the excited state caused by colliding with another molecule known as quencher. General quenchers are halogens, oxygen, amines and electron-poor molecules. Static quenching occurs usually in the ground state upon interaction between the fluorophore and the quenching thereby forming a non-fluorescent complex.

Quenching is stated by the Stern-Volmer equation:

$$F_0/F = 1 + K[Q] = 1 + k_q\tau_0[Q] \quad (1.3)$$

Where  $F_0$  and  $F$  are the intensities in the absence and presence of the quencher respectively,  $K$  is the Stern-Volmer quenching constant,  $k_q$  is the bimolecular quenching constant,  $\tau_0$  is the unquenched lifetime and  $[Q]$  is the concentration of the quencher. Quenching depends on the distance between the fluorophore and the quencher thus  $K$  is relatively low when the quencher can't reach the fluorophore. Whereas,  $K$  is large when the fluorescent molecule is free in solution and the quencher can easily interact with it. Fluorescence quenching study gives an insight regarding the position of the probe and to study and determine the permeability and fluidity of membranes [94].

## 6. Steady-State and Time-Resolved Fluorescence

Steady state measurements are the most common type of fluorescence measurements. After continuous illumination, a sample arrives at steady state where the intensity is recorded versus wavelength. Meanwhile time-resolved measurement which aims at measuring intensity decays is done when a sample is exposed to a pulse of light for a short time.

For a fluorophore that shows a single decay time, the intensity  $I$  is expressed as

$$I(t) = I_0 e^{-t/\tau} \quad (1.4)$$

With  $I_0$  the intensity at  $t=0$  instantly after the pulse.

The steady-state intensity  $I_{SS}$  is correlated to the decay time by

$$I_{SS} = \int_0^{\infty} I_0 e^{-t/\tau} dt = I_0 \tau \quad (1.5)$$

Both measurements are important, steady state measurements shows average intensities while time resolved ones reveal two decay times for a probe existing in two conformations [94].

## 7. Fluorescence for Probing Membranes

Fluorescence allows the study of dynamics of proteins and lipids thus it has lots of advantages over classical microscopy methodologies.

The use of fluorescence for probing membranes has many advantages over classical microscopy techniques since it provides information about minute details reaching single molecule sensitivity, and permits the study of the dynamics of lipids and proteins on narrow timescales. Probing can be either direct, by visualizing a fluorescent component of the membrane such as green fluorescent proteins, or by inserting fluorescent compounds or dyes into the membrane. The only problem is the significant size of the probes relative to the small phospholipid molecules [97].

Moreover, fluorescence anisotropy measured by the use of polarized light shows the order and the existence of domains in the membrane, in addition, generalized polarization is a good approach to study the phase transition. Baumgart et al. applied generalized polarization to study the polarity of membrane. By computing the ratio of the fluorescence intensity in the liquid ordered phase  $L_o$  and that in liquid disordered phase  $L_d$  generalized polarization GP can be calculated as follows [98]:

$$GP = (I_o - I_d)/(I_o + I_d) \quad (1.6)$$

## Chapter 2

# Interaction of Curcumin with Biosurfactant Rhamnolipids: Controlling Tautomer for On-Off Ratiometric Fluorescence Temperature Sensing

### 2.1 Introduction

Curcumin is a natural yellow-orange pigment present in the Indian spice turmeric; it is extracted from the roots of the perennial herb *Curcuma longa* Linn [3]. Curcumin exists mainly in the keto enol isomer. The massive increase in research studies targeting curcumin over the past decade is due to its wide range of biological activities. Curcumin expresses an antioxidant, anti-cancer and anti-inflammatory effects [11]. Recently, curcumin was shown to be effective against devastating diseases both Parkinson [99] and Alzheimer [100]. In addition to biological effects, curcumin is successfully established as a probe to study liposome properties [101], and sensing applications [102]. Moreover curcumin has been used to investigate polymer properties [103] and silver nanoparticle green synthesis [104]. The major hurdle in using curcumin for diseases treatment is its low aqueous solubility thus limiting its availability in biological systems [105]. The solubility of curcumin can be enhanced by increasing the pH of the medium. However, curcumin is known to undergo rapid hydrolytic degradation in alkaline medium [9]. Several approaches targeted the enhancement of curcumin solubility and bioavailability. These studies include incorporation into liposomes and phospholipids [106], encapsulation of curcumin into CD-MOFs [107] and as polymer nanoparticles [108], in addition to several cyclodextran inclusion complexes [109]. Moreover an effective approach was to encapsulate curcumin in surfactant micelles [110]. Surfactants are chemical compounds that display surface activity. Surfactants

show propensity for interfaces of unlike polarities (liquid - liquid or liquid - air) and are soluble in both organic and aqueous solvents. This property is a consequence of their amphiphilic structures, which hold both a hydrophilic head and a hydrophobic tail [23]. Studies showed that curcumin solubility is improved in micellar solutions, but few studies targeted the physicochemical properties of curcumin in the latter systems [111, 112]. The chemical stability of curcumin at pH 5 and 8 was investigated and it was shown that SDS and TX-100 micelles are highly efficient in stabilizing curcumin compared to TTAB micelles. An 1800 times improvement in curcumin chemical stability was reported in the presence of SDS and TX-100. Moreover, cationic micelles were shown to suppress alkaline hydrolysis of curcumin at pH 13 with a 90% yield [110]. The aim of this is to study the interaction between curcumin and rhamnolipids, which are glycolipid biosurfactants produced mainly by *Pseudomonas aeruginosa* and constitute the most intensively investigated biosurfactants. Biosurfactants hold an advantage over their synthetic counter parts for being biocompatible. RLs possess several physiological functions that are greatly important for the producing bacterium as well as several applications in industry. These roles include immune modulators [57] and virulence elements [58], antimicrobials [59] and biofilm development [54]. The industrial applications for RLs are in fields of bioremediation and enhanced oil recovery (EOR) [60], pharmaceuticals and therapeutics [61], cosmetics [62], and soil remediation along with plant pathogen elimination [64].

In this study we use steady state fluorescent and UV-vis spectroscopic measurements to report the interaction between curcumin and rhamnolipids, which was shown to be dependent on the charging state of curcumin. Steady state fluorescent measurements were exploited to explore the accessibility of curcumin into the rhamnolipids hydrophobic core applying a hydrophilic quencher (iodide) and another hydrophobic one (CPB) to study the position of curcumin with respect to the rhamnolipids system. Our study is the first to report the encapsulation of curcumin into rhamnolipids micelle and its outcome regarding the chemical stability of curcumin at pH 7 and pH 8. In addition to the impact of rhamnolipids on the thermal spectral properties of curcumin showing that the resonance stability of the keto-enol-enolate in aqueous medium is highly affected and sensitive to temperature. This equilibrium of the keto-enol curcumin isomers was shown to be temperature dependent, a relation that presents a potential ratiometric fluorescence temperature sensor.

## **2.2 Materials and Methods**

### **2.2.1 Materials**

Rhamnolipids (RLs) was acquired from AGAE Technology (USA). Curcumin, pyrene and CPB were obtained from Sigma-Aldrich and used as received. The solvents used were of spectroscopic grade and obtained from Sigma-Aldrich. The stock solution of rhamnolipids  $\sim 1\text{g/L}$  was prepared in double distilled water. Because of poor solubil-

ity, the stock solution of curcumin was made in spectroscopic grade ethanol. A few microliters of the stock sample of curcumin ( $\sim 1$  mM) was taken in a vial and added to a final sample for measurement in buffer. Steps were taken to ensure that the final concentration of ethanol was negligible, less than 0.1% in the measurement sample, to avoid affecting the sample.

## 2.2.2 Spectroscopic measurements

The absorption spectra were recorded at room temperature using a JASCOV-570 UV-vis-NIR spectrophotometer. The steady-state fluorescence measurements were recorded with a resolution increment of 1 nm, slit 5 using a HORIBA Jobin Yvon Fluorolog-3 fluorometer and the FluorEssence program. The excitation source was a 100 W xenon lamp, and the detector used was an R-928 operating at a voltage of 950 V. To regulate the temperature, a thermostat was coupled with the sample holder. The final temperature was noted in the sample compartment using a thermometer rather than thermostat.

## 2.3 Results and discussion

### 2.3.1 Interaction of Curcumin with Rhamnolipids

The UV-visible absorption spectra of curcumin in different concentration of RLs are demonstrated in Figure 2.1A. Curcumin exists in enol form with trans geometry in solution because of its  $\beta$ -diketone moiety [10]. This planar geometry facilitates the  $\pi$ -systems of the two feruloyl chromophores to interact with each other through the central  $sp^2$ -hybridized carbon atom causing a common conjugated  $\pi$ -system [113]. In the absence of RLs, the absorption spectrum of curcumin is characterized by broad peak at  $\sim 428$  nm and a small shoulder at  $\sim 355$  nm. The peak at  $\sim 428$  nm corresponds to enol form (due to conjugated diferuloyl structure) and the band at  $\sim 355$  nm corresponds to  $\beta$ -diketone form (due to lack of conjugation between two feruloyl units in  $\beta$ -diketo form, thus, absorption di-keto form is solely because of feruloyl units)[113]. Note that weakly allowed  $\pi(\text{HOMO}-1) \rightarrow \pi^*(\text{LUMO})$  transition and virtually forbidden  $n \rightarrow \pi^*(\text{LUMO})$  transition also absorb around this region [114]. The band at  $\sim 355$  nm due to  $\beta$ -diketo form of curcumin appears as shoulder in neutral /acidic condition (in the absence of surfactant), which has been attributed to stronger specific interaction with water due to dualistic nature of water (proton donor and proton acceptor) [115]. With RLs concentration, the absorbance of curcumin at  $\sim 428$  nm continued to increase, at the same time the band at  $\sim 355$  nm turned out to be unresolved, instead at higher concentration of RLs the absorption spectrum of curcumin became narrower and structured with a minor band at  $\sim 445$  nm. Disappearance of the band at  $\sim 355$  nm is expected during incorporation of curcumin into hydrophobic pocket of RLs micelle. The formation of new band at  $\sim 440$  nm is similar to results obtained in micelle [116].



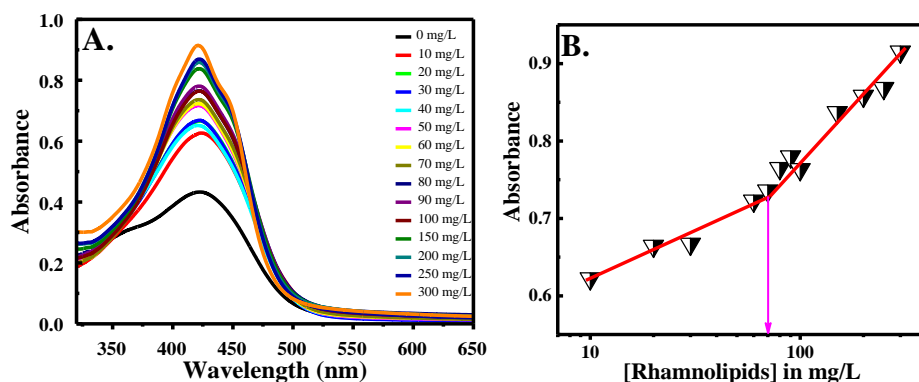


Figure 2.1: (A) UV-visible absorption spectra of curcumin in different concentration of rhamnolipids in neutral pH condition; (B) Plot of absorbance vs. rhamnolipid concentration. Arrow directs towards critical micelle concentration.

The change in absorbance with RLs concentration illustrated two different trends as depicted in Figure 2.1B. The intersecting point of these two different linear lines, gave a RLs concentration of  $\sim 70$  mg/L. Like any other surfactant solution, rhamnolipids form micelle only after a certain concentration, known as critical micelle concentration (cmc) due assembly of monomer surfactant units. This value is similar to reported cmc value earlier [117, 118, 119]. There are various approaches reported in literature to determine cmc. Often variation of certain physical properties such as conductivity, surface tension, osmotic pressure etc. is studied in different monomer concentration and cmc is estimated based on abrupt change of such physical properties. In addition, cmc of rhamnolipids varies on kinds and composition of rhamnolipids. Therefore, we measured the electrical conductivity and molar conductivity. The break in molar conductivity vs. RLs concentration was observed, which must have originated from micellisation/aggregation of RLs [120]. The concentration corresponding to breaking point is cmc. The estimated value for cmc was found to be 60-70 mg/L, which is similar to value obtained by UV-visible spectral measurement of curcumin. Recently spectroscopic methods, especially fluorescence technique, has been an easy and convenient tool to determine cmc, however, in such case fluorescence parameter of probe molecule should sense variation in surfactant concentration. Curcumin has been successfully applied to determine cmc of micelle [116] and nano-aggregates [103]. The fluorescence spectra of curcumin were measured in two different excitation wavelengths, at  $\lambda_{ex} = 355$  nm for  $\beta$ -diketone and at  $\lambda_{ex} = 425$  nm for enol forms of curcumin. At  $\lambda_{ex} = 425$  nm, curcumin in neutral buffer condition gave an emission maximum at  $\sim 540$  nm, which shifted to blue with RLs concentration and at higher concentration of RLs remained constant at 492 nm (see Figure 2.2A). Similar results were obtained at  $\lambda_{ex} = 355$  nm (compare Figure 2.2B) indicating the emitting species is the same in both the excitation wavelengths. The blue shift in emission maximum has been correlated with formation of micellar structure where curcumin tends to get buried in. In both the excitation wavelengths, the emission maximum is similar to one observed for curcumin

embedded liposomes [101]. The increase in fluorescence intensity at  $\sim 492$  nm with RLs concentrations demonstrated two different trends (see Figure 2.2C) and in both cases the breaking point could be able to estimate cmc and was found to be  $\sim 70$  mg/L, which corroborates earlier observation.

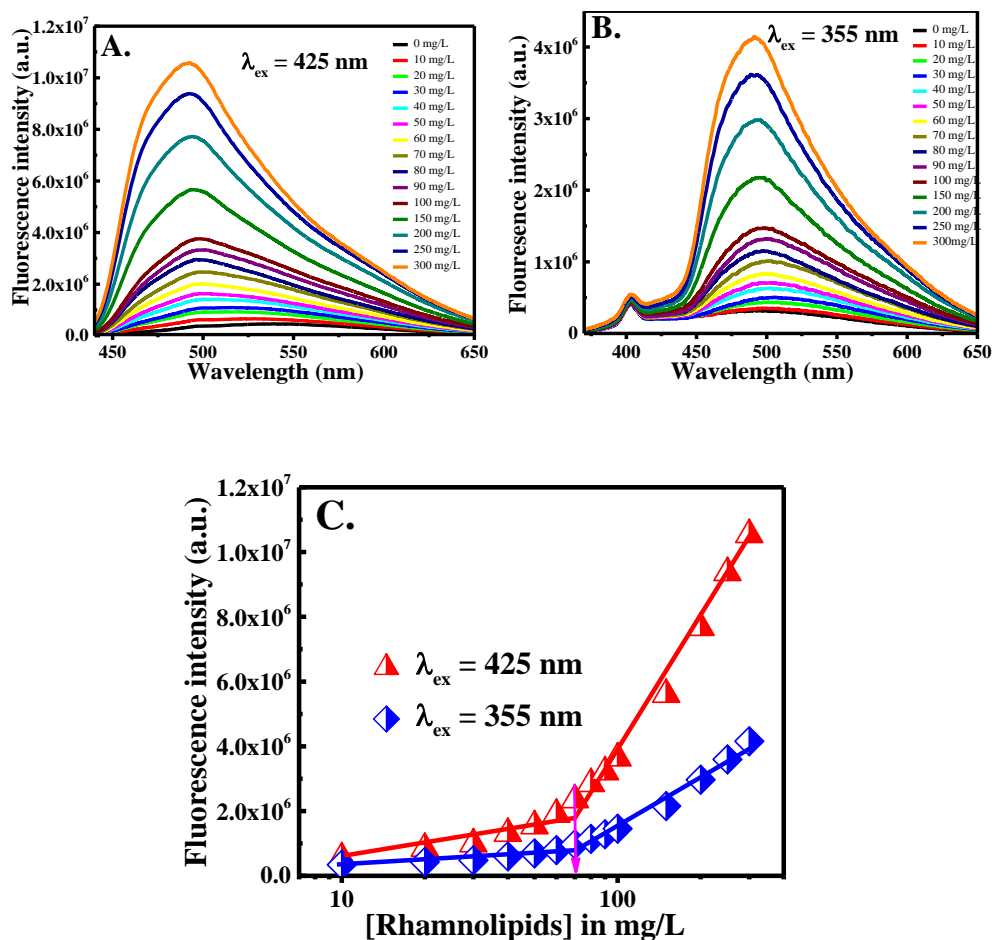


Figure 2.2: Fluorescence spectra of curcumin in difference concentration of rhamnolipids in neutral pH condition at  $\lambda_{ex} = 425$  nm for  $\beta$ -diketone form (A) and  $\lambda_{ex} = 355$  nm for enol form (B); (C) Plot of fluorescence intensity vs. rhamnolipid concentration. Arrow directs towards critical micelle concentration.

### 2.3.2 Effect of pH on Micellization

Curcumin exhibits a clear and intense absorption peak in the UV- visible spectral region at  $\sim 430$  nm in the in acidic medium (pH 4). Upon interaction with rhamnolipids, this absorption was shifted to 420 nm at pH 4 as depicted in Figure 2.3A. In neutral media at pH 7 the absorption of curcumin exhibited a blue shift of 10 nm from 428 nm in the absence of rhamnolipids to an absorption peak at 418 nm (see Figure 2.3B). The

interaction between curcumin and rhamnolipids in basic medium was investigated at two different pHs, first at 8 and then at 13, where the curcumin species present is different at the two pHs. At pH 8 a slight shift of 5 nm was observed as shown in Figure 2.3C, from 425 nm in the absence of RLs to a maximum absorption at 420 nm in the presence of RLs. It is well established that curcumin possesses three pKa values (8.38, 9.88 and 10.51) [121] consequent of the deprotonation of the three hydroxyl groups of curcumin. Therefore, at pH 13 curcumin is completely deprotonated to form the negatively charged species,  $\text{Cur}^{3-}$ . At pH 13 the absorption spectrum of the negatively charged species  $\text{Cur}^{3-}$  articulated no difference in the presence of rhamnolipids compared to that in the absence of RL with a maximum absorption at 468 nm at both stated conditions (see Figure 2.3D) suggesting  $\text{cur}^{3-}$  has relatively weak interaction with RLs.

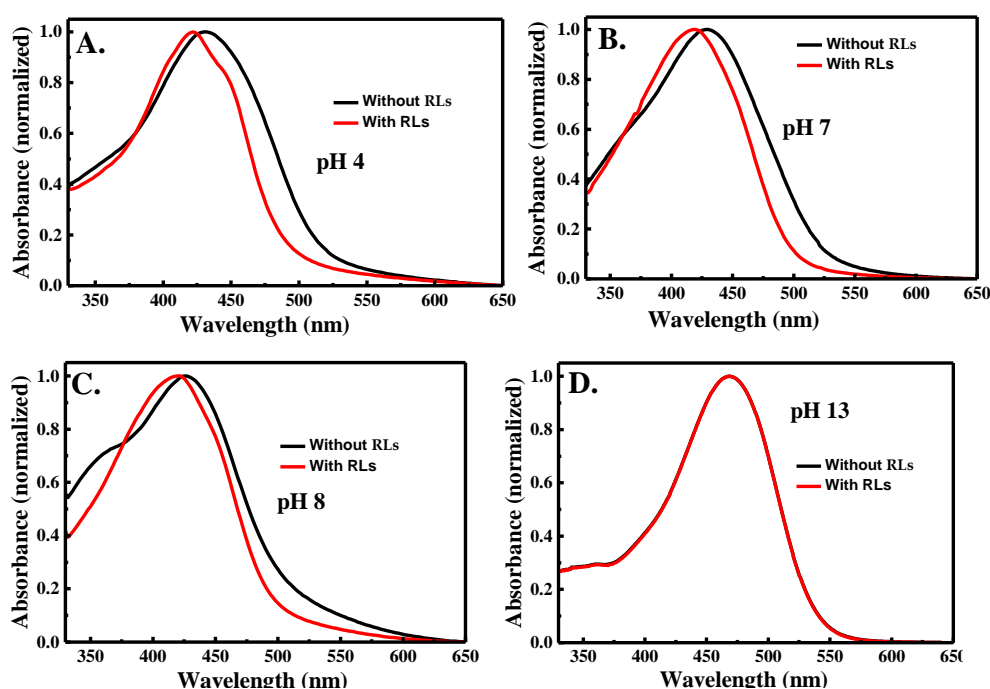


Figure 2.3: UV-visible absorption spectra of curcumin in the absence (black) and presence (red) of rhamnolipids at pHs (A) 4; (B) 7; (C) 8 and (D) 13. Absorbance is normalized to maximum value.

To further investigate this phenomenon and the interaction between curcumin and rhamnolipids, fluorescence titrations of curcumin were done at three different pHs with increasing concentrations of rhamnolipids. The fluorescence intensity of curcumin was significantly improved in the presence of RLs. This increase in the intensity reveals a strong interaction between curcumin and RLs. At pHs 4 and 7 as the concentration of rhamnolipids increases, expectedly the emission of the uncharged protonated form of curcumin excited at both wavelengths 425 nm and 355 nm increases in identical pattern. It should be noted that the fluorescence emission maximum of curcumin at pH 4.0 did not change irrespective excitation wavelengths (see Figure 2.4 A&B) and remained

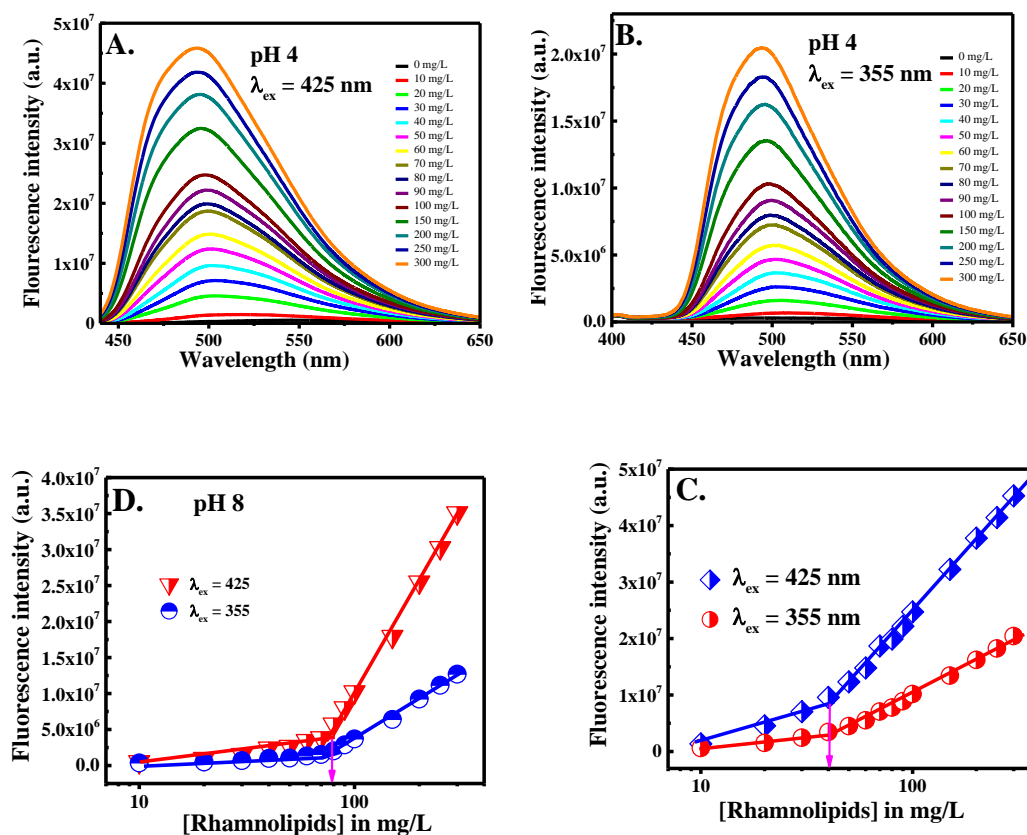


Figure 2.4: Fluorescence spectra of curcumin in difference concentration of rhamnolipids in pH 4.0 condition at  $\lambda_{ex} = 425$  nm for  $\beta$ -diketone form (A) and  $\lambda_{ex} = 355$  nm for enol form (B); Plot of fluorescence intensity vs. rhamnolipid concentration for pH 4 (C) and pH 8 (D). Arrow directs towards critical micelle concentration.

at  $\sim 540$  nm and with increase in RLs concentration the emission maximum shifted to blue,  $\sim 492$  nm and the spectrum became narrower, which is similar to results observed at neutral pH condition earlier (Figure 2.2 A&B). At pH 8.0 the emission maximum slightly blue shifted at excitation wavelength 355 nm compared to at 425 nm, however, in this pH too the shift in emission maximum of curcumin in RLs was similar and centered at  $\sim 492$  nm. However at pH 13, the fluorescence spectra of curcumin were completely different at  $\lambda_{ex} = 355$  nm vs.  $\lambda_{ex} = 425$  nm (see Figure 2.5 A&B). The emission maximum of curcumin in all the pHs (4, 7, 8 and 13) were similar at excitation wavelength 425 nm, however, at excitation wavelength 355 nm, there was a remarkable difference, especially at pH 13. The absorption of deprotonated form is at  $\sim 460$  nm with a minor peak at  $\sim 355$  nm. When excited at 355 nm, curcumin did not show emission peak at  $\sim 460$  nm at pH 4, 7, and 8 despite a minor absorption band at  $\sim 355$  nm. This is because after excited at 355 nm, emission of  $\beta$ -diketone form undergoes excited state hydrogen transfer [10, 114, 10, 122] to form a six membered ring

structure [123], thus the emission obtained is solely from six membered ring structure enol form of curcumin. However, at pH 13.0, curcumin in water gave two peaks, one at  $\sim 540$  nm and other one at  $\sim 440$  nm (see inset of Figure 2.5B). Coincidentally, we did not find any literature report on fluorescence spectral behavior of curcumin at pH 8 and 13 at  $\lambda_{ex} = 355$  nm. At pH 13.0 it is expected that curcumin exists completely in deprotonated  $cur^{3-}$  form. Since most of the protons are deprotonated, there is little chance for  $\beta$ -diketone form to undergo excited state hydrogen transfer to form six membered emitting species, thus, emission of  $\beta$ -diketone form was observed even though a good fraction of the molecules undergo excited state hydrogen transfer to emit at  $\sim 540$  nm. This observation is similar to emission observed for curcumin associated PAH nanocapsules at  $\lambda_{ex} = 355$  nm [123]. Increase in RLs concentration further reduces the possibility of excited state hydrogen transfer, thus, the emission is dominated by that of  $\beta$ -diketone form of curcumin at  $\lambda_{ex} = 355$  nm. Since fluorescence intensity of curcumin successfully determines cmc of RLs in neutral pH condition, effect of acidic and alkaline pH on cmc of RLs was investigated by measuring fluorescence of curcumin. As can be seen in Figure 2.4 C&D and Figure 2.5C, cmc of RLs could be successfully detected at pH 4, 8 and 13 using fluorescence intensity variation of curcumin both at  $\lambda_{ex} = 355$  nm and 425 nm, except at  $\lambda_{ex} = 425$  nm for pH 13, which did not illustrate any regular variation with RLs concentration suggesting enol form of curcumin interacts poorly with RLs at pH 13, whereas  $\beta$ -diketone form has no issue while interacting with RLs at pH 13. This is possible as at pH 13 RLs is in deprotonated form and would preferentially choose  $\beta$ -diketone form over enol form to avoid repulsive interaction. Interestingly, the cmc of RLs increases linearly with increase in pH of the solution as shown in Figure 2.5D. Rhamnolipids form lipid like vesicles in the size ranges 10-500 nm having structure similar to biological membrane at low pH, whereas at pH 7 rhamnosyl moiety is negatively charged and RLs form lamella like structure or lipid aggregates. Since greater interactive forces exist between the undissociated rhamnolipid molecules at pH=4.0 resulting in a greater compaction at the surface monolayer. But RLs may undergo deprotonation at higher pH. Thus, increase in pH increases the size of micelle by enhancing cmc.

### 2.3.3 Accessibility of Probe Molecule in Rhamnolipids Micelle

To have an insight regarding the accessibility of curcumin with respect to the rhamnolipids micelle, experiments were performed by following fluorescence quenching method at pH 7. Quenching was done using two different quenchers, a hydrophobic quencher CPB which can interact with curcumin when positioned inside the hydrophobic compartment of the micelle while iodide which is a hydrophilic quencher can access curcumin at the surface of the micelle. Similarly, pyrene was used a well-established probe molecule that is known to present at the Stern layer of micelle (micellar interface). As seen in Figure 2.6A, fluorescence of pyrene was quenched linearly in the concentration range 0 to 300  $\mu$ M of CPB in pH 7 without RLs, but the quenching rate was slow. The fluorescence intensity of curcumin was followed at different concentration of both

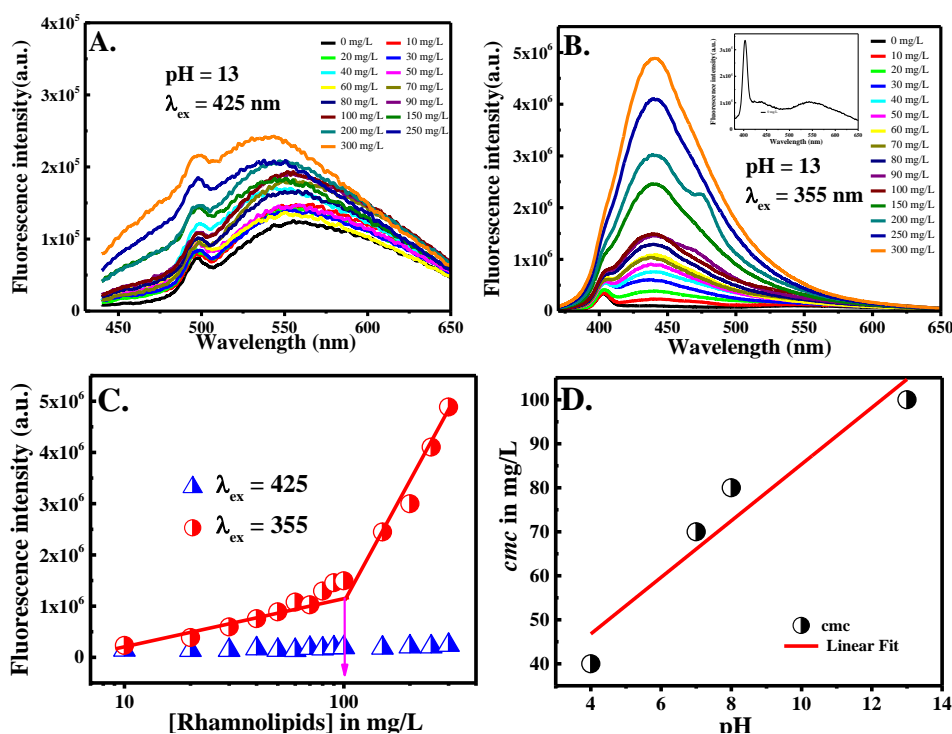


Figure 2.5: Fluorescence spectra of curcumin in difference concentration of rhamnolipids in pH 13.0 condition at  $\lambda_{ex} = 425$  nm for  $\beta$ -diketone form (A) and  $\lambda_{ex} = 355$  nm for enol form (B); (C) Plot of fluorescence intensity vs. rhamnolipid concentration for pH 13. Arrow directs towards critical micelle concentration; (D) Plot of cmc vs. pH

the quenchers. Considering steady state conditions, the relationship derived by Stern and Volmer describes quenching as:

$$F_0/F = 1 + K_{SV}(Q) \quad (2.1)$$

where  $F_0$  and  $F$  are the fluorescence intensities of the fluorophore in the absence and presence of the quencher (Q) respectively and  $K_{SV}$  is the Stern-Volmer quenching constant. The Stern Volmer plot is given in Figure 2.6B estimated Stern Volmer quenching constant of pyrene by CPB in the absence of RLs and is given in Table 2.1. However, when quenching experiment was carried out in the presence of RLs (above cmc), the quenching rate remarkably enhanced exponentially and started saturating at above 100  $\mu$ M of CPB. At high concentration, quenching rate is expected to get saturated due to quenching sphere of action [94]. Therefore, the Stern Volmer constant for fluorescence quenching of pyrene by CPB in the presence of RLs was estimated in 0 - 100  $\mu$ M of CPB and was found to be  $\sim 10$  fold higher than in the absence of RLs (see Table 2.1). Since the quenching by CPB is due to electron transfer process from pyrene to  $N^+$ -atom of pyridinium salt in CPB [124], such a high rate of quenching is rational because of fact that RLs facilitate to bring close together pyrene and  $N^+$ -atom of pyridinium salt during micellisation. Similarly, when fluorescence quenching of curcumin by CPB

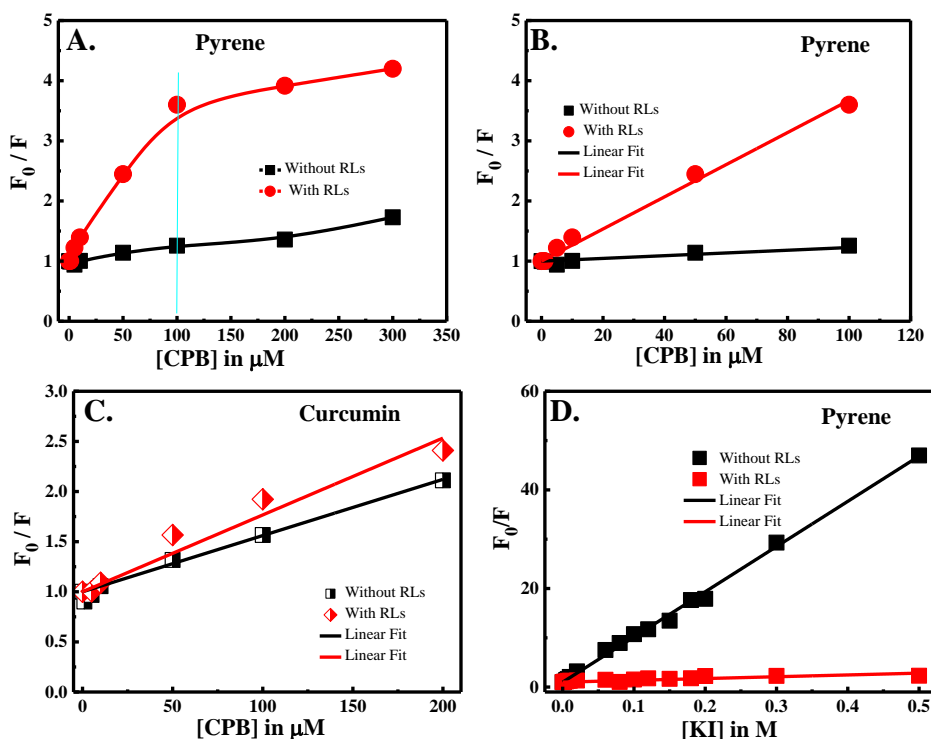


Figure 2.6: Fluorescence quenching of pyrene by CPB, corresponding Stern-Volmer plot is shown in (B); (C) Stern-Volmer plot for fluorescence quenching of curcumin by CPB; (D) Stern-Volmer plot for fluorescence quenching of pyrene by KI.

was carried out in the absence and presence of RLs, the quenching rate was  $\sim 1.5$  folds higher in the presence of rhamnolipids compared to in the absence of RLs (see Figure 2.6C). At pH 7, curcumin exists in its neutral form (90%) and 10% anionic. Thus the fluorescence of the neutral form dominates, with that of the anionic form being negligible. Therefore, poor partition of curcumin into micellar phase is ruled out. This slower rate of quenching of curcumin compared to pyrene is due to the fact that curcumin intercalates deep into the hydrophobic pocket of micelle, thus, reducing the distance for close contact between  $N^+$ -atom of pyridinium salt and curcumin, this discourages a strong fluorescence quenching. Similar observation has been noted in nanoaggregates.<sup>7</sup> For comparison, a hydrophilic quencher KI was used for both pyrene and curcumin. In the absence of rhamnolipids, the  $K_{sv}$  value for quenching of pyrene by KI was  $92 M^{-1}$  (see Figure 2.6D) indicating a high quenching effect, which was greatly reduced in the presence of rhamnolipids to a value of  $4 M^{-1}$ , which correspond to 25 fold decrease in the rate of quenching. Similarly, fluorescence of curcumin was reduced 6 folds by KI in the presence of RLs compared to in absence. Fluorescence quenching experiments clearly indicates that fluorescence of the micelle-encapsulated curcumin is quenched greatly by the hydrophobic quencher CPB compared by the less hydrophobic quencher iodide. Thus a higher percentage of curcumin is positioned inside the micelle, which

agrees with the increase in the stability of curcumin at pH 7 (discussed later on) in the presence of rhamnolipids.

Table 2.1: Add caption

Probe	$K_{SV}$ in $M^{-1}$ with Rhamnolipids		$K_{SV}$ in $M^{-1}$ without Rhamnolipids	
	Cpb	KI	CPB	KI
Pyrene	$2.7 \times 10^4$	3.7	$2.2 \times 10^3$	91.7
Curcumin	$7.7 \times 10^3$	0.39	$5.6 \times 10^3$	2.3

### 2.3.4 Ratiometric Fluorescence Temperature Sensing

To check the impact of temperature, UV-visible absorption spectrum of curcumin was carried out in the absence and presence of rhamnolipids in temperature ranges 15 to 70 °C. As shown in Figure 2.7A in the absence of RLs the absorption spectrum of curcumin showed a decrease in the absorbance at  $\sim 428$  nm with increase in temperature whereas the absorption at  $\sim 355$  nm increased with temperature, thus, shifting the tautomeric equilibrium towards diketo form. This is possible because increase in temperature is expected to break the intramolecular (or intermolecular with solvent molecules) hydrogen bonding of enol form, favoring towards diketo form, which breaks the conjugation between two feruloyl units. Interestingly, in the presence of rhamnolipids the decrease in absorbance at 425 nm occurred in a slower manner (see Figure 2.7B), which could be due to suppression of hydrolytic degradation of curcumin in the presence of RLs (discussed subsequently). On the other hand the peak at 355 nm continued to increase as expected suggesting RLs has little role in influencing transformation to diketo form. However, when ratio of absorbance at 355 nm vs. 425 nm of curcumin was plotted in the absence and presence of RLs, best linear correlation was obtained in the presence of RLs ( $R^2 = 0.994$ ) compared to in the absence of RLs ( $R^2 = 0.947$ ) as shown in Figure 2.7C.

When fluorescence spectra were measured at  $\lambda_{ex} = 425$  nm (enol form, Figure 2.8A) and  $\lambda_{ex} = 355$  nm (for diketo form, Figure 2.8B) in the absence of RLs, interestingly, the spectrum obtained after excitation at 425 nm expressed a broad spectrum with an emission maximum at  $\sim 500$  nm at low temperature. The intensity of emission at 500 nm decreased slightly upon increasing the temperature from 10 degrees till 35 degrees then it increased to attain a maximum at 45 degrees. As temperature increased further till 90 degrees, the intensity of emission decreased with it thus indicating the degradation of curcumin under the effect of temperature. However, at  $\lambda_{ex} = 355$  nm, the emission spectrum exhibited a different pattern. Exciting at 355 nm resulted in a maximum at 510 nm when the temperature was 10 °C but this fluorescence intensity was lower than that obtained after exciting at 425 nm. As temperature increased, a 10 nm blue shift in the emission was gradually attained from 10 till 40 degrees. Similarly as temperature was increased further from 45 to 70 °C the emission wavelength blue



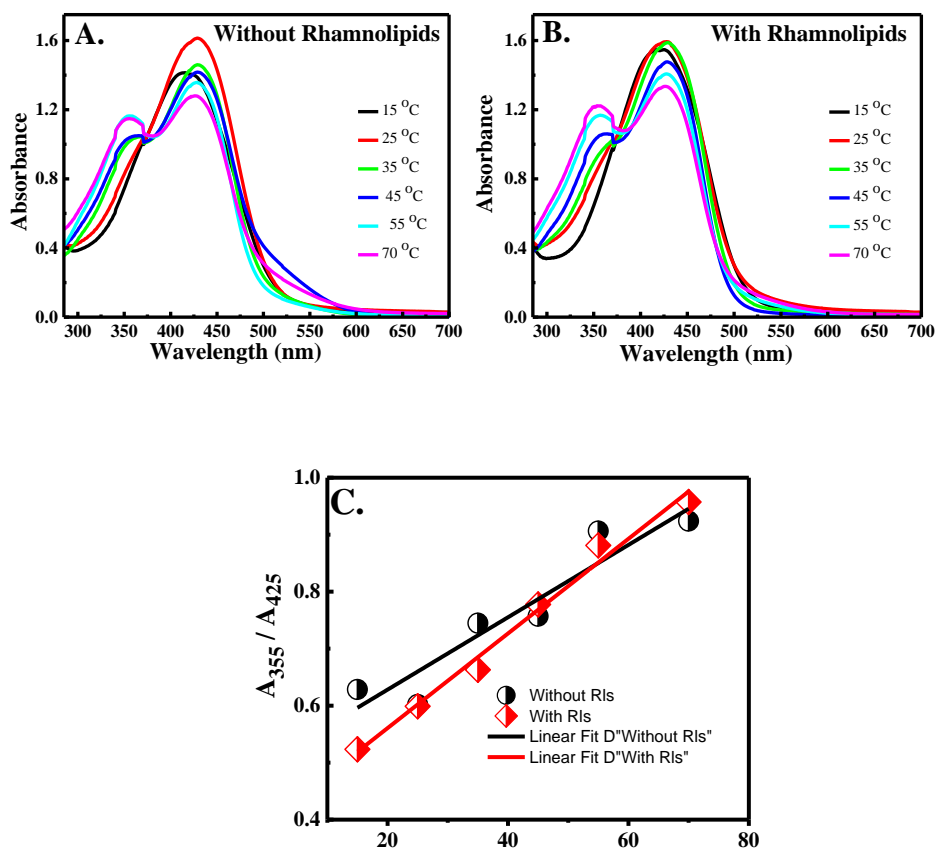


Figure 2.7: UV-visible absorption spectra of curcumin in neutral buffer at different temperature in the absence (A) and presence of rhamnolipids; (C) Plot absorbance ratio ( $A_{355}/A_{425}$ ) vs. temperature.

shifted further to 470 nm. Finally, at 90 degrees, the emission maximum occurred at 437 nm, thus, a huge 73 nm blue shift was observed between 10 degrees and 90 °C at  $\lambda_{ex} = 355$  nm, which could be attributed to transformation from enol form to diketo form of curcumin. The correlation of ratio of fluorescence intensity at 430 nm and 530 nm vs. temperature was done (see Figure 2.8C) at  $\lambda_{ex} = 355$  nm, it gave a good linear changes but the deviation between 40 and 75 °C was visible. This deviation could be due to degradation of curcumin during our measurement time at pH 7. When effect of temperature was studied for curcumin embedded rhamnolipids, at  $\lambda_{ex} = 425$  nm initially a marginal blue shift and increase in fluorescence intensity was observed from 10 to 15 °C, a blue shift in the emission spectrum is usually a result of weaker interaction between the fluorophore and the surrounding medium. Hence we can say that the resonance stability in the keto-enol-enolate in aqueous medium is highly affected and sensitive to temperature. But further increase in temperature lowered the fluorescence intensity and marginally shifted the spectrum towards red wavelength region (see Figure 2.9A). At  $\lambda_{ex} = 355$  nm (see Figure 2.9B), curcumin embedded in RLs gave an

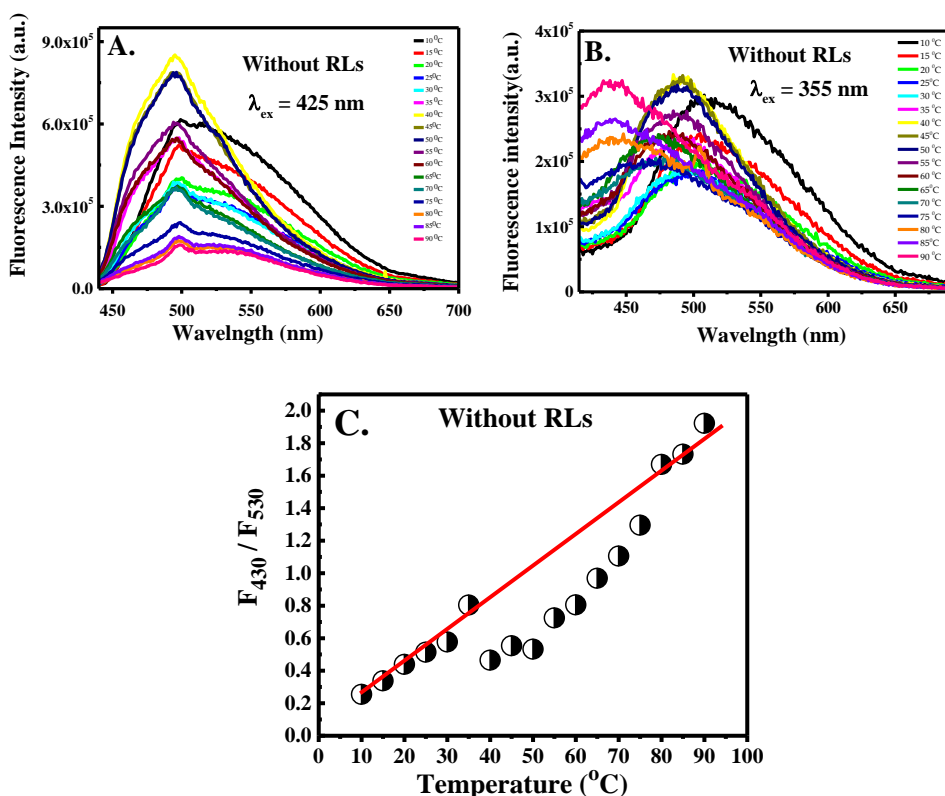


Figure 2.8: Fluorescence spectra of curcumin in difference temperature without rhamnolipids at  $\lambda_{ex} = 425$  nm for  $\beta$ -diketone form (A) and  $\lambda_{ex} = 355$  nm for enol form (B); (C) Plot of fluorescence intensity ratio ( $F_{430}/F_{530}$ ) vs. temperature.

emission maximum at  $\sim 502$  nm and with increase in temperature the peak shifted towards red wavelength region by decreasing the fluorescence intensity. However, the fluorescence intensity at  $\sim 430$  nm improved with increase in temperature. The thermal energy resulting from heating the sample is likely to be responsible of breaking intramolecular hydrogen bonding thus exposing the polar groups of curcumin to the solvent, thus, a red shift resulting from interactions between the exposed polar groups of the keto-enol-enolate group in curcumin and the polar solvent is obtained. This could be possible that the six membered cyclic ring in curcumin (due to intramolecular hydrogen transfer between enolic -OH and carbonyl group) opens up by lowering the conjugation effect and increasing its energy, which not only exposes the polar group to solvent molecules but also stabilizes the diketone form as evident from absorption spectra and increase in fluorescence intensity at  $\sim 430$  nm. However, increase in temperature can also hold back and obstruct the intermolecular H-bonding between the isomer and the solvent, such possibility can't be ruled out completely. As shown in Figure 2.9C, the variation in fluorescence intensity ratio between 430 nm and 530 nm vs. temperature was systematic in the presence of RLs which could be due to stability in keto-enol trans-

formation, thus, curcumin embedded in RLs could potentially be useful as ratiometric fluorescence sensor for temperature.

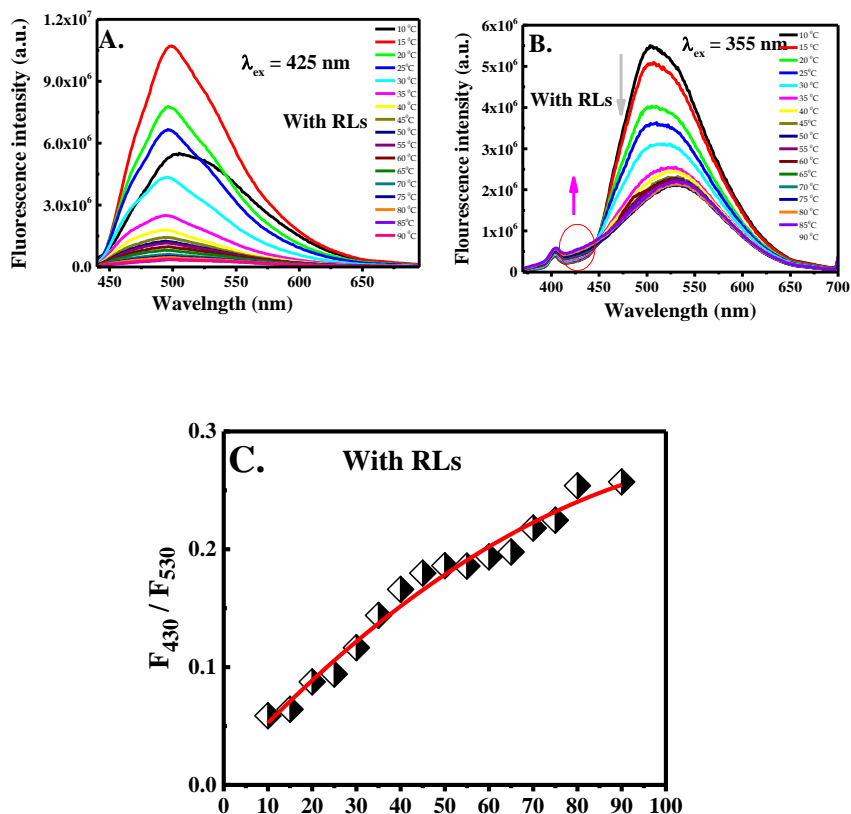


Figure 2.9: Fluorescence spectra of curcumin in difference temperature in the presence of rhamnolipids at  $\lambda_{ex} = 425$  nm for  $\beta$ -diketone form (A) and  $\lambda_{ex} = 355$  nm for enol form (B); (C) Plot of fluorescence intensity ratio ( $F_{430}/F_{530}$ ) vs. temperature.

### 2.3.5 Stability of Curcumin in Rhamnolipids

Curcumin's degradation in aqueous medium has been related to hydrolysis, where it has been shown that this degradation occurs faster at a pH above 7. In alkaline medium, curcumin undergoes rapid hydrolytic degradation where it first undergoes deprotonation followed by fragmentation into bi-products that have been identified by HPLC and mass spectrometry and found to be trans-6-(4'-hydroxy-3'-methoxyphenyl)-2,4-dioxo-5-hexanal as the main product, which further degrades to vanillin, ferulic acid, and feruloyl methane [5]. The kinetics of degradation of curcumin at the different pHs (4, 7, 8 and 13) was investigated in the presence and absence of rhamnolipids. The degradation of curcumin was measured over 24 hrs by recording the decrease in the absorbance at the maximum. The results of the kinetic studies are shown in the Figure 2.10. In the absence of RLs at pH 4, the absorption maxima decreased to approximately 60% of

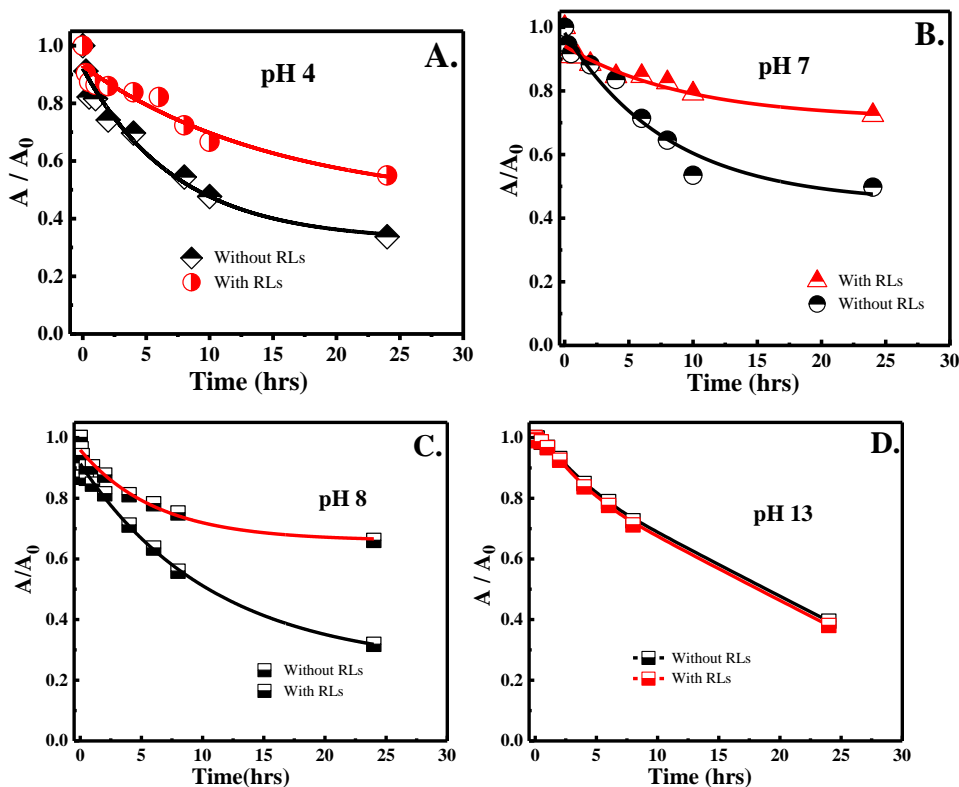


Figure 2.10: Stability of curcumin measured by UV-visible spectrophotometer at  $\lambda_{abs}^{max}$  of curcumin at pHs (A) 4; (B) 7; (C) 8 and (D) 13.

the original value in 24 hrs, whereas in the presence of RLs at the same pH, 46% of curcumin degraded in the same time interval (see Figure 2.10A). At pH 7, degradation of curcumin reduced from 50% in the absence of RLs to 30% presence of RLs in 24 hrs (see Figure 2.10B). Similarly at pH 8 the degradation of curcumin decreased appreciable from 70% to 35% in the presence of RLs (see Figure 2.10C). However, no remarkable change was observed for  $\text{Cur}^{3-}$  species (at pH 13, see Figure 2.10D) in the absence and presence of RLs, and this is as expected due to absence of interaction between RLs and the  $\text{Cur}^{3-}$  as indicated by the absorption spectra earlier. The degradation of curcumin is significantly reduced in the presence of rhamnolipids compared to free curcumin in buffer solutions. The ratio between the degradation in buffer pH 4 in the absence of RLs and in the presence of the latter shows that the degradation is almost 1.5 times slower with rhamnolipids. Likewise in both pH 7 and pH 8, stability of curcumin was enhanced by 2 folds. To our knowledge, these results are the first work to show the ability of RLs to stabilize curcumin and suppress degradation. The difference between the rates of degradation of curcumin at pH 8 and that at pH 13 suggests that in basic media, the fully deprotonated form may have a different degradation pathway than that present at pH 8. The difference in the behavior of curcumin at pH 8

to that at pH 13 is related to the charged species present in solution. In fact pKa value of 8.31 corresponds to the deprotonation of the enolic hydroxyl group. Hence, at pH 8 applying Henderson-Hasselback equation, shows that around 30% of the curcumin is deprotonated. While at pH 13 curcumin is fully deprotonated. Thus we suggest that the interaction between the non-polar neutral rhamnolipids and curcumin depends on the charging state of the latter. Such a claim is indicated by the outcome regarding the effect of RLs on the rate of degradation. The suppression of hydrolysis at pHs 7 and 4 was close to that at pH 8 with a negligible effect for rhamnolipids on Cur<sup>3-</sup>.

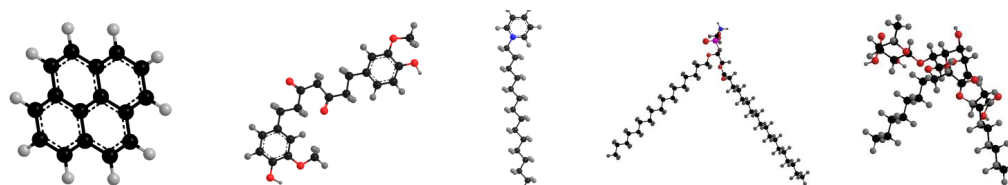
## Chapter 3

# Intercalation of Rhamnolipids with 1, 2-Dioctadecanoyl-sn-glycero-3-phosphocholine Liposomes Enhances Membrane Fluidity, Permeability and Stability of Curcumin

### 3.1 Introduction

Curcumin is chemically 1, 7-bis-(4-hydroxy-3-methoxyphenyl)-1, 6-heptadiene-3, 5-dione (see Scheme 3.1A) or simply diferuloylmethane, which is a polyphenolic phytochemical substance extracted from the roots of the perennial herb *Curcuma longa* Linn [125]. Curcumin is well known for its wide range of biological activities [11]; it is effective against many inflammatory diseases [126], such as pancreatitis arthritis [12], colitis [13], allergy and inflammatory bowel disease [14]. This impact is mainly due to the down-regulation of inflammatory molecules. The potential of curcumin against different autoimmune diseases has been reported as well, including Lupus nephritis [127], multiple sclerosis [15], diabetes [16] and scleroderma psoriasis [128]. Extensive research is being currently carried out to apply curcumin as a potential drug for anti-cancer activities [129, 130, 131] and anti-amyloid behavior [132]. Moreover, curcumin is useful for metal nanoparticles synthesis and its interaction in heterogeneous media can determine shape and size during nanorods synthesis [133]. However its poor solubility [9] and poor stability especially in neutral/alkaline medium [134] remain important concerns. Several studies have targeted the enhancement of curcumin bioavailability and its delivery. These studies include incorporation into liposomes and phospholipids [106], surfactants [135], encapsulation as polymer nanoparticles [108], polyethylene glycol [136], and several cyclodextran inclusion complexes [105]. Encapsulation of curcumin in liposome offers another good alternative. Membrane bound curcumin

is now available as a dietary supplement in the name of BCM-95.



Scheme 3.1: Structure of (A) Pyrene; (B) Curcumin; (C) CPB; (D) DSPC; (E) Rhamnolipids

Liposomes are small artificial spherical vesicles made of curved lipid bilayers that include portion of the surrounding solvent into their inside [1]. Liposomes are of important interest since they can trap and release two compounds of different solubility: a lipid soluble material and a water soluble one [137]. Moreover due to their biocompatibility and low toxicity, food and pharmaceutical industries have extensively investigated liposomal systems and their applications [138, 139, 140]. Liposomes are formed by dissolving lipid molecules mainly phospholipids, which are amphiphilic molecules having a hydrophilic head section and hydrophobic tail. The most used lipids are phospholipids, especially the neutral phosphatidylcholine and the several negatively charged ones that differ by the fatty acid chain in the hydrophobic moiety of the molecule, these include phosphatidylethanolamine, phosphatidylglycerol, phosphatidylserine and phosphatidic acid. The most abundant lipid in animal cell membrane is phosphatidylcholine, which gives structural framework. Phosphatidylcholine primarily functions as part of the permeability barrier in the outer leaflet. It is also primary substrate of phospholipase D enzymes that produce the signaling lipids-phosphatidic acid and lysophosphatidic acid. 1,2-Dioleoyl-*sn*-glycero-3-phosphocholine (DSPC) (see Scheme 3.1B) is an 18-carbon chain phosphatidylcholine.

On the other hand, surfactants are chemical compounds that exhibit surface activity and are useful in modulating liposomes properties. Surfactants show tendency for interfaces of unlike polarities (liquid-liquid or liquid-air) and are soluble in both organic and aqueous solvents [23]. This property is a result of their amphiphilic structures, which contain both a hydrophilic head and a hydrophobic tail [23] Biosurfactants are surface-active biomolecules of microbial origin among which are Rhamnolipids (RLs) [24] (see Scheme 3.1C). RLs are glycolipid biosurfactants produced mainly by *Pseudomonas aeruginosa* [27] and can be described as glycosides that are composed, of a rhamnose moieties (that constitute the glycon part) and lipid part (that makes the aglycon part connected by an O-glycosidic bond) [28]. RLs are characterized by unique physiochemical properties namely surface activity, wetting ability, detergency, and other amphipathic-related qualities [141, 142, 143, 144]. These properties render RLs physiological functions that are highly important for the producing organism as well as many applications in industry [145]. Several studies have reported the interaction between liposomes and

surfactants. Studies targeted the topological changes of liposomes that are induced upon interactions with surfactants [146], in addition to effect of anionic surfactants on both the disintegration of liposomes [147] and mixed liposome solubilization [148]. Moreover, few reports assessed the thermodynamics of liposome-surfactant interactions [149] and other work that aimed at understanding the effect of physiochemical interaction of cationic surfactants with model membranes on the antimicrobial effect of the former [150]. To our knowledge there is little report on influence of RLs on liposomes properties, which is the aim of this work.

Fluorescent probes have been ideal candidates to study the properties of liposomes. Curcumin is a fluorescent molecule and its photo-physical properties are greatly reliant on the polarity of the environment and the pH of the medium [151]. The absorption maximum of curcumin is at  $\sim 420$  nm in the largest part of the polar solvents, yet in hydrogen bond acceptor and donor solvents, it is shifted to  $\sim 430$ - $434$  nm, excluding methanol where it is around  $423$ - $428$  nm [151]. In acidic media, the absorption maximum of curcumin is at  $\sim 422$  nm, however, at pH greater than 7, the yellow color of curcumin turns bright red, with the absorption maximum shifting to  $\sim 463$  nm caused by the ionization of phenolic OH group [121]. We have successfully established curcumin as a molecular probe to investigate liposome characteristics [152, 101, 153]. In this study, we have applied curcumin as a molecular probe to investigate the properties of DSPC liposomes that is not yet explored. It is found that curcumin strongly partition into DSPC liposomes and can effectively determine the phase transition temperature of DSPC liposomes. However, at higher concentrations, curcumin can influence phase transition temperature of DSPC liposomes. This probing concept has been further extended to examine the impact of RLs on DSPC membrane properties. This is the first study that applies curcumin as a probe to study the interaction between a biosurfactant and a phospholipid membrane and brings new insight on modulation of liposomes properties induced by the biosurfactant (RLs). The phase transition temperature of DSPC liposomes is influenced by RLs and it decreases with increase in percentage of RLs in DSPC liposomes. The study proves that intercalation of RLs with DSPC liposomes improve stability of curcumin by enhancing permeability and fluidity of the liposomes opening the possibility of using such mix system for drug delivery.

## **3.2 Materials And Methods**

### **3.2.1 Materials**

DSPC was obtained from Avanti. Rhamnolipids, curcumin, pyrene and Cetylpyridinium bromide (CPB) were obtained from Sigma-Aldrich and used as received. The solvents used were of spectroscopic grade and obtained from Sigma-Aldrich. The stock solution of membrane was prepared in 50 mM mono- and dibasic phosphate buffer at pH 7.0. Further dilution was made in 50 mM mono- and dibasic phosphate buffer at



pH 7.0. Because of poor solubility, the stock solution of curcumin was made in spectroscopic grade ethanol. A few microliters of the stock sample of curcumin (~ 1 mM) was taken in a vial and added to a final sample for measurement in buffer. Steps were taken to ensure that the final concentration of ethanol was negligible, less than 0.1% in the measurement sample, to avoid affecting the sample.

### **3.2.2 Preparation of liposomes**

DSPC liposomes were prepared by the solvent evaporation method [154]. The desired amount of DSPC phospholipid was dissolved in 15 mL of a chloroform/methanol mixture (1:1 volume ratio). The solvents were evaporated using a rotary evaporator at 57-60 °C. The membrane formed was dried under vacuum for 10 min. Then glass beads were added, and enough phosphate buffer at pH 7.0 was used to form liposomes at a concentration of 1 mM. The mixture was vortexed rigorously for 15 min and finally heated for 30 min at 65 °C, about 14 °C above the phase transition temperatures for DSPC. When required, further dilution was made in 50 mM mono- and dibasic phosphate buffer at pH 7.0. The prepared liposomes were multilamellar vesicles (MLVs).

### **3.2.3 Incorporation of RLs**

Stock solutions, ~1g/L was prepared in double distilled water. The solutions were prepared by adding the desired volume (a few microliters) of RLs stock of appropriate concentration to the liposome (MLV) solution at 37 °C.

### **3.2.4 Spectroscopic measurements**

The absorption spectra were recorded at room temperature using a JASCOV-570 UV-vis-NIR spectrophotometer. The steady-state fluorescence measurements were recorded with a resolution increment of 1 nm, slit 5 using a HORIBA Jobin Yvon Fluorolog-3 fluorometer and the FluorEssence program. The excitation source was a 100 W xenon lamp, and the detector used was an R-928 operating at a voltage of 950 V. To regulate the temperature, a thermostat was coupled with the sample holder. The final temperature was noted in the sample compartment using a thermometer rather than thermostat.

## **3.3 Results And Discussion**

### **3.3.1 Interaction and stabilization curcumin in DSPC liposomes**

Degradation of curcumin in physiological buffer solution is well reported [5] and for its applicability, stabilization of curcumin in neutralbuffer condition is significant [155]. The degradation products of curcumin are trans-6-(4'-hydroxy-3'-methoxy- phenyl)-2,4-dioxo-5-hexanal as the main product, which further decomposes to vanilin, ferulic

acid, and feruloyl methane [5]. All these degradation products have different visible absorption than curcumin, thus, effect of the degradation products on the main absorption maximum of curcumin is negligible. Thus, UV-visible absorption spectrum of curcumin has been used to understand the degradation process of curcumin [110]. In the present case, the degradation of curcumin was studied at physiologically significant buffer, pH 7.0, in presence and absence of DSPC. The UV-visible absorption spectra of curcumin with initial concentration of 25  $\mu\text{M}$  in the presence of 100  $\mu\text{M}$  DSPC concentration was monitored as shown in Figure 3.2A. A control measurement was done for curcumin at pH 7.0 phosphate buffer solution without DSPC (to increase solubility of curcumin a small amount of methanol was used). In neutral condition, 47% of curcumin degraded in 8 hrs in buffer solution compared to 37% degradation when associated with DSPC (see Figure 3.2B), thus, presence of DSPC liposomes significantly stabilizes curcumin in neutral pH conditions.

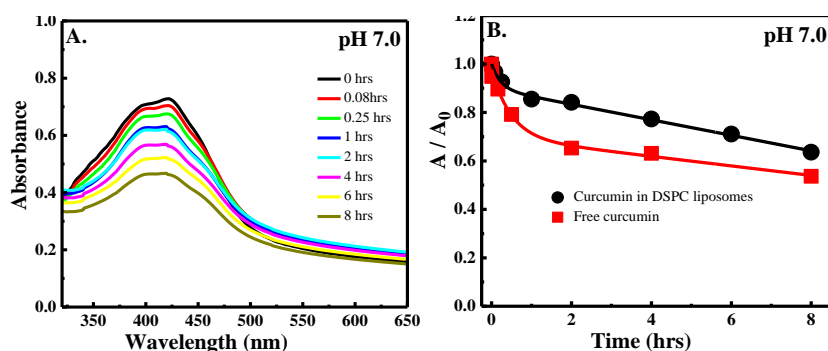


Figure 3.2: (A) UV-visible absorption spectra of curcumin in DSPC liposomes at pH 7.0 buffer solution during different time interval; (B) Rate of degradation of curcumin at pH 7.0 buffer solution in the absence and presence of DSPC liposomes.

The suppression of the degradation of curcumin in this condition is possibly caused by interaction of curcumin with the DSPC liposomes. An evidence of this interaction is shift in the absorption spectrum of curcumin observed in DSPC liposomes. In neutral buffer condition (pH  $\sim$ 7) we found a 10 nm blue shift in the absorption maximum of curcumin associated with DSPC as absorption maximum of curcumin in DSPC liposomes was observed at  $\sim$ 420 nm compared to at  $\sim$ 430 nm for the free curcumin (see Figure 3.3A). Moreover, the peak of curcumin in DSPC liposomes broadened with a relatively small shoulder at 397 nm. Such structure in absorption spectrum has also been noted for curcumin in Gemini [156] and neutral [116] surfactant solutions as well as in DMPC/DPPC liposomes [152], thus, indicating association of curcumin with DSPC liposomes. Similarly, in acidic medium at pH 4.0, the UV-visible spectrum of curcumin revealed in Figure 3.3B showed a strong absorption peak  $\sim$ 432 nm, which was shifted to  $\sim$ 423 nm in DSPC liposomes at pH 4.0 suggesting acidic environment does not affect association of curcumin with DSPC liposomes. However, in an alkaline medium

at pH 13 the absorption maximum of curcumin in DSPC liposomes was found to be at  $\sim 468$  nm (see Figure 3.3C). It is established that in aqueous medium, curcumin possess 3 pKa values, 8.38, 9.88, and 10.5 [121]; these values correspond the de-protonation of the three hydroxyl groups. At pH 13, curcumin is de-protonated to give a negatively charged species  $\text{Cur}^{3-}$ . In UV-Vis spectrum, completely de-protonated curcumin absorbs with a maximum at  $\sim 468$  nm. The shape of absorption spectrum and absorption maximum of de-protonated curcumin was not affected by the presence of DSPC liposomes. Since there is little influence by DSPC liposomes on S0-S1 electronic transition of deprotonated form of curcumin,  $\text{Cur}^{3-}$ , compared to protonated form of curcumin (cur), association of curcumin with liposomes is pH dependent.

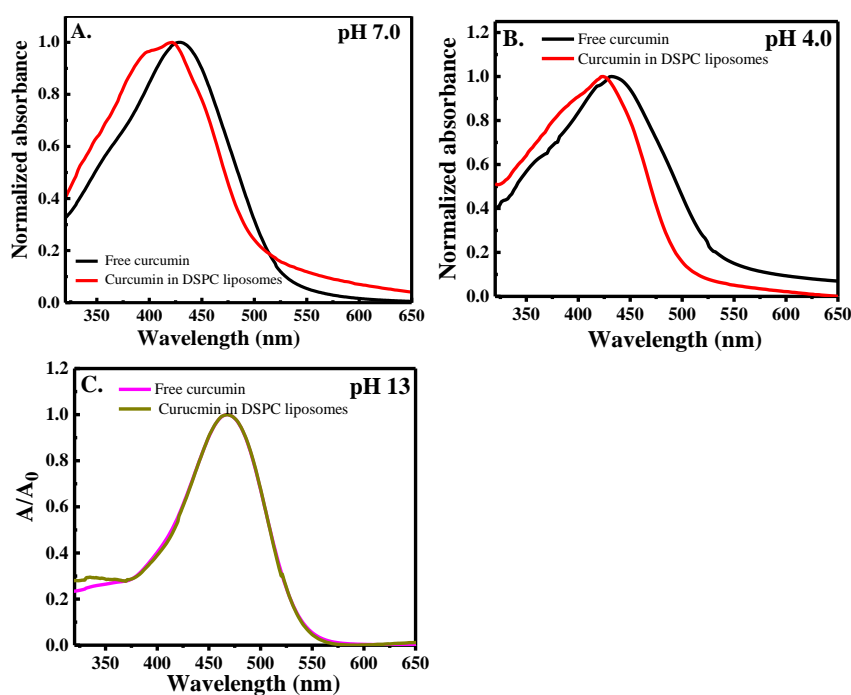


Figure 3.3: Normalized UV-visible absorption spectra of curcumin in the absence and presence of DSPC liposomes at (A) pH 7.0; (B) 4.0 and (C) 13.0 buffer solution.

The interaction between curcumin and DSPC liposomes was further investigated by fluorescence titration, which is a sensitive, accurate and simple method. Since association of curcumin with DSPC liposomes can be affected by different phases of liposomes, the fluorescence spectra of curcumin in different concentrations of DSPC liposomes were measured in both the phases: the solid-gel phase and liquid crystalline phase, as shown in Figure 3.4A & 3.4B. The fluorescence intensity of curcumin was significantly enhanced in the presence of DSPC irrespective of solid-gel or liquid crystalline phases. This increase in the intensity reveals a strong interaction between curcumin and DSPC liposomes. Heightening of curcumin fluorescence intensity in water

has been reported with micelles, membranes and methanol [151, 157]. The rate of increase in the intensity of fluorescence in solid-gel was greater than that in liquid-crystalline phase; however in both there is a blue shift of 57 nm magnitude in the emission spectra of curcumin in the presence of DSPC compared to curcumin in buffer solution. This >50 nm shift further reconfirms the association of curcumin with DSPC liposomes.

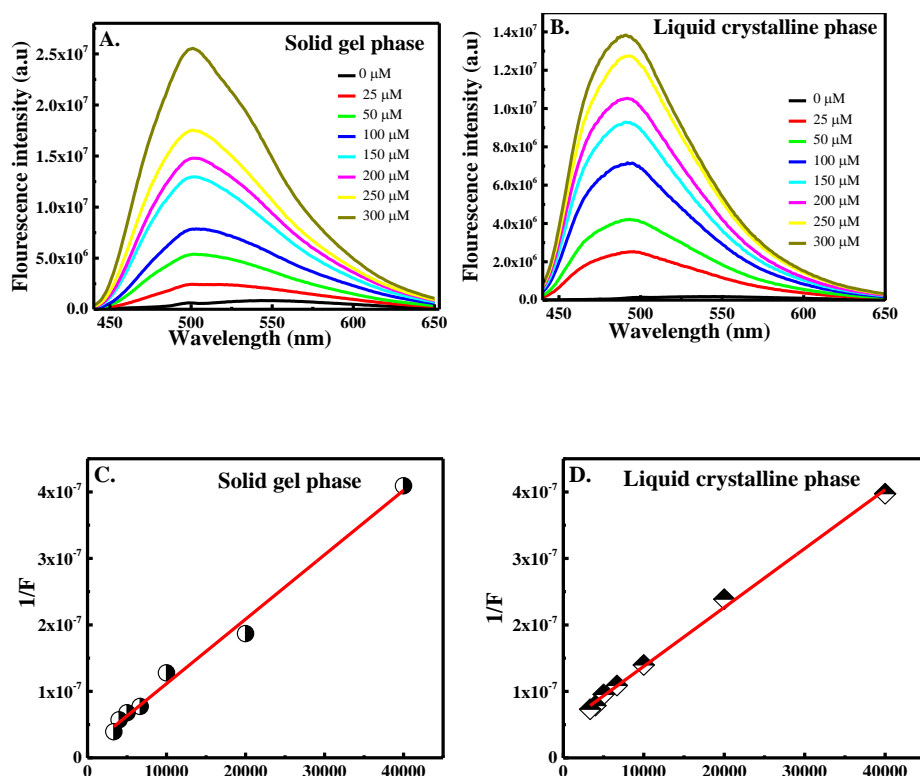


Figure 3.4: Fluorescence emission spectra of curcumin in various concentrations of DSPC liposomes in (A) solid gel phase and (B) liquid crystalline phase. Plot of  $1/F$  vs  $1/[DSPC]$  in solid gel phase (C) and liquid crystalline phase (D). Fluorescence intensity was measured at excitation wavelength 425 nm and emission wavelength 492 nm.

### 3.3.2 Partition coefficient of curcumin in DSPC liposomes

The partition coefficient ( $K_p$ ) indicates the fraction of the lipophilic molecule associated with the lipid. The change in the fluorescence intensity of curcumin in the aqueous phase and after association with the liposomes presents a potential tool to evaluate  $K_p$ . The partition coefficient of curcumin into DSPC liposomes is expressed as [158]:

$$K_p = (CUR_a / DSPC)(CUR_f / M) \quad (3.1)$$

where  $CUR_\alpha$  is the molar concentration of curcumin associated with the membrane;  $CUR_f$ , DSPC and  $M$  are molar concentration of free curcumin in aqueous medium,

liposomes/phospholipid membranes and water respectively. Knowing that curcumin fluorescence intensity in water is weak compared to that obtained for curcumin incorporated with the liposome, it can be inferred that the fluorescence of curcumin is proportional to the amount of curcumin associated with the membrane, thus the fluorescence  $F$  can be written as:

$$K_p = cCURa \quad (3.2)$$

where  $c$  is a proportionality constant.

Considering that the total curcumin concentration is  $CUR = CURa + CURf$  then it is possible to write

$$F = F_0 \times DSPC / (M / K_p + DSPC) \quad (3.3)$$

where  $F_0 = cCUR$  is the maximum fluorescence obtained from total curcumin incorporated into the liposomes. The molar concentration of the DSPC membrane is less than 0.2% of the total volume, thus, the molar concentration of water can be considered as that of pure water and it can be rewritten as:

$$F = F_0 \times DSPC / (55.6 / K_p + [DSPC]) \quad (3.4)$$

Or

$$\frac{1}{F} = [55.6 / K_p F_0] (1 / DSPC) + \frac{1}{F_0} \quad (3.5)$$

The equation presented above indicates that the plot of the reciprocal of fluorescence intensity as a function of the reciprocal of the membrane concentration is a linear curve and  $K_p$  can be calculated from the slope and intercept. The partition coefficient of curcumin into DSPC was calculated by plotting reciprocal of fluorescence intensity ( $1/F$ ) versus the reciprocal of DSPC concentration ( $1/[DSPC]$ ) as depicted in Figure 3.4D (for solid gel) and 3E (for liquid crystalline phase).  $K_p$  for both the solid gel phase at 25°C and the liquid crystalline at 58°C was calculated from the above equation and the results are summarized in Table 3.1. The partition coefficient of curcumin into DSPC at the solid gel phase was found to be  $8.38 \times 10^4$ . The partition coefficient increased by a factor of 3.6 in the liquid crystalline phase and estimated to be  $3.08 \times 10^5$  suggesting that the partition of curcumin into DSPC at the liquid crystalline phase is more than that at the solid gel phase. This trend is similar to our earlier observation for both DMPC [13] and DPPC [14] liposomes and logical due to the fact that the permeability of the liposome at the liquid crystalline phase is higher than that at the solid gel phase where the former is characterized by flexibility compared to the rigidity and the latter is known to be dense form (see Figure 3.4D). As the permeability increases, the incorporation of curcumin into the membrane is expected to enhance.

### 3.3.3 Determination of phase transition temperature of DSPC liposomes

Phase transition is an important aspect of the liposomes and it affects various important functions of membranes. Florescence is a sensitive method where it requires

smaller samples unlike DSC measurements; therefore, we have recently established using curcumin as a fluorescence probe to reliably detect phase transition temperature of DMPC [101] and DPPC liposomes [153]. In this case we further extended our study to measure phase transition temperature of DSPC liposome having a longer carbon chain and higher phase transition temperature where the concentration of DSPC liposomes was fixed at 100  $\mu\text{M}$  and that of curcumin was at 5  $\mu\text{M}$ . Phase transition of DSPC can be divided into two stages. The first one is pre-transition where DSPC liposomes undergo a transition from solid gel to a rippled gel phase and it occurs around 35 degrees [159]. The major phase change occurs along with the melting of the acyl chains in the hydrophobic part of the membrane. This transition into the liquid crystalline phase of DSPC occurs near 54°C. As shown in Figure 3.5A, along with the increase in temperature, the fluorescence intensity of curcumin in DSPC liposomes increased to a maximum at the phase transition temperature ( $T_m$ ), after  $T_m$ , the intensity decreased as the system became homogeneous at the liquid phase. Such a behavior is related to the changes in the permeability and the fluidity of the DSPC liposomes. Before the  $T_m$ , as the system is shifting from the dense solid gel phase to the less compacted liquid crystalline phase, the chance of curcumin permeating the DSPC membrane is enhanced, as it has been shown with the  $\sim 3.7$  times increase in the partitioning of curcumin into DSPC at the liquid phase compared to the solid gel phase before. This increase in the permeability results in an enhancement in the fluorescence intensity of curcumin as more molecule enters the hydrophobic phase. In addition the observed blue shift in the emission spectrum of curcumin from 512 nm to 492 nm (see Figure 3.5A) occurring along with the increase in the temperature confirms the partitioning of curcumin into the hydrophobic core of the membrane. This observation is consistent with earlier work [101]. Beside the permeability of the membrane another factor should be considered which is the microviscosity or fluidity of the environment. The fluorescence of curcumin is not only dependent on the permeability rather it is affected by the viscosity or the fluidity of the medium, which accounts for the decrease in the emission intensity after the phase transition temperature. Therefore the fluorescence of curcumin was dominated by the permeability factor prior to the  $T_m$  and by viscosity or the fluidity factor after attaining phase transition temperature. Thus a maximum was obtained at the phase transition temperature, which further reconfirms that curcumin can be successfully used to measure phase transition temperature of membranes, the phase transition temperature measured for DSPC liposomes in this case was found to be at 54°C as depicted in Figure 3.5C, which agrees with the values reported in literature [159].

It is also reported that at higher concentration curcumin does influence the phase transition temperature at high molar ratio, though at low concentration it has no. This has been established for DMPC [101] and DPPC [153] liposomes but its impact of DSPC has not been inspected. Therefore, the molar concentration of curcumin was increased and the phase transition was measured at the following proportions between curcumin concentration and [DSPC]: 1:20, 1:10, 1:5, 1:2 and 1:1. Interestingly, when

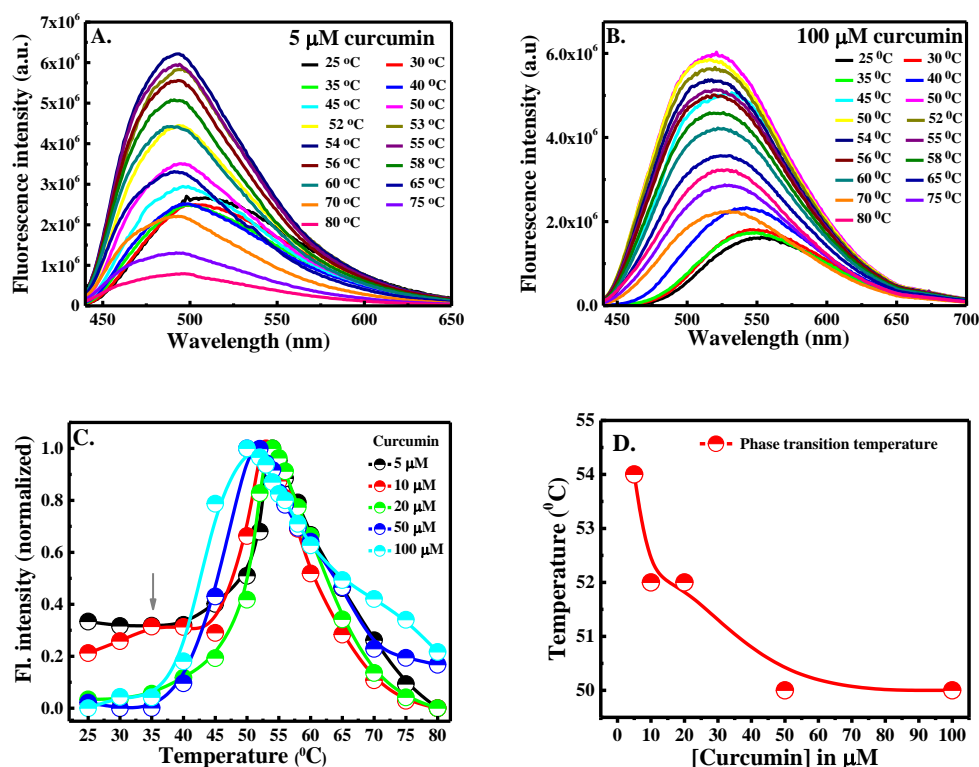


Figure 3.5: Fluorescence emission spectra of 5  $\mu$  M (A) and 100  $\mu$  M (B) curcumin in DSPC liposomes (100  $\mu$ M); (C) Profile of fluorescence intensity of curcumin vs. temperature at various concentration of curcumin concentration in DSPC liposomes; (D) Variation in phase transition temperature of DSPC liposomes with curcumin concentration.

the curcumin concentration was increased to 50  $\mu$ M ([curcumin]: [DSPC] = 1:2); and 100  $\mu$ M ([curcumin]: [DSPC] = 1:1) in DSPC liposomes, the fluorescence emission maximum was found to be red shifted to  $\sim$ 550 nm (see Figure 3.5B;  $\sim$ 545 nm in the presence of 50  $\mu$ M of curcumin) compared to  $\sim$ 512 nm (see Figure 3.5A) obtained in the presence of 5  $\mu$ M of curcumin suggesting at this concentration ( $>$  50  $\mu$ M) of curcumin large population is exposed to aqueous medium, thus, penetration of curcumin gets saturated at higher concentration ( $>$  50  $\mu$ M). With increase in temperature of curcumin embedded DSPC liposomes, the fluorescence emission maximum blue shifted to  $\sim$ 492 nm and  $\sim$ 525 nm in the presence of 50  $\mu$ M and 100  $\mu$ M of curcumin respectively. This is a clear indication that most of the curcumin gets buried into the DSPC liposomes in liquid crystalline phase at 50  $\mu$ M of curcumin whereas majority amount curcumin still partially exposed to aqueous media in the liquid crystalline phase at 100  $\mu$ M of curcumin. However, the variation of curcumin population in different depth of liposomes did not affect during estimation the phase transition temperature [101]. As the concentration of curcumin increased, the phase transition temperature broad-

ened as shown in Figure 3.5C, with shift from 54 °C at 5  $\mu\text{M}$  of curcumin to 50 °C at 100  $\mu\text{M}$  of curcumin as depicted in Figure 3.5D. Moreover, the shoulder that marks the pre-transition stage faded as the concentration of curcumin increased to become at an equal proportion with that of the phospholipid. This outcome indicates the interposition of curcumin molecules between the acyl chains of DSPC thus disrupting the regular packing in both phases. It has been displayed in early studies that at high curcumin concentrations, curcumin molecules tend to form oligomers that occupy the deep core of the membrane and that diverge between them and the thickness of the bilayers results in thinning of the membrane to compensate the length of the curcumin oligomers [160].

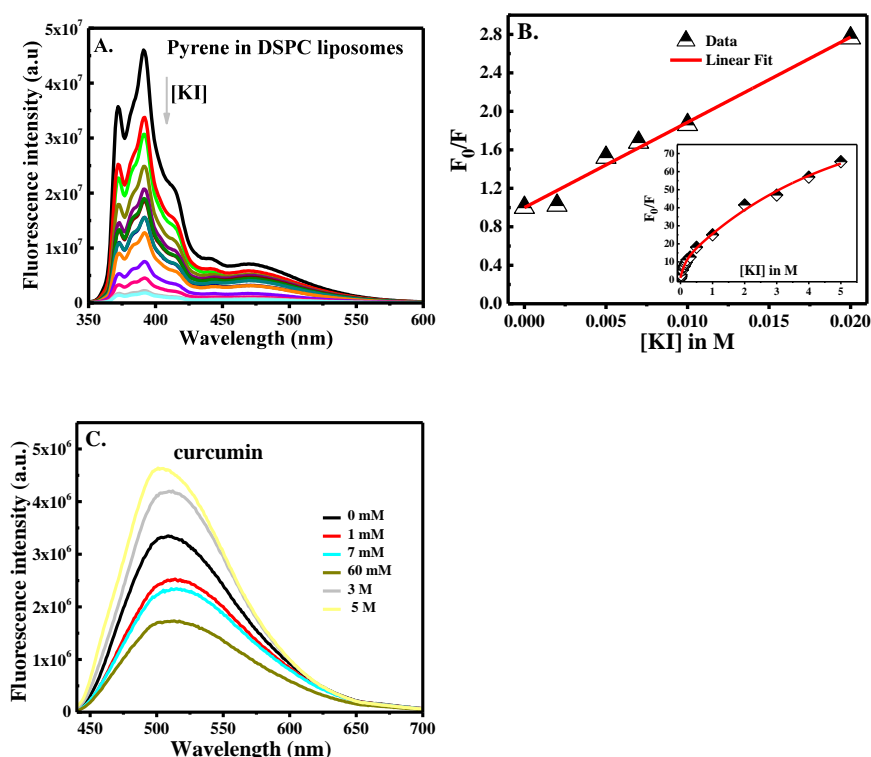


Figure 3.6: (A) Fluorescence spectra of pyrene in DSPC liposomes with different concentration of KI; (B) Stern-Volmer plot for fluorescence quenching of pyrene by KI (0 to 20 mM) in DSPC liposomes, inset shown the same plot for KI 0 to 5 M; (C) Fluorescence spectra of curcumin in DSPC liposomes with different concentration of KI.

### 3.3.4 Fluorescence quenching study in DSPC liposomes

Lipophilicity is one of the significant parameters usually used to predict membrane permeability and is roughly associated with the passive transport across cell membranes



and the capability of a compound to partition and intercalate into a membrane. Quenching of fluorescence probes in bio-membrane systems are of an important interest. In these investigations, the use of appropriate quenchers could provide valued information regarding the permeability and fluidity of membrane systems. Changes in the membrane permeability are reflected in changes in the rate constant of the quenching reaction or ease of entry of the quencher to the probe, which is usually incorporated within the membrane hydrophobic core. Initially pyrene (see Scheme 3.1D) as a well-reported external fluorescence probe for liposomes was applied for quenching experiment by KI. The fluorescence intensity of pyrene was measured at different concentration of quencher. The fluorescence intensity of pyrene was quenched by KI in the absence and presence of DSPC liposomes (shown in Figure 3.6A). Under steady state conditions the relationship derived by Stern and Volmer describes quenching as

$$F_0/F = 1 + K_{SV}[Q] \quad (3.6)$$

where  $F_0$  and  $F$  are the fluorescence intensities in the absence and presence of different quencher concentration ( $[Q]$ ), respectively, and  $K_{SV}$  is the Stern-Volmer quenching constant. The Stern-Volmer plot for fluorescence quenching of pyrene by KI in DSPC liposomes was found to be linear till 20 mM (see Figure 3.6B) and at higher concentration of KI it is saturated as expected due to quenching sphere action (see inset of Figure 3.6B). The  $K_{SV}$  value estimated for pyrene in aqueous environment was found to be  $\sim 102 \text{ M}^{-1}$  [103] whereas in the presence of 100  $\mu\text{M}$  DSPC liposomes was  $\sim 88 \text{ M}^{-1}$ . This  $\sim 13\%$  decrease in quenching rate is expected, though not substantial, because pyrene is expected to locate at the interface of liposomes, thus partially exposing to aqueous environment. Fluorescence quenching of curcumin by KI in DSPC liposomes followed two different patterns as shown in Figure 3.6C. At low concentrations of KI (below 60 mM), the fluorescence intensity of curcumin was quenched by KI but further increase in KI concentration recovered the lost fluorescence and above 1 M of KI an enhancement in fluorescence intensity of curcumin was observed in DSPC liposomes. In contrast a single trend was obtained for fluorescence quenching of curcumin by KI in buffer solution without DSPC liposomes i.e. the fluorescence intensity of curcumin decreased from 0 to 5 M of KI. In aqueous environment curcumin and  $\text{I}^-$  are in close contact to cause quenching of curcumin fluorescence, however, in liposomes curcumin is largely present in hydrophobic environment whereas  $\text{I}^-$  in aqueous medium discouraging close contact between curcumin and  $\text{I}^-$ . Moreover, the difference in the fluorescence quenching by KI between pyrene and curcumin in DSPC liposomes can be related to the different in their structures. Due to entropic reasons, pyrene is positioned close to the head groups of the bilayer which is confirmed by fluorescence experimental approaches [161, 162, 163]. This location, which partially increases close contact between pyrene and  $\text{I}^-$  whereas curcumin intercalates parallel to the lipid bilayers of the liposome [152] and largely reduces contact between curcumin and  $\text{I}^-$ . At higher concentration of KI, more curcumin molecules are helped and pushed by KI into the deep lipid bilayers due to salting out effect, which rather enhance overall fluorescence intensity of curcumin.

### 3.3.5 Effect of rhamnolipids on stability of curcumin in DSPC liposomes

The absorption spectra of curcumin at pH 7.0 did not change in the absence and presence of 10 to 150 % of RLs in DSPC liposomes. A representative UV-visible absorption spectrum for 10 % of RLs in DSPC liposome is shown in Figure 3.7A (compare with Figure 3.3A). In the neutral condition at pH 7, the absorption maximum was unaltered by rhamnolipids in DSPC liposomes but with time the absorbance decreased due to degradation (see Figure 3.7A). Interestingly, the stability of curcumin was further enhanced with increasing concentrations of RLs in DSPC liposomes till 8 hrs (degradation of curcumin in DSPC liposomes decreased from 37 % in absence of RLs to 20 % in presence of 150 % RLs after 8 hrs), however, after 24 hrs the most stable condition was found to be 50 % RLs where degradation was about 32 % compared to 43 % in the absence of RLs and 35 % in the presence of 150 % of RLs in DSPC liposomes as shown in Figure 3.7B. Since degradation of curcumin in alkaline pH is often reported [110], degradation of curcumin in de-protonated form,  $\text{Cur}^{3-}$ , was investigated. Like in pH 7.0, the decrease in absorbance of  $\text{Cur}^{3-}$  at  $\sim 468$  nm was monitored in this case for testing the stability. The absorbance of  $\text{Cur}^{3-}$  in DSPC liposomes in the presence (Figure 3.7C) and absence of RLs reduced with time. As expected after 24 hrs degradation of  $\text{Cur}^{3-}$  in DSPC liposomes was 50 % in pH 13.0 (see Figure 3.7D) compared to 43 % for curcumin in pH 7.0. However, in the presence of 50 % RLs in liposomes, stability of  $\text{Cur}^{3-}$  improved and the degradation rate remained 26 %, which is even better than for curcumin at pH 7.0. Nevertheless, further increase in RLs concentration did not help rather increased in degradation rate of  $\text{Cur}^{3-}$  (see Figure 3.7D). Thus a different type of interaction occurs with the completely deprotonated form of curcumin compared to that of the protonated form in DSPC liposomes.

### 3.3.6 Effect of rhamnolipids on partition coefficient of curcumin into DSPC liposomes

The partition of curcumin into DSPC liposomes in the presence of RLs was studied by keeping RLs concentration constant at 100 % and varying the DSPC concentrations. In this case the concentration of curcumin was maintained at 5  $\mu\text{M}$ , which was less than the concentration of the phospholipid concentration. In the presence of 100 % RLs, the fluorescence intensity of curcumin increased with the increase in DSPC liposome concentration in both solid gel phase and liquid crystalline phase (see Figure 3.8A). The partition coefficient was estimated as described earlier, a representative plot for the determination partition coefficient of curcumin in liquid crystalline phase of DSPC liposomes in the presence of RLs is shown in Figure 3.8B. The partition coefficient values are summarized in Table 3.1, which clearly establishes that the partition coefficient of curcumin into DSPC in the solid gel phase was enhanced by  $\sim 22$  folds in the presence of RLs compared to that in the absence of RLs, this indicates presence of RLs increases permeability of DSPC liposomes in solid gel phase. This increase

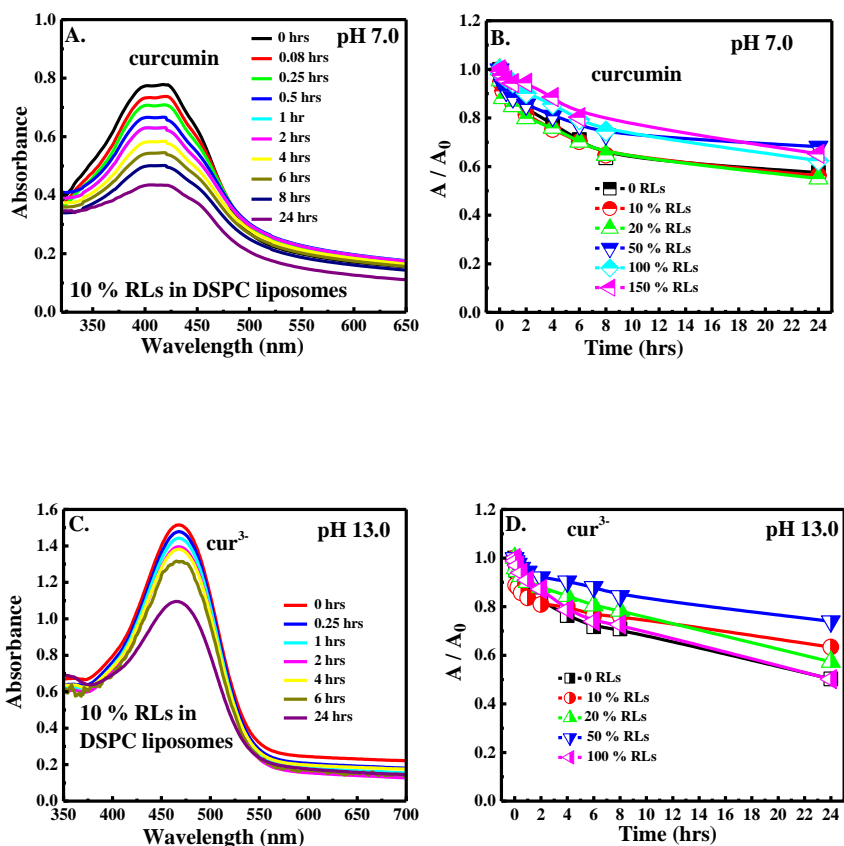


Figure 3.7: UV-visible absorption spectra of curcumin in 10 % of RLs in DSPC liposomes at pH 7.0 (A) and pH 13.0 (C) buffer solution during different time interval; Rate of degradation of curcumin at pH 7.0 (B) and pH 13.0 (D) buffer solution in the absence and presence of different % of RLs in DSPC liposomes.

permeability of curcumin is also in an agreement with the enhanced stability of curcumin in the presence of RLs as seen at two different pHs earlier. However in liquid crystalline phase, the increase was mild, the partition was enhanced only by a factor of  $\sim 1.9$ , compared to that at the solid gel phase where enhancement was  $\sim 22$  fold. This can be explained based on the fact that in the solid gel phase the liposomes are closely packed, thus the interaction between the liposome and the glycolipids molecules alters the permeability and fluidity of membranes thereby pushing the curcumin into the hydrophobic region. However in the liquid crystalline phase the interaction between rhamnolipids and the liposomes is weakened due to the change in the membrane state, thus not helping in the partitioning of curcumin, which maintains a close value to that in the absence of RLs.

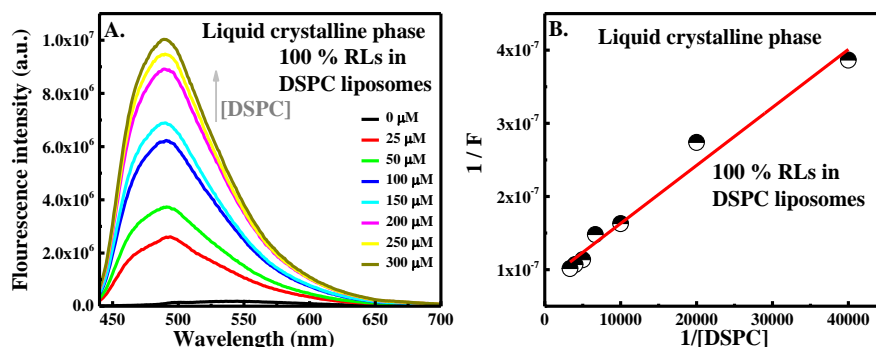


Figure 3.8: (A) Fluorescence emission spectra of curcumin in various concentrations of DSPC liposomes in the presence of 10 % RLs in liquid crystalline phase; (B) Plot of  $1/F$  vs.  $1/[DSPC]$  in the presence of 10 % RLs in liquid crystalline phase. Fluorescence intensity was measured at excitation wavelength 425 nm and emission wavelength 492 nm.

### 3.3.7 Effect of RLs on fluidity of DSPC liposomes

Fluidity of DSPC liposomes was measured by fluorescence quenching of pyrene by KI. Like observed earlier (for without RLs), the fluorescence of pyrene was quenched by KI in the presence of various concentrations of RLs in DSPC liposomes. The quenching rate was established using Stern-Volmer plot as shown in Figure 3.9A. Stern-Volmer constant ( $K_{SV}$ ) remarkably decreased in the presence of 10 % of RLs in DSPC liposomes, however, with further increase in % of RLs the reduction was reasonable as depicted in Figure 3.9B. To complement this result, instead of a hydrophilic quencher (KI), a hydrophobic quencher molecule Cetylpyridinium bromide (CPB) (see Scheme 3.1E) was applied. In aqueous environment, CPB quenches the fluorescence of pyrene by electron transfer process, where electron in the excited state is transferred from the aromatic ring of pyrene to electron deficient N-atom of CPB [124]. In the meantime in liposomes CPB intercalates within the hydrophobic part of the membrane with its charged moiety exposed at the surface, thus, liposome encourages contact between CPB and hydrophobic probe like pyrene. The fluorescence of pyrene was expectedly quenched by CPB in DSPC liposomes as shown in Figure 3.9C. The Stern-Volmer quenching constant was evaluated for pyrene in DSPC liposomes in the concentration range 0-100 μM of CPB. The Stern-Volmer constant for fluorescence quenching of pyrene by CPB increased linearly in the beginning with RLs concentration and at higher RLs concentration it saturated as depicted in Figure 3.9D. This is logical as increase in fluidity of liposomes in the presence of RLs facilitates more pyrene to enter the interface of liposomes and help in bringing N-atom of CPB and pyrene moiety come together. When pyrene was replaced with curcumin to investigate quenching rate by KI in the presence of various concentration of RLs in DSPC liposomes, the Stern-Volmer constant decreased with increase in percentage RLs in DSPC liposomes

as shown in Figure 3.10A, which is in the line of results obtained for pyrene as external probe molecule. Similarly, the fluorescence intensity of curcumin consistently was quenched by CPB in DSPC liposomes (see Figure 3.10B) without affecting the shape of the emission spectra. However, in the presence of RLs in DSPC liposomes, the fluorescence-quenching rate of curcumin by CPB decreased. The Stern-Volmer plots for fluorescence quenching of curcumin by CPB in the presence of different percentage of RLs in DSPC liposomes are demonstrated in Figure 3.10C. The Stern-Volmer constant for curcumin as external probe molecule decreased exponentially with increase in RLs percentage in DSPC liposomes (see Figure 3.10D). This trend is quite opposite to that observed for pyrene as external probe molecule. Nonetheless, this difference is due to the difference in the structure of pyrene and curcumin and their relative position with respect to the phospholipid membrane. Because increase in permeability of the DSPC liposomes in the presence of RLs allows curcumin to penetrate deeper within the membrane, as curcumin intercalates and exist parallel to lipid bilayer unlike bulky pyrene that stays at the interface. More curcumin penetrate deeply into the lipid bilayer greater becomes the distance between curcumin and N<sup>+</sup>-atom of CPB, and larger distance reduces the quenching rate (see Scheme 3.11). These results support the conclusion that rhamnolipids increase the permeability and fluidity of the liposomes.

### 3.3.8 Effect of RLs on the phase transition of DSPC liposomes

To further understand and study the effect of RLs on modulation of membrane properties, the phase transition of DSPC was monitored with increasing % of rhamnolipids using curcumin as external fluorescence probe. The fluorescence spectrum of curcumin in the presence of 10 % of RLs in DSPC liposomes was monitored in different temperature (see Figure 3.12A) similar to procedure mentioned earlier. From the fluorescence intensity of curcumin vs. temperature profile phase transition temperature was deduced. In the presence of 10 % RLs a remarkable broadening in the shape of fluorescence intensity of curcumin vs. temperature profile of DSPC liposomes was obtained. The shift in the phase transition temperature was also appreciable, which is similar to the results obtained for 100 % of curcumin in DSPC liposomes. Further increase in percentage of RLs in DSPC liposomes, enhanced the broadness in the shape of fluorescence intensity of curcumin vs. temperature profile of DSPC liposomes by shifting the phase transition temperature further to the lower end as shown in Figure 3.12B. Similar shift (to lower temperature) and broadening in phase transition temperature has been observed in DSC measurement [164]. The lowest phase transition temperature value was obtained at 150 % of RLs in DSPC liposomes. The correlation between phase transition temperatures and the % of RLs in DSPC liposomes is shown in Figure 3.12C. When associated with the membrane, the lipid moiety of the glycolipidic biosurfactants is most likely to disrupt the close packing of the phospholipid membrane thereby decreasing the temperature at which this solid packing changes to a liquid-crystalline nature. This change in the packing is accompanied with an increase in the permeability of the liposome, which is so far reflected in the gross enhancement of the partition co-

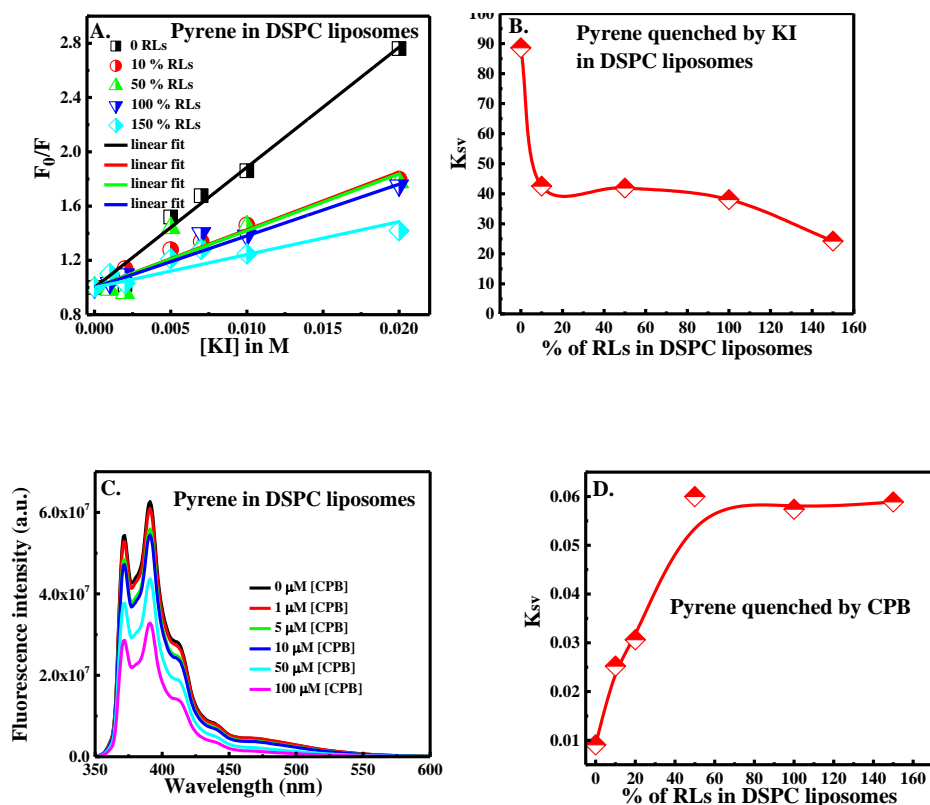


Figure 3.9: (A) Stern-Volmer plots for fluorescence quenching of pyrene by KI (0 to 20 mM) in DSPC liposomes in the presence of different amount of RLs; (B) Plot of  $K_{sv}$  vs. % of RLs in DSPC liposomes during fluorescence quenching of pyrene by KI; (C) Fluorescence spectra of pyrene in DSPC liposomes with different concentration of CPB; (D) Plot of  $K_{sv}$  vs. % of RLs in DSPC liposomes during fluorescence quenching of pyrene by CPB.

efficient at solid gel phase as well as the enhanced stabilization of curcumin at different pHs. Moreover, the sharpness in the phase transition was lost with the peak broadening with increasing rhamnolipids concentrations hence, the fusion between the solid gel phase and the liquid crystalline state is encouraged with increasing percentage of rhamnolipids to liposome concentration.

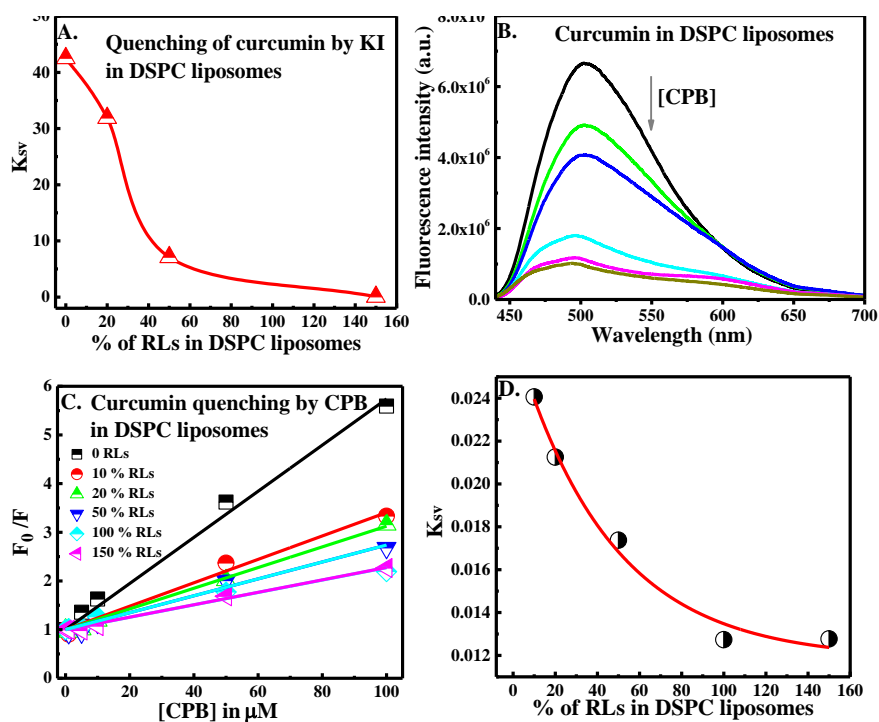
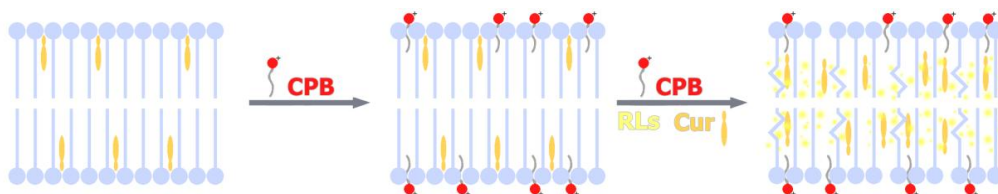


Figure 3.10: (A) Plot of  $K_{sv}$  vs. % of RLs in DSPC liposomes during fluorescence quenching of curcumin by KI; (B) Fluorescence spectra of curcumin in DSPC liposomes with different concentration of CPB; (C) Stern-Volmer plots for fluorescence quenching of pyrene by CPB (0 to 100  $\mu\text{M}$ ) in DSPC liposomes in the presence of different amount of RLs; (D) Plot of  $K_{sv}$  vs. % of RLs in DSPC liposomes during fluorescence quenching of curcumin by CPB.



Scheme 3.11: Illustration of contact between curcumin and CPB in DSPC liposomes in the absence and presence of rhamnolipids.

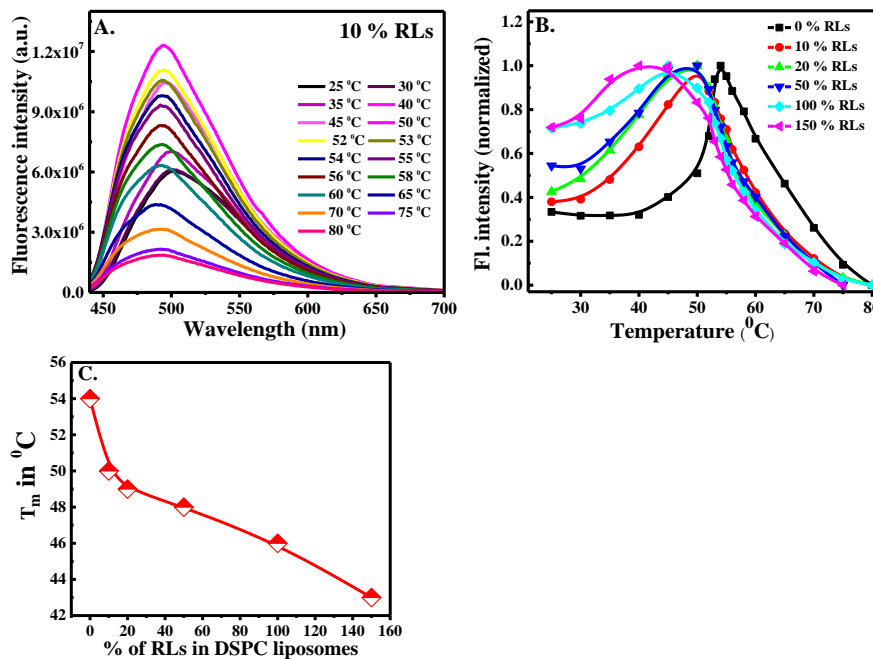


Figure 3.12: (A) Fluorescence emission spectra of 5 μM curcumin in 10 % of RLs in DSPC liposomes (100 μM); (B) Profile of fluorescence intensity of curcumin vs. temperature at various % of RLs in DSPC liposomes; (C) Variation in phase transition temperature of DSPC liposomes with % of RLs in DSPC liposomes.

Table 3.1: Partition Coefficients of Curcumin into DMPC Liposomes

Curcumin in DSPC	Partition coefficients	
	Solid gel phase	Liquid crystalline phase
Without Rhamnolipids	$8.38 \times 10^4$	$3.08 \times 10^5$
With Rhamnolipids (1:1)	$1.9 \times 10^6$	$5.9 \times 10^5$



## **Chapter 4**

# **Encapsulation of curcumin in cyclodextrin-metal organic frameworks: Dissociation of loaded CD-MOFs enhances stability of curcumin**

### **4.1 Introduction**

Phytochemicals derived from natural foods including spices, fruits and vegetables have recently drawn great interest because of their health promotion activities. Curcumin (see Figure 4.1), a major component of turmeric, is a yellow pigment extracted from the ground rhizome of curcuma [7] commonly used as a spice and food colorant. The last two decades have generated much of enthusiasm among researchers to explore the application of curcumin based on its beneficial biological and pharmacological activities. It has been reported for its various important biological applications as an anti-inflammatory molecule [165] along with an antioxidant activity and expressing an anticancer effect by inhibiting angiogenesis [166] and affecting major cell signaling pathways [167]. Curcumin is a fluorescent molecule; its photo physical properties are greatly reliant on the polarity of the environment and the pH of the medium [168]. Curcumin has been a good candidate for fluorescence probing [101, 153] and sensing [102, 169] applications. The absorption maximum of curcumin is at 420 nm in the largest part of the polar solvents, yet in hydrogen bond acceptor and donor solvents, it is shifted to 430-434 nm, excluding methanol where it is around 423-428 nm [151]. In acidic media, the absorption maximum of curcumin is at 422 nm, however, at pH greater than 7, the yellow color of curcumin turns bright red, with the absorption maximum shifting to 463 nm caused by the ionization of phenolic OH group [121]. Curcumin is well known for its instability in neutral and alkaline conditions, under-

going a hydrolytic degradation to feruloyl methane, ferulic acid and vanillin [105]. Still, the exposure of curcumin to alkaline foods or components may be hard to avoid, thus, it should be confined from physical and chemical damage before its industrial use. Several approaches have been tried to improve the delivery of curcumin in its intact hydrophobic form. These include several encapsulation-based systems as polymer nanoparticles [108], phospholipids [106], polyethylene glycol conjugates [136], and surfactants [135]. In addition curcumin can be stabilized by forming metallo-complexes with divalent cations prepared in water/glycerol system [170]. However, for food application the encapsulating agent should be non-toxic and edible. Among these possibilities to encapsulate curcumin for food applications, several cyclodextrin inclusion complexes have been tested [109].

A.

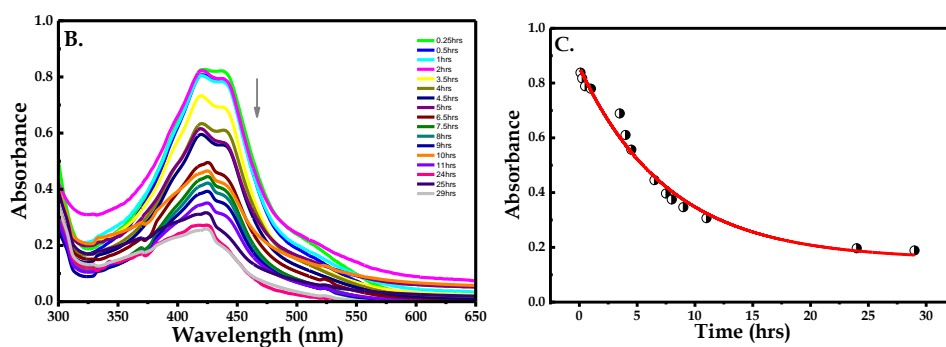
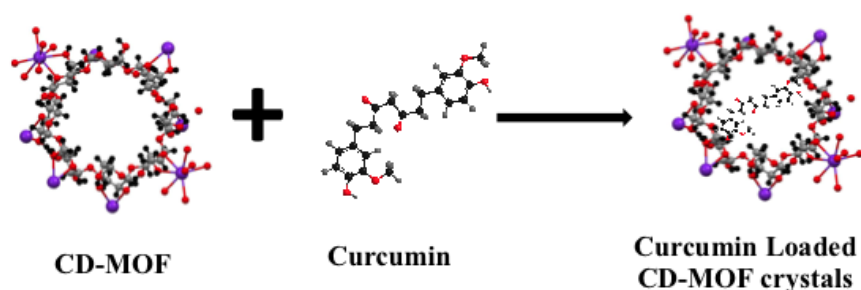


Figure 4.1: Interaction between CD-MOF and curcumin

In the past decade, Metal-Organic Frameworks (MOFs), a novel class of crystalline porous materials emerged to be one of the most investigated areas. Structurally, MOFs are composed of an organic linker and a metal cluster connected mainly through coordination bonds and arranged in an extended 3D network, spatially organized obtaining cavities of a regular size [171]. Due to their extremely high surface areas, ex-

tending beyond  $6000 \text{ m}^2 / \text{g}$  [172, 173, 174] along with a relatively thermal and mechanical stability, MOFs have demonstrated a great prospective for a varied array of applications [175, 176, 177, 176]. There are various kinds of MOFs reported, one of the important class is edible MOFs prepared from natural products. Among these edible MOFs, Cyclodextrin-MOFs (CD-MOFs), as shown Figure 4.1A, is produced by using  $\gamma$ -cyclodextrin ( $\gamma$ -CD) [178], a symmetrical cyclic oligosaccharide obtained from starch and composed of eight asymmetric  $\alpha$ -1, 4-linked dglucopyranosyl moieties [179]. The building units in CD-MOFs are connected by potassium ions, in aqueous media at suitable temperature and pressure, producing a body-centered cubic structure [179]. The storage ability of CD-MOFs has been already established using two different experimental approaches with rhodamine in an aqueous methanolic solution and 4-phenylazophenol in  $\text{CH}_2\text{Cl}_2$  [179]. In addition to its selective  $\text{CO}_2$  adsorption under low pressure [180], CD-MOFs -that are synthesized from natural components under benign conditions- hold promises for therapeutic and biological applications. In this manuscript we have investigated encapsulation of curcumin in CD-MOFs. To our knowledge this is the first report where encapsulation of curcumin in CD-MOFs has been carried out and stability of curcumin in such system is reported. Encapsulation of curcumin in CD-MOFs is characterized by various methods and found that curcumin inhabits in the pores of CD-MOFs without affecting the crystallinity of CD-MOFs. The interaction between curcumin and CD-MOFs are found to be strong through a hydrogen bond type interaction between OH group of cyclodextrin moiety of CD-MOF and phenolic hydroxyl group of curcumin. The absorption and fluorescence spectral study indicates the pores encapsulating curcumin in CD-MOFs have similar solvent environment like methanol. Furthermore, the dissociation of loaded curcumin-CD-MOF crystals in water leads to the formation of a unique water soluble complex in which curcumin appears to be chemically stable in alkaline media (pH=11.5). These interesting findings pave the way to explore CD-MOFs as promising benign system to store and stabilize curcumin for food applications.

## 4.2 Materials And Methods

### 4.2.1 Material

$\gamma$ -cyclodextrin (purity > 99%, food grade) was donated by Wacker Chemical Corporation (Adrian, MI, US). Potassium hydroxide, pellets (ACS reagent, purity  $\geq 85\%$ ) was purchased from Columbus Chemical Industries, Inc. (Phoenix, AZ, US). Methanol (purity > 99.8%) was purchased from Sigma-Aldrich Corp. (Saint Louis, MO, US). Dichloromethane (purity > 99%) contains 50-150 ppm amylene as stabilizer; chloroform contains 100-200 ppm amylenes as stabilizer (purity  $\geq 99.5\%$ ), and hexane (purity  $\geq 98\%$ ) were also purchased from Sigma-Aldrich Corp. (Saint Louis, MO, US). Diethyl ether (purity > 99.8%) and water were purchased from Avantor Performance Materials (Center Valley, PA, US). Curcumin was obtained from Sigma-Aldrich and used as

received.

### 4.2.2 Sample Preparation

CD-MOFs were synthesized from food grade components as described by Smaldone et al. [179] whereby 1.0 mole-equivalent of the cyclodextrin (1.30 g) was dissolved in 20 mL deionized distilled water with 8.0 mole-equivalent of potassium hydroxide (0.45 g) under magnetic stirring for 6 to 12 h at 500 rpm. The ratio of metal salt (KOH) to  $\gamma$ -CD was 1:8. The solution was filtered and sealed in a beaker containing 50 mL methanol to allow for vapor diffusion over a period of 7 days at  $23 \pm 0.1^\circ\text{C}$  and  $50 \pm 2\%$  RH after which approximately 85% yield of CD-MOF crystals were obtained (1.5 to 1.6 g).

The activation process frees the pores from any residual moisture entrapped during synthesis. The crystals were filtered, washed two or three times with 20 to 30 mL of methanol to remove all extra unlinked potassium ions, and allowed to dry in air for 30 min. The collected crystals were soaked in methanol for 3 days before being filtered and dried under vacuum ( $P = 1$  Torr) for 10 h at  $25^\circ\text{C}$  followed by 12 h at  $45^\circ\text{C}$ . This process ensures complete evacuation of the solvents from the pores. Consequently, the crystals were either used immediately or stored over Drierite<sup>®</sup> desiccant.

To study the inclusion of curcumin, 10 mg of CD MOF crystals were dispersed in 3ml of methanol. Curcumin dissolved in methanol was added to get a final concentration  $25\mu\text{M}$ . For the spectroscopic measurements the crystal were sonicated to get a good dispersion in methanol. However for the dissolved part the crystals were washed thoroughly with methanol until the supernatant was clear and 3 ml of water were added to dissolve the loaded CD MOF crystals.

### 4.2.3 Spectroscopic measurement

UV-visible absorption spectra were recorded using a SCOV-570 UV-VIS-NIR Spectrophotometer. Steady state fluorescence measurements were performed by a Jobin-Yvon-Horiba fluorimeter, emission and excitation slits were both set at 5 nm, equipped with a 100 W Xenon lamp and an R-928 detector operating at 950 V. FTIR spectra were recorded on FT-IR-Raman spectrometer Thermo-Nicolet. The spectra were collected in the  $4,000 - 650\text{ cm}^{-1}$  range.

### 4.2.4 Surface area and pore volume measurements

The surface area of the activated CD-MOF crystals was determined using an autosorb iQ-Micropore-XR (Quantachrome Instruments, Boynton Beach, FL, USA) gas analyzer using nitrogen gas. The Brunauer-Emmett-Teller (BET) and Langmuir methods were used to determine the surface area with  $P/P_0$  varying from 10<sup>-5</sup> to 0.99  $P/P_0$ . Micropore volumes were calculated at radius of 2 nm and relative pressure 0.5  $P/P_0$ , whereas total pore volumes were obtained at the relative pressure  $P/P_0 = 0.99$ . Samples were run in triplicates.

## 4.2.5 X-ray diffraction (XRD)

XRD data was collected for the CD-MOF crystals using a Bruker D8 advance X-ray diffractometer (Bruker AXS GmbH, Karlsruhe, Germany) at 40 kV, 40 mA (1,600 W) using Cu K $\alpha$  radiation ( $\lambda = 1.5418 \text{ \AA}$ ), with a 1.2 mm primary beam slit and 2.0 mm detector slit. The X-ray scans were carried out for  $2\theta$  between 4 and 40 degrees at  $0.02^\circ$  increments. Data was collected in triplicates.

## 4.3 Results And Discussion

### 4.3.1 Inclusion of curcumin into CD-MOF pores

Given the stability, high surface area, large-pore-aperture characteristic of CD-MOF, in addition to its biocompatibility we decided to study the inclusion of the potent anti-inflammatory molecule curcumin into CD-MOF. Activated crystals of CD-MOF were immersed in methanol, curcumin prepared in methanol was added to the soaked CD-MOF crystals. The amount of curcumin in the supernatant was measured through ultraviolet-visible (UV-Vis) spectrophotometry. The obtained spectra over a period of 30 hours are depicted in Figure 4.1a and the characteristic absorbance at 440 nm was examined as plotted in Figure 4.1B and the characteristic absorbance at 440 nm was examined as plotted in Figure 14.1C. The same experiment was carried out for curcumin prepared in methanol in the absence of CD-MOF as a control. In the presence of CD-MOF a continuous decrease in absorbance at 440 nm of curcumin in the supernatant was observed while that of the control (in the absence of CD-MOF) the absorbance remained almost unchanged except after 7 hours a minor decrease was observed. Since reduction in absorbance at the absorption maximum is often related to degradation of curcumin in solution [5], the control experiment reconfirms that there is no degradation of curcumin in methanol during our experimental condition, which is consistent with other report [11]. Thus, decrease in absorbance of the supernatant solution in the presence of CD-MOF clearly confirms a reduction in the amount of curcumin in the supernatant due to encapsulation into the CD-MOFs (see Figure 4.1C. The encapsulation rate of curcumin into CD-MOFs was estimated by applying a first order kinetics. The half-life of encapsulation was determined as 5.41 hours indicating encapsulation into the pores is a relatively slow process under our experimental conditions. After encapsulation procedure was completed, CD-MOF (loaded with curcumin) crystal was washed several time in methanol to remove free and weakly adsorbed curcumin on the surface of the CD-MOF. The final curcumin loaded CD-MOFs crystals were dark pink. These crystals were used for further characterization to understand the interaction between curcumin and CD-MOF.

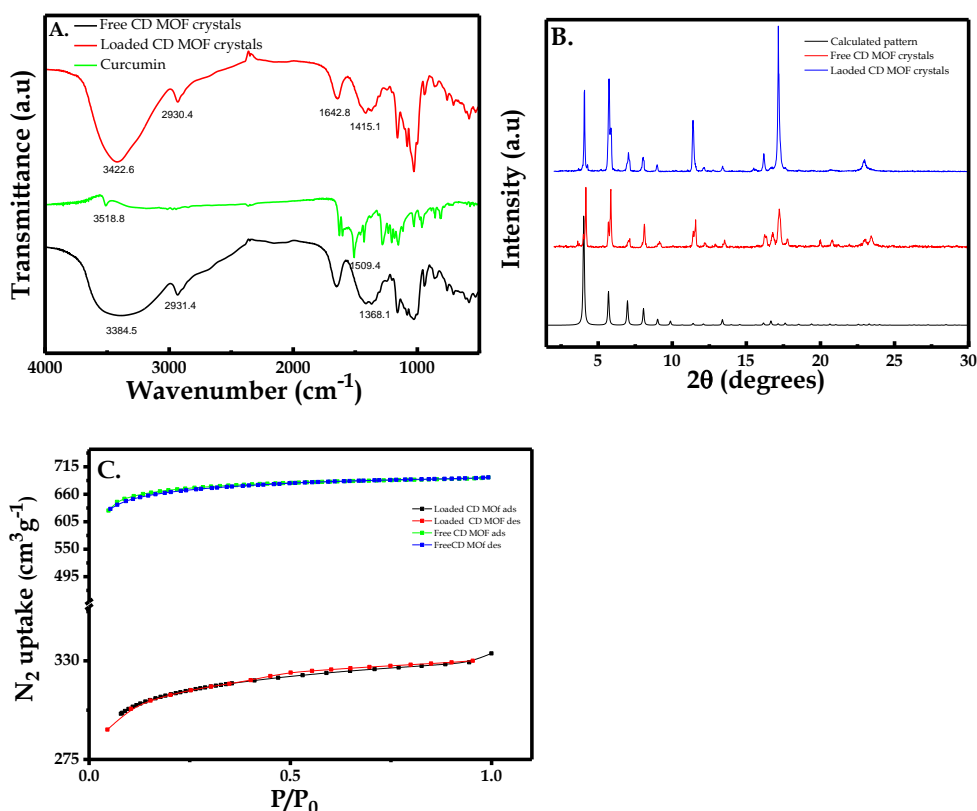


Figure 4.2: FT-IR spectra of curcumin, free CD MOF and the curcumin loaded CD-MOFs.

### 4.3.2 Characterization of the loaded CD MOF crystals

The dark pink colored crystals were characterized by their IR, Powder X-ray diffraction (PXRD) and BET analysis. For characterization, the amount of CD-MOFs used was 30 mg where the concentration of curcumin used for encapsulation was  $100 \mu\text{M}$ . The FT-IR spectrum (Figure 4.2) showed a great shift in the transmittance of the loaded CD-MOFs compared to that of the free one with the latter transmitting at  $3884 \text{ cm}^{-1}$  corresponding to the OH stretching of the cyclodextran moiety. In contrast the curcumin loaded one transmitted, at  $3422 \text{ cm}^{-1}$  indicating a possible interaction between the OH group of CD-MOFs and curcumin. Prominent peaks at  $3518 \text{ cm}^{-1}$  for the hydroxyl (phenolic) vibration of curcumin was not detected in the FT-IR spectra of curcumin loaded CD-MOFs suggesting a hydrogen type of bonding between OH group of cyclodextrin moiety of CD-MOFs and phenolic hydroxyl group of curcumin. Another major shift was observed where free CD-MOFs transmit at  $1368 \text{ cm}^{-1}$  and the loaded one at  $1415 \text{ cm}^{-1}$ . Incidentally, these peak positions are in the same region where curcumin prominently absorbs for its functional groups.  $1600 \text{ cm}^{-1}$  for benzene ring skeleton stretching of curcumin is in the same region of free CD-MOFs. Similarly,  $1280 \text{ cm}^{-1}$  for Ar-O stretching and  $1500 \text{ cm}^{-1}$  for C=O and C=C vibrations of

curcumin overlaps with free CD-MOFs. Therefore, not much can be concluded about the interaction in this region except involvement of -OH and phenolic group, which could be attributed to H-bonding type of interaction. Interestingly, the broadness in the peak of the free CD-MOFs due to the intra-molecular hydrogen bonding is persistence in the loaded CD-MOF indicating curcumin doesn't disturb the structure of CD-MOFs. The PXRD patterns as depicted in Figure 4.2B further clearly showed that curcumin doesn't disrupt the crystallinity of the CD-MOFs with a slight shift in the positions of the peaks. The porosity of the activated CD-MOF was verified by measuring the  $N_2$  gas adsorption of the sample as shown in Figure 4.2C. The typical isotherm exhibits steep  $N_2$  uptake in the low-pressure areas for ( $P/P_0 < 0.05$ ), hence validating the micro porosities of these materials, and the BET surface area for CD-MOF was estimated to be  $1030 \text{ m}^2 \text{ g}^{-1}$ . Similarly, the BET surface area of the loaded CD-MOF crystals was measured and found to be  $800 \text{ m}^2 \text{ g}^{-1}$ . This decrease in the surface area is a further proof of the interaction taking place between curcumin and the CD-MOFs crystals as curcumin is occupying some of the empty pores of the CD-MOFs.

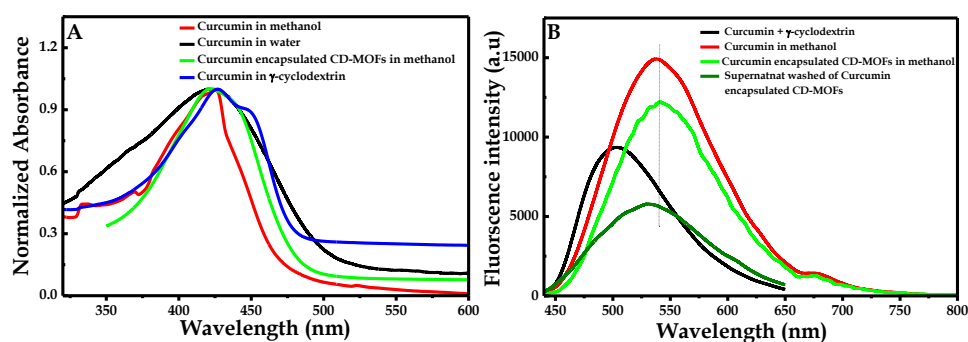


Figure 4.3: Powder X-ray diffraction patterns for free CD-MOFs crystals washed by methanol (in black) and loaded CD-MOFs crystals with curcumin (in red) compared to the calculated pattern of CD-MOFs (blue).

### 4.3.3 Spectroscopic study

After several washings by methanol to remove free and weakly adsorbed curcumin on the surface of the CD-MOFs, the absorption spectrum of the curcumin loaded CD-MOFs crystals dispersed in methanol was measured. As shown in Figure 4.3A, the crystals absorbed at 425 which is the characteristic curcumin peak in methanol, whereas free CD-MOFs crystals dispersed in methanol showed no absorption around 425 nm. The absorption of CD-MOFs in the visible region is a strong indication for the presence of curcumin within the CD-MOFs crystals, which is directly reconfirmed from the color change of CD-MOFs after encapsulation of curcumin. The fluorescence spectrum of these dispersed crystals was investigated. The fluorescence emission spectrum, at 425 nm excitation wavelength, (Figure 4.3B) obtained for the curcumin loaded CD-MOFs

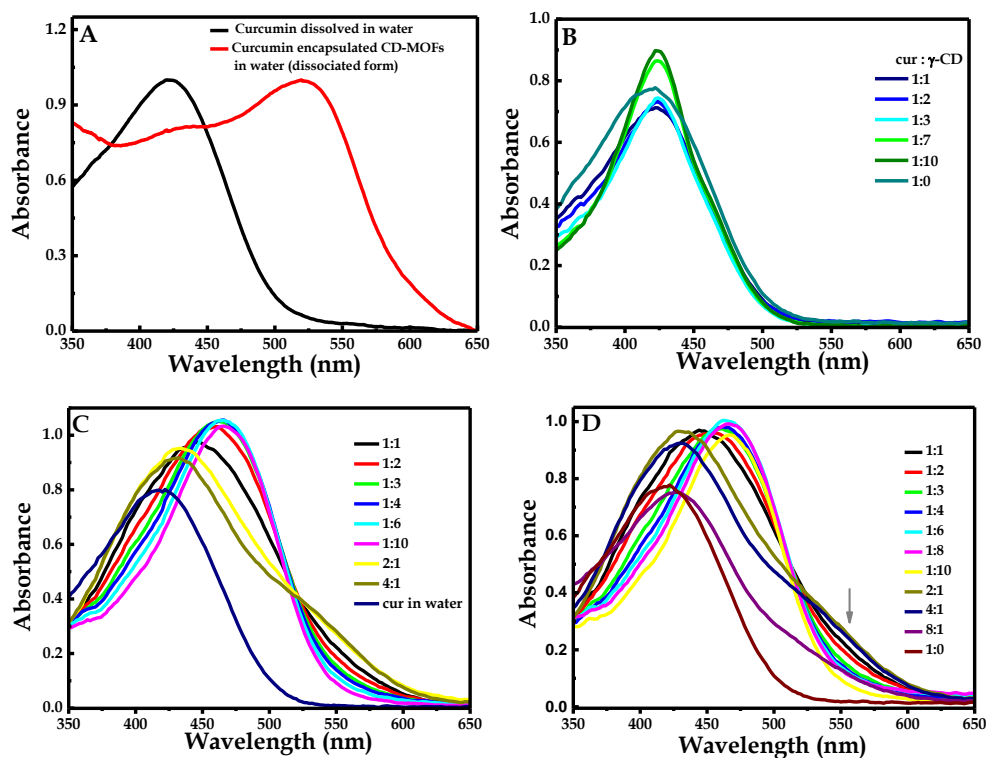


Figure 4.4:  $N_2$  adsorption isotherms, for activated samples of free CD-MOFs and curcumin loaded CD-MOFs. Filled and open symbols represent adsorption and desorption branches, respectively. Connecting traces are for guidance only.

crystals dispersed in methanol is identical to that of curcumin in methanol, thus, the interaction between curcumin and the CD-MOFs crystals preserves the photo-physical properties of curcumin. Curcumin has been shown to be a good probe molecule to sense local environment of the heterogeneous systems [181, 182]. The fluorescence spectra for curcumin encapsulated CD-MOFs and the supernatant washed of curcumin loaded CD-MOFs were found to be similar and showed a negligible blue shift compared to curcumin in methanol. In contrast, the fluorescence spectrum of curcumin in  $\gamma$ -cyclodextrin is remarkably blue shifted  $\sim 40$  nm, indicating the local microenvironment of curcumin inside the  $\gamma$ -cyclodextrin is more hydrophobic and less polar compared to that inside CD-MOFs. This confirms that the interaction between curcumin and  $\gamma$ -cyclodextrin is different from that between curcumin and CD-MOFs. This could be rational due to presence of potassium ion in CD-MOFs, which could facilitate the interaction and/or coordination of curcumin with CD-MOFs. It also establishes the local microenvironment inside the pores of CD-MOFs is similar to that of methanol.



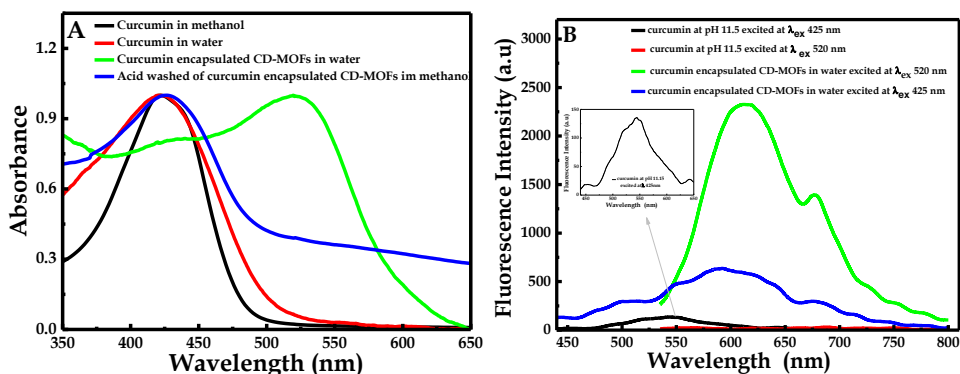


Figure 4.5: (A) UV-visible absorption spectra of the free curcumin in water (in black), methanol (in red), in  $\gamma$ -cyclodextrin (in blue) and curcumin encapsulated CD-MOFs crystals in methanol (in green); (B) Fluorescence emission spectra of free curcumin in methanol (red), in curcumin encapsulated CD-MOFs crystals (in green) and that of curcumin in methanol (in black), both excited at 425 nm. Curcumin:  $\gamma$ -CD = 1:10.

#### 4.3.4 Dissociation of curcumin loaded CD-MOF crystals

Two approaches for the destruction of the CD-MOF structure were followed. The first was dissolving the loaded CD-MOF crystals in water and the second one was treating them by an acidic solution in methanol. It is known that dissolving CD-MOF crystals in water results in dissociation of the framework, hence releasing  $\gamma$ -cyclodextrin and KOH into the solution thereby creating a basic medium. Interestingly, destroying the curcumin loaded CD-MOFs in water changed the color of the solution. A pink color was observed upon dissolving the loaded MOF crystals in water instead of a dark pink color in methanol, and the absorption spectrum showed a maximum at 520 nm (Figure 4.4A). In most of the polar solvents, the absorption maximum of curcumin is at  $\sim 420$  nm, and it is shifted in hydrogen bond acceptor and donor solvents to  $\sim 430$ , except in methanol where it is around 425 nm [11]. A shift in the absorption maximum of curcumin is reported in basic medium where curcumin absorbs at 463 nm [11] with bright red color, this shift is caused by the ionization of phenolic OH group. Shen and Ji [123] theoretically predicted an absorption maximum at 531 for curcumin caused by the de-protonation of the phenolic OH group. Moreover, a study performed by Zsila et al [113] for curcumin in KOH-ethanolic solution reported an absorption maximum at 535 nm, however, free curcumin molecules are quite unstable at above pH 7 in pure aqueous solution, thereby limiting further investigations of curcumin properties in basic medium. In our case when the absorption spectrum of the dissociated curcumin loaded CD-MOF in water showed a broad peak at  $\sim 520$  nm, the pH of the solution was measured and found to be 11.5.

In order to identify the absorption peak and predict the nature of the complex existing at pH 11.5 between curcumin and  $\gamma$ -cyclodextrin in the presence of  $K^+$  ions in water, different controls experiments were carried out. In the first case (Figure 4.4B),

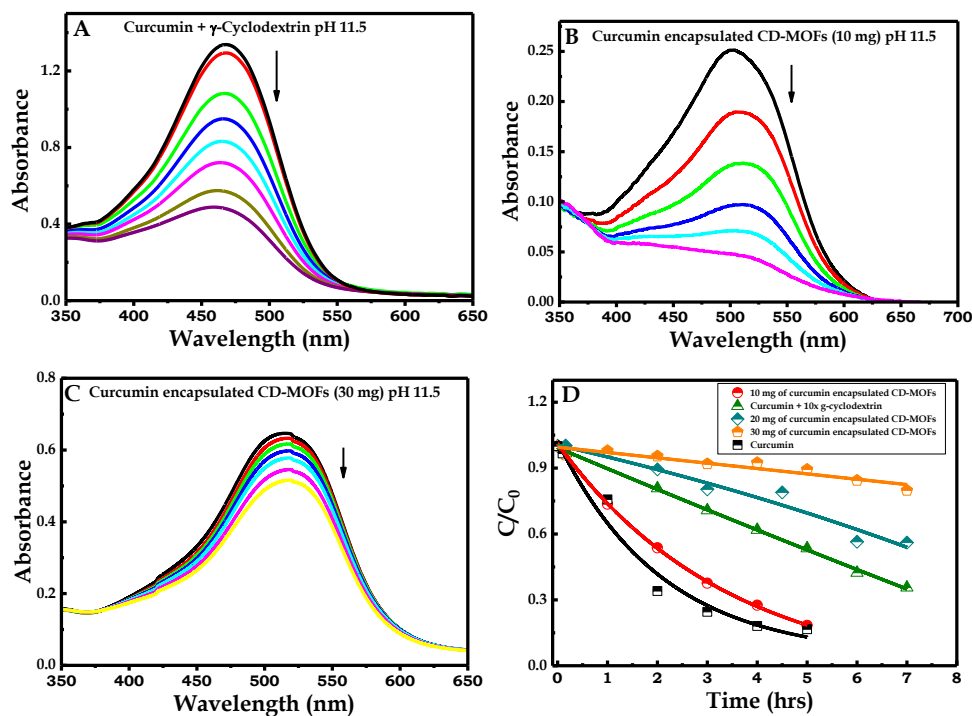


Figure 4.6: (A) UV-vis absorption spectrum of the dissolved loaded CD-MOF crystals (red) with curcumin in water and that of curcumin alone in water (black); (B) UV-vis absorption spectrum of curcumin (25  $\mu$ M) in the presence of different concentrations of  $\gamma$ -cyclodextrin in water; (C) UV-vis absorption spectrum of curcumin (25  $\mu$ M) in different concentrations of KOH in water; (D). UV-vis absorption spectrum of curcumin (25  $\mu$ M) in different concentration of ( $\gamma$ -CD: KOH) complex in water.

the influence of different molar ratio of curcumin to  $\gamma$ -cyclodextrin on absorption spectrum of curcumin was examined. A solution of curcumin with concentration 25  $\mu$ M in water was prepared and to this solution  $\gamma$ -cyclodextrin solution was added in portions to have various curcumin to  $\gamma$ -cyclodextrin molar ratio. The absorption maximum of curcumin was not affected by in different molar ratio of  $\gamma$ -cyclodextrin, but as the molar ratio of  $\gamma$ -cyclodextrin (curcumin: $\gamma$ -cyclodextrin = 1:0 to 1:10) increased the absorption spectrum became narrower. Narrowing of absorption spectrum of curcumin in micellar medium has also been observed [183] and can be an indication that at higher molar ratio most of the curcumin are completely buried inside the hydrophobic pocket of  $\gamma$ -cyclodextran. There are also report that one curcumin can bound to two cyclodextrin units [184], thus need of higher molar ratio with  $\gamma$ -cyclodextran for complete encapsulation is rational though spectra for 1:7 and 1:10 were found to be identical due to saturation. This excludes the possibility that band at  $\sim$ 520 nm observed for curcumin with the dissociated CD-MOFs framework is due to curcumin- $\gamma$ -cyclodextran complex formation. The second possibility could be due to complexation between curcumin and

$K^+$  ion. Absorption spectra of curcumin and KOH in various molar ratios are shown in Figure 4.4C. As illustrated in the spectra, 1:1 molar ratio of curcumin:KOH red shifted the absorption spectra to  $\sim 450$  nm with a new minor peak (band) at  $\sim 550$  nm. With further increase the molar ratio of curcumin:KOH from 1:1 to 1:10 shifted the spectra more toward red wavelength region, however, decreasing the band at  $\sim 550$  nm and completely abolishing for 1:10 of curcumin:KOH. The red shift is expected as in completely deprotonated form curcumin has absorption maximum at  $\sim 463$  nm [11]. Interestingly, when the molar ratio of curcumin:KOH was increased to 2:1 and 4:1 the main peak at  $\sim 450$  nm (for 1:1 molar ratio) showed a blue shift with an enhancement of the band at  $\sim 550$  nm suggesting this band could be due to one potassium ion bound to multiple numbers of curcumin. To test, whether  $\gamma$ -cyclodextrin has any role in this complex, solution of  $\gamma$ -cyclodextrin to KOH (1:1) was prepared and added in portions to a curcumin solution  $25 \mu\text{M}$ . Interestingly, the absorption spectra (Figure 4.4D) showed a shoulder at  $\sim 530$  nm instead of  $\sim 550$  nm (Figure 4.4C) for the solutions of 2:1 and 4:1 curcumin to  $\gamma$ -CD-KOH solution (Figure 4.4D). At a higher concentration of curcumin in the 8:1 solution, no shoulder appears. As well as going from 1:1 to 1:10, no shoulder was found expect a shift in the main absorption peak to  $\sim 465$  nm due to deprotonated form of curcumin. This spectral study proposes that the band observed at  $\sim 520$  nm in the dissociated loaded CD-MOF is because of the formation of an adduct between curcumin, potassium ion and  $\gamma$ -cyclodextrin.

To study the importance of encapsulation of curcumin in the extended porous structure of CD-MOFs in the formation of the adduct, we investigated the association of curcumin with dissociated CD-MOF and compared with that of dissociated curcumin loaded CD-MOFs. As depicted in Figure S1A (see Supporting Information), when curcumin was added to dissolved CD-MOFs in water, a (color) solution was obtained, the absorption spectrum gave a maximum at  $\sim 450$  nm and a weak intensity shoulder at 520 nm. Due to the weak intensity of the 520 nm shoulder which is characteristic of the adduct formation (Figure 4.4A), we can conclude that the formation of this complex via addition of curcumin to the dissolved CD-MOF is not favorable. This result clearly demonstrates the importance of the encapsulation of curcumin within the pores of the CD-MOF crystals prior the formation of the water soluble adduct. To appreciate the role of water molecules during the complex formation, the curcumin loaded CD-MOF crystals were dissolved in methanol solution by adding hydrochloric acid to the MOF crystals dispersed in methanol. It is well established that treating MOFs structures with acid results in the dissociation and destruction of the framework [172]. As shown in Figure 4.5A, after treating the loaded CD-MOFs crystals with acid the absorption spectrum is identical to that of curcumin observed in methanol, although it is slightly broadened like that of curcumin in water. Thus, water plays a significant role during the complex formation via dissociation of curcumin-loaded CD-MOF in water.

In order to study the emission properties of the adduct formed via dissociation of curcumin loaded CD-MOFs, fluorescence spectra of the complex were recorded at  $\lambda_{ex} = 425$  nm and 520 nm and compared with the emission spectra of free curcumin. As shown in Figure 4.5B, curcumin at pH 11.5 excited at 425 nm gave an emission spec-

trum with a maximum at ~540 nm whereas when excited at 520 nm, as expected no emission was found as curcumin does not absorb at this wavelength. Similarly, the dissolved curcumin loaded CD-MOF crystals were excited at 425 nm and 520 nm. When at excited at 425 nm, the dissolved curcumin loaded CD-MOF crystals (the obtained adduct) gave a moderate intense fluorescence emission spectra with an emission maximum at 600 nm. This emission is a remarkably ~50 nm red shift from curcumin alone, which could be because of two reasons, either due to change in local environment of curcumin or due to a new emissive species. Interestingly, when excited at 520 nm the adduct showed an emission spectrum with a remarkable enhancement in fluorescence intensity and emission maximum at ~600 nm. This result confirms that at both excitation 425 nm and 520 nm the same species is emitting; this species is different from the curcumin alone, thus demonstrating a cooperative complex formation between curcumin, potassium ion and  $\gamma$ -cyclodextrin.

To understand the pH dependent stability of the dissociated curcumin loaded CD-MOFs crystals, the absorption and fluorescence spectra were recorded at different pH using buffer solutions. Figure S1B (see Supporting Information) shows absorption spectra of dissolved curcumin loaded CD-MOFs at different pH. Interestingly, the absorption at 520 nm exists only at pH 11.5 and at lower or higher pH the absorption spectra were similar to that of curcumin. For instance, absorption of curcumin loaded CD-MOF crystals gave a blue shift at pH 13 to 470 nm, and was further shifted at pH 4, 5, 7 and 10 to 430 nm. In Figure 4.5C, the effect of pH on the fluorescence spectrum was presented. When excited at 425 nm (see Figure S1C, Supporting Information), the curcumin loaded CD-MOF crystals at pH 4, 5, 7 and 8 gave emit from 450 to 600 nm region with a maximum at ~540 nm indicating the emission is due to solely curcumin, where as at pH 11.5 emission was in the 500 to 700 nm region with maximum at ~600 nm. At pH 13 a similar spectrum with lower intensity was obtained suggesting at this pH a small amount of the potassium-curcumin is still present. As expected when excited at 520 nm (Figure 4.5C), there was no fluorescence observed at pH 4, 5, 7 and 8, whereas a low fluorescence was obtained at pH 13 and a remarkably high fluorescence intensity with an emission maximum at ~600 nm was found for pH 11.5, which further demonstrate that the adduct has a strong absorption and emission properties that are different from that of curcumin. Curcumin has 3 pKa values ranging from 7.75 to 10 [121]. Therefore, the complexation occurs in completely deprotonated form of curcumin and as soon as the pH of the medium was lowered, the fluorescent complex collapses. Nevertheless, increasing the pH further to more alkaline medium, ~pH 13, the complex is not stable. This finding indicates potassium ion of CD-MOFs is associated with at least on phenolate ion and other enolic ion of curcumin.

## **Stabilization of curcumin in dissociated CD-MOF**

In the first part, we studied the physical interaction between curcumin and the CD crystals demonstrated by the IR spectrum, UV-visible and fluorescence spectra, we also demonstrated that the incorporation of curcumin in the cavities of CD-MOF is cru-

cial for the formation of the adduct upon dissolving the loaded CD-MOF. The second part of this study was built on stability of curcumin in the CD-MOF structure. Several studies have reported the interaction of curcumin with the family of cyclodextran, such as  $\alpha$ ,  $\beta$ , and  $\gamma$ -CD [184, 185, 186]. Curcumin is relatively stable in organic solvent like methanol but it is quite unstable in aqueous alkaline medium. Similarly, stabilization of curcumin with cyclodextrin was reported in alkaline medium at pH 8 [105]. There are limited studies that ever managed to stabilize curcumin at high pH conditions. The effect of interaction of curcumin with CD-MOFs crystals on the degradation of curcumin was investigated in water since curcumin is relatively stable in organic solvents. It is noteworthy that dissociation of the loaded crystals in water leads to the formation of a water soluble complex that involves the association between curcumin, potassium cations and CD. In the current study, the UV-Vis absorption spectra of the dissolved curcumin loaded MOF crystals were recorded for 8 hrs in water at alkaline condition as shown in Figure 4.6. The degradation rate was fitted to first order kinetics as shown in Figure 4.6D. Free curcumin showed a high level of degradation in 2 hrs and continued for 8 hrs period (See Figure 4.6D). The results illustrated that curcumin undergoes rapid degradation at pH 11.5 with a half-life of 1.45 hr. Recent work has established that curcumin exists in solution in the keto-enol tautomeric form [11]. Under alkaline conditions, the enol group of curcumin becomes de-protonated and it is likely to undergo degradation by a retro-aldol condensation reaction catalyzed by the hydroxide anion. In the past curcumin has been encapsulated in p-sulfonatocalix[4]arene, but in alkaline condition (pH 9.2) degradation of curcumin has been not affected in p-sulfonatocalix[4]arene [187]. On the other hand, stability of curcumin in  $\gamma$ -cyclodextrin has been reported [105, 188]. For comparison we checked stability of curcumin in 10 times of  $\gamma$ -cyclodextrin concentration (so that all the curcumin molecules present in solution are bound to  $\gamma$ -cyclodextrin) as shown in Figure 4.6A. Degradation of curcumin in the presence of  $\gamma$ -cyclodextrin continued with a half-life of 56 hr, which is  $\sim 39$  times more stable than curcumin alone. Harada et al. have reported half-life of  $\sim 0.09$  hr for free curcumin and 4.46 hr for  $\gamma$ -cyclodextrin in PBS buffer at pH 7.4 [188], thus, our results are better than reported in literature. Since pH of the buffer solution and molar ratio of cyclodextrin:curcumin could influence stability of curcumin, the higher stability of curcumin in  $\gamma$ -cyclodextrin must be due to higher molar ratio of cyclodextrin:curcumin (10:1) in our case compared to 1:1 molar ratio by Harada et al. [188]. When 10 mg of the curcumin encapsulated CD-MOFs crystals was studied, it can be seen from Figure 4.6B, the measurement showed no appreciable difference from that of free curcumin at pH 11.5 in water with a half-life of 2.36 hr (a marginal increase). However, as the amount of CD-MOFs increased to 20 mg, the stability of curcumin increased with a half-life of 10.22 hr, which is still lower than that of curcumin in 10-times  $\gamma$ -cyclodextrin. Further increase of CD-MOFs to 30 mg increased to stability of curcumin (Figure 4.6C) with a half-life of above one million hours at pH 11.5. Thus, in the presence of sufficient amount of CD-MOFs, stability of curcumin enhanced substantially due to incorporation within the pores of the crystals.

## Chapter 5

### Conclusion

The studies revealed that interaction of curcumin with rhamnolipids is pH dependent. It was shown that in acidic, neutral and slightly alkaline medium (pH 8),  $\beta$ -diketone form of curcumin undergoes excited state hydrogen transfer and emits solely from enol form, which is not affected by the presence of rhamnolipids. The study also explored fluorescence spectral behavior of curcumin in extremely alkaline condition, pH 13, which was not reported earlier. In this condition curcumin emits from both  $\beta$ -diketone as well as enolic ESHT forms, however, increase in rhamnolipids preferentially increases formation of  $\beta$ -diketone tautomer by completely revoking ESHT process of curcumin. Similarly, fluorescence of curcumin could detect cmc of rhamnolipids. It was established that increase in pH increases cmc of rhamnolipids suggesting structural change of rhamnolipids micelle. Fluorescence quenching by CPB proved that curcumin stays deep inside the hydrophobic pocket of rhamnolipid aggregates/micelle that decreased the distance between  $N^+$ -atom of pyridinium ion and curcumin, thus, marginally affecting its quenching behavior. At the same time fluorescence quenching of pyrene by CPB suggested a strong electron transfer from pyrene to  $N^+$ -atom of pyridinium ion, which is possible only when pyrene stays near to the Stern layer of rhamnolipids micelle. Enol to  $\beta$ -diketone tautomer was found to be sensitive to temperature. Increase in temperature encouraged emission from  $\beta$ -diketone tautomer over enolic ESHT.

Hydrolysis of curcumin was significantly reduced with DSPC. Curcumin was remarkably associated with DSPC liposomes and the partitioning of curcumin into the hydrophobic core of DSPC was enhanced by a factor of 3.6 in the liquid crystalline phase compared to that in the solid gel phase mainly due to the increase in membrane fluidity. The spectroscopic characteristics of curcumin were successfully shown in the pre-transition as well as phase transition temperature of DSPC liposome. The influence of RLs on DSPC liposome properties was remarkable. Quenching of fluorescence probes pyrene and curcumin in bio-membrane systems are of an important interest. In these investigations, the use of appropriate quenchers could provide valuable information regarding the permeability and fluidity of membrane systems. Changes in the membrane permeability are reflected in changes in the rate constant of the quenching

reaction or ease of entry of the quencher to the probe, which is usually incorporated within the membrane hydrophobic core. Permeability and fluidity of DSPC liposomes were affected by RLs. The permeability of the membrane increased with increasing concentrations of RLs as revealed by the enhanced partitioning of curcumin into DSPC at both phases in the presence of RLs. RLs lowered the phase transition temperature, and broadened it as an indication of fusion of solid gel and liquid crystalline phases. Moreover increase fluidity of DSPC liposomes was reflected by reducing the degradation of curcumin further when DSPC liposomes were intercalated with RLs, thus, the present study opens up the possibility of using such mix system for curcumin and other unstable drug delivery application. Curcumin was successfully encapsulated in CD-MOFs. The encapsulation kinetics was relatively slow with a half-life of 5.41 hr under our experimental conditions. The results established that curcumin exists in the pores of CD-MOFs through a hydrogen bond type interaction between OH group of cyclodextrin moiety of CD-MOFs and phenolic hydroxyl group of curcumin. Presence of curcumin also does not disturb the crystallinity of CD-MOFs. The solvent polarity of the pores inside the CD-MOFs was found to be methanolic. Dissociation of the curcumin loaded CD-MOF in water did not separated curcumin from the dissolved framework but resulted in formation of an adduct in which the interaction was found to be unique in nature through complexation of potassium ion with curcumin and CD. The formation of this new complex, which absorbed at 520 nm and emitted at 600 nm, depends strongly on the incorporation of curcumin within the pores of CD-MOFs. The dissociated framework incorporating curcumin molecules showed an important enhancement in the chemical stability, of curcumin in water in alkaline conditions. In conclusion, CD-MOFs can be a promising benign system to store and stabilize curcumin for food applications.

# Bibliography

- [1] A. Jesorka and O. Orwar, "Liposomes: technologies and analytical applications," *Annu. Rev. Anal. Chem.*, vol. 1, pp. 801–832, 2008.
- [2] T. Esatbeyoglu, P. Huebbe, I. Ernst, D. Chin, A. E. Wagner, and G. Rimbach, "Curcumin—From molecule to biological function," *Angewandte Chemie International Edition*, vol. 51, no. 22, pp. 5308–5332, 2012.
- [3] B. Brouk *et al.*, *Plants consumed by man*. Academic Press Inc.(London) Ltd., 1975.
- [4] J. Milobedzka, V. Kostanecki, and V. Lampe, "Structure," *Chem Ber*, vol. 43, p. 2163, 1910.
- [5] Y.-J. Wang, M.-H. Pan, A.-L. Cheng, L.-I. Lin, Y.-S. Ho, C.-Y. Hsieh, and J.-K. Lin, "Stability of curcumin in buffer solutions and characterization of its degradation products," *Journal of pharmaceutical and biomedical analysis*, vol. 15, no. 12, pp. 1867–1876, 1997.
- [6] S. V. Jovanovic, S. Steenken, C. W. Boone, and M. G. Simic, "H-atom transfer is a preferred antioxidant mechanism of curcumin," *Journal of the American Chemical Society*, vol. 121, no. 41, pp. 9677–9681, 1999.
- [7] R. Sharma, A. Gescher, and W. Steward, "Curcumin: the story so far," *European journal of cancer*, vol. 41, no. 13, pp. 1955–1968, 2005.
- [8] J.-K. Lin, M.-H. Pan, and S.-Y. Lin-Shiau, "Recent studies on the biofunctions and biotransformations of curcumin," *Biofactors*, vol. 13, no. 1-4, pp. 153–158, 2000.
- [9] H. H. Tønnesen and J. Karlsen, "Studies on curcumin and curcuminoids," *Zeitschrift für Lebensmittel-Untersuchung und Forschung*, vol. 180, no. 5, pp. 402–404, 1985.
- [10] S. M. Khopde, K. Indira Priyadarsini, T. Mukherjee *et al.*, "Effect of solvent on the excited-state photophysical properties of curcumin," *Photochemistry and photobiology*, vol. 72, no. 5, pp. 625–631, 2000.



- [11] K. I. Priyadarsini, “The chemistry of curcumin: from extraction to therapeutic agent,” *Molecules*, vol. 19, no. 12, pp. 20 091–20 112, 2014.
- [12] W.-G. Yu, G. Xu, G.-J. Ren, X. Xu, H.-Q. Yuan, X.-L. Qi, K.-L. Tian *et al.*, “Preventive action of curcumin in experimental acute pancreatitis in mouse,” *The Indian journal of medical research*, vol. 134, no. 5, p. 717, 2011.
- [13] J. Epstein, G. Docena, T. T. MacDonald, and I. R. Sanderson, “Curcumin suppresses p38 mitogen-activated protein kinase activation, reduces il-1 $\beta$  and matrix metalloproteinase-3 and enhances il-10 in the mucosa of children and adults with inflammatory bowel disease,” *British Journal of Nutrition*, vol. 103, no. 06, pp. 824–832, 2010.
- [14] H. Hanai and K. Sugimoto, “Curcumin has bright prospects for the treatment of inflammatory bowel disease,” *Current pharmaceutical design*, vol. 15, no. 18, pp. 2087–2094, 2009.
- [15] C. Natarajan and J. J. Bright, “Curcumin inhibits experimental allergic encephalomyelitis by blocking il-12 signaling through janus kinase-stat pathway in t lymphocytes,” *The Journal of Immunology*, vol. 168, no. 12, pp. 6506–6513, 2002.
- [16] P. S. Babu and K. Srinivasan, “Influence of dietary curcumin and cholesterol on the progression of experimentally induced diabetes in albino rat,” *Molecular and cellular biochemistry*, vol. 152, no. 1, pp. 13–21, 1995.
- [17] M.-C. Jiang, H.-F. Yang-Yen, J. J.-Y. Yen, and J.-K. Lin, “Curcumin induces apoptosis in immortalized nih 3t3 and malignant cancer cell lines,” 1996.
- [18] S.-S. Han, S.-T. Chung, D. A. Robertson, D. Ranjan, and S. Bondada, “Curcumin causes the growth arrest and apoptosis of b cell lymphoma by downregulation of egr-1, c-myc, bcl-x l, nf- $\kappa$ b, and p53,” *Clinical immunology*, vol. 93, no. 2, pp. 152–161, 1999.
- [19] B. Gupta and B. Ghosh, “Curcuma longa inhibits tnf- $\alpha$  induced expression of adhesion molecules on human umbilical vein endothelial cells,” *International journal of immunopharmacology*, vol. 21, no. 11, pp. 745–757, 1999.
- [20] A. S. Jaiswal, B. P. Marlow, N. Gupta, and S. Narayan, “ $\beta$ -catenin-mediated transactivation and cell–cell adhesion pathways are important in curcumin (diferuylmethane)-induced growth arrest and apoptosis in colon cancer cells.” *Oncogene*, vol. 21, no. 55, 2002.
- [21] J. S. Flier, L. H. Underhill, and J. Folkman, “Clinical applications of research on angiogenesis,” *New England Journal of Medicine*, vol. 333, no. 26, pp. 1757–1763, 1995.

- [22] J. L. Arbiser, N. Klauber, R. Rohan, R. van Leeuwen, M.-T. Huang, C. Fisher, E. Flynn, and H. R. Byers, "Curcumin is an in vivo inhibitor of angiogenesis." *Molecular Medicine*, vol. 4, no. 6, p. 376, 1998.
- [23] J. D. Desai and I. M. Banat, "Microbial production of surfactants and their commercial potential." *Microbiology and molecular Biology reviews*, vol. 61, no. 1, pp. 47–64, 1997.
- [24] S. Lang and D. Wullbrandt, "Rhamnose lipids–biosynthesis, microbial production and application potential," *Applied Microbiology and Biotechnology*, vol. 51, no. 1, pp. 22–32, 1999.
- [25] K. Arima, A. Kakinuma, and G. Tamura, "Surfactin, a crystalline peptidelipid surfactant produced by bacillus subtilis: Isolation, characterization and its inhibition of fibrin clot formation," *Biochemical and biophysical research communications*, vol. 31, no. 3, pp. 488–494, 1968.
- [26] A. M. Abdel-Mawgoud, F. Lépine, and E. Déziel, "Rhamnolipids: diversity of structures, microbial origins and roles," *Applied microbiology and biotechnology*, vol. 86, no. 5, pp. 1323–1336, 2010.
- [27] F. Jarvis and M. Johnson, "A glyco-lipide produced by pseudomonas aeruginosa," *Journal of the American Chemical Society*, vol. 71, no. 12, pp. 4124–4126, 1949.
- [28] J. R. Edwards and J. A. Hayashi, "Structure of a rhamnolipid from pseudomonas aeruginosa," *Archives of biochemistry and biophysics*, vol. 111, no. 2, pp. 415–421, 1965.
- [29] A. Abalos, F. Maximo, M. A. Manresa, and J. Bastida, "Utilization of response surface methodology to optimize the culture media for the production of rhamnolipids by pseudomonas aeruginosa at 10," *Journal of chemical technology and biotechnology*, vol. 77, no. 7, pp. 777–784, 2002.
- [30] E. Déziel, Y. Comeau, and R. Villemur, "Two-liquid-phase bioreactors for enhanced degradation of hydrophobic/toxic compounds," *Biodegradation*, vol. 10, no. 3, pp. 219–233, 1999.
- [31] E. Déziel, F. Lépine, S. Milot, and R. Villemur, "Mass spectrometry monitoring of rhamnolipids from a growing culture of pseudomonas aeruginosa strain 57rp," *Biochimica et Biophysica Acta (BBA)-Molecular and Cell Biology of Lipids*, vol. 1485, no. 2, pp. 145–152, 2000.
- [32] N. M. Pinzon and L.-K. Ju, "Improved detection of rhamnolipid production using agar plates containing methylene blue and cetyl trimethylammonium bromide," *Biotechnology letters*, vol. 31, no. 10, pp. 1583–1588, 2009.

- [33] I. Siegmund and F. Wagner, "New method for detecting rhamnolipids excreted by pseudomonas species during growth on mineral agar," *Biotechnology Techniques*, vol. 5, no. 4, pp. 265–268, 1991.
- [34] D. Jain, D. Collins-Thompson, H. Lee, and J. Trevors, "A drop-collapsing test for screening surfactant-producing microorganisms," *Journal of Microbiological Methods*, vol. 13, no. 4, pp. 271–279, 1991.
- [35] P. Wood and I. Siddiqui, "Determination of methanol and its application to measurement of pectin ester content and pectin methyl esterase activity," *Analytical biochemistry*, vol. 39, no. 2, pp. 418–428, 1971.
- [36] A. K. Koch, O. Käppeli, A. Fiechter, and J. Reiser, "Hydrocarbon assimilation and biosurfactant production in pseudomonas aeruginosa mutants." *Journal of Bacteriology*, vol. 173, no. 13, pp. 4212–4219, 1991.
- [37] A. Mechaly, V. Belakhov, Y. Shoham, and T. Baasov, "An efficient chemical-enzymatic synthesis of 4-nitrophenyl  $\beta$ -xylobioside: A chromogenic substrate for xylanases," *Carbohydrate research*, vol. 304, no. 2, pp. 111–115, 1997.
- [38] S. Arino, R. Marchal, and J.-P. Vandecasteele, "Identification and production of a rhamnolipidic biosurfactant by a pseudomonas species," *Applied Microbiology and Biotechnology*, vol. 45, no. 1-2, pp. 162–168, 1996.
- [39] W. H. Noordman, M. L. Brusseau, and D. B. Janssen, "Adsorption of a multi-component rhamnolipid surfactant to soil," *Environmental science & technology*, vol. 34, no. 5, pp. 832–838, 2000.
- [40] L. A. Morici, A. J. Carterson, V. E. Wagner, A. Frisk, J. R. Schurr, K. H. Zubertrup, D. J. Hassett, B. H. Iglewski, K. Sauer, and M. J. Schurr, "Pseudomonas aeruginosa alginate represses the rhl quorum-sensing system in a biofilm-specific manner," *Journal of bacteriology*, vol. 189, no. 21, pp. 7752–7764, 2007.
- [41] J. Gartshore, Y. Lim, and D. Cooper, "Quantitative analysis of biosurfactants using fourier transform infrared (ft-ir) spectroscopy," *Biotechnology letters*, vol. 22, no. 2, pp. 169–172, 2000.
- [42] S. A. Monteiro, G. L. Sasaki, L. M. de Souza, J. A. Meira, J. M. de Araújo, D. A. Mitchell, L. P. Ramos, and N. Krieger, "Molecular and structural characterization of the biosurfactant produced by pseudomonas aeruginosa daupé 614," *Chemistry and physics of lipids*, vol. 147, no. 1, pp. 1–13, 2007.
- [43] M. M. Burger, L. Glaser, and R. M. Burton, "The enzymatic synthesis of a rhamnose-containing glycolipid by extracts of pseudomonas aeruginosa," *Journal of Biological Chemistry*, vol. 238, no. 8, pp. 2595–2602, 1963.

- [44] G. Hauser and M. L. Karnovsky, "Rhamnose and rhamnolipide biosynthesis by *Pseudomonas aeruginosa*," *Journal of Biological Chemistry*, vol. 224, no. 1, pp. 91–105, 1957.
- [45] ———, "Studies on the biosynthesis of l-rhamnose," *Journal of Biological Chemistry*, vol. 233, no. 2, pp. 287–291, 1958.
- [46] L. Glaser and S. Kornfeld, "The enzymatic synthesis of thymidine-linked sugars ii. thymidine diphosphate l-rhamnose," *Journal of Biological Chemistry*, vol. 236, no. 6, pp. 1795–1799, 1961.
- [47] W. Southard, J. Hayashi, and S. Barkulis, "Studies of streptococcal cell walls iv.: The conversion of d-glucose to cell wall l-rhamnose1," *Journal of bacteriology*, vol. 78, no. 1, p. 79, 1959.
- [48] G. Soberón-Chávez, F. Lépine, and E. Déziel, "Production of rhamnolipids by *Pseudomonas aeruginosa*," *Applied Microbiology and Biotechnology*, vol. 68, no. 6, pp. 718–725, 2005.
- [49] E. Déziel, F. Lépine, S. Milot, and R. Villemur, "rhlA is required for the production of a novel biosurfactant promoting swarming motility in *Pseudomonas aeruginosa*: 3-(3-hydroxyalkanoyloxy) alkanolic acids (haas), the precursors of rhamnolipids," *Microbiology*, vol. 149, no. 8, pp. 2005–2013, 2003.
- [50] F. Lépine, E. Déziel, S. Milot, and R. Villemur, "Liquid chromatographic/mass spectrometric detection of the 3-(3-hydroxyalkanoyloxy) alkanolic acid precursors of rhamnolipids in *Pseudomonas aeruginosa* cultures," *Journal of mass spectrometry*, vol. 37, no. 1, pp. 41–46, 2002.
- [51] H. Zhong, G. M. Zeng, J. X. Liu, X. M. Xu, X. Z. Yuan, H. Y. Fu, G. H. Huang, Z. F. Liu, and Y. Ding, "Adsorption of monorhamnolipid and dirhamnolipid on two *Pseudomonas aeruginosa* strains and the effect on cell surface hydrophobicity," *Applied microbiology and biotechnology*, vol. 79, no. 4, pp. 671–677, 2008.
- [52] U. A. Ochsner and J. Reiser, "Autoinducer-mediated regulation of rhamnolipid biosurfactant synthesis in *Pseudomonas aeruginosa*," *Proceedings of the National Academy of Sciences*, vol. 92, no. 14, pp. 6424–6428, 1995.
- [53] A. M. Lazdunski, I. Ventre, and J. N. Sturgis, "Regulatory circuits and communication in gram-negative bacteria," *Nature Reviews Microbiology*, vol. 2, no. 7, pp. 581–592, 2004.
- [54] T. Köhler, L. K. Curty, F. Barja, C. Van Delden, and J.-C. PecheRe, "Swarming of *Pseudomonas aeruginosa* is dependent on cell-to-cell signaling and requires flagella and pili," *Journal of bacteriology*, vol. 182, no. 21, pp. 5990–5996, 2000.

- [55] R. Beal and W. Betts, "Role of rhamnolipid biosurfactants in the uptake and mineralization of hexadecane in *Pseudomonas aeruginosa*," *Journal of Applied Microbiology*, vol. 89, no. 1, pp. 158–168, 2000.
- [56] L. Guerra-Santos, O. Käppeli, and A. Fiechter, "Pseudomonas aeruginosa biosurfactant production in continuous culture with glucose as carbon source." *Applied and environmental microbiology*, vol. 48, no. 2, pp. 301–305, 1984.
- [57] R. C. Read, P. Roberts, N. Munro, A. Rutman, A. Hastie, T. Shryock, R. Hall, W. McDonald-Gibson, V. Lund, G. Taylor *et al.*, "Effect of pseudomonas aeruginosa rhamnolipids on mucociliary transport and ciliary beating," *Journal of Applied Physiology*, vol. 72, no. 6, pp. 2271–2277, 1992.
- [58] P. Cosson, L. Zulianello, O. Join-Lambert, F. Faurisson, L. Gebbie, M. Benghezal, C. van Delden, L. K. Curty, and T. Köhler, "Pseudomonas aeruginosa virulence analyzed in a dictyostelium discoideum host system," *Journal of Bacteriology*, vol. 184, no. 11, pp. 3027–3033, 2002.
- [59] A. Sotirova, D. Spasova, D. Galabova, E. Karpenko, and A. Shulga, "Rhamnolipid–biosurfactant permeabilizing effects on gram-positive and gram-negative bacterial strains," *Current microbiology*, vol. 56, no. 6, pp. 639–644, 2008.
- [60] R. Maier and G. Soberon-Chavez, "Pseudomonas aeruginosa rhamnolipids: biosynthesis and potential applications," *Applied Microbiology and Biotechnology*, vol. 54, no. 5, pp. 625–633, 2000.
- [61] E. Gharaei-Fathabad, "Biosurfactants in pharmaceutical industry: a mini-review," *American Journal of Drug Discovery and Development*, vol. 1, no. 1, pp. 58–69, 2011.
- [62] N. Lourith and M. Kanlayavattanakul, "Natural surfactants used in cosmetics: glycolipids," *International journal of cosmetic science*, vol. 31, no. 4, pp. 255–261, 2009.
- [63] E. Rosenberg and E. Ron, "High- and low-molecular-mass microbial surfactants," *Applied Microbiology and Biotechnology*, vol. 52, no. 2, pp. 154–162, 1999.
- [64] P. Vatsa, L. Sanchez, C. Clement, F. Baillieul, and S. Dorey, "Rhamnolipid biosurfactants as new players in animal and plant defense against microbes," *International journal of molecular sciences*, vol. 11, no. 12, pp. 5095–5108, 2010.
- [65] A. Wagner and K. Vorauer-Uhl, "Liposome technology for industrial purposes," *Journal of drug delivery*, vol. 2011, 2010.

- [66] N. Maurer, D. B. Fenske, and P. R. Cullis, "Developments in liposomal drug delivery systems," *Expert opinion on biological therapy*, vol. 1, no. 6, pp. 923–947, 2001.
- [67] A. Akbarzadeh, R. Rezaei-Sadabady, S. Davaran, S. W. Joo, N. Zarghami, Y. Hanifehpour, M. Samiei, M. Kouhi, and K. Nejati-Koshki, "Liposome: classification, preparation, and applications," *Nanoscale Res Lett*, vol. 8, no. 1, p. 102, 2013.
- [68] K. Khosravi-Darani and M. Mozafari, "Nanoliposome potentials in nanotherapy: A concise overview," *International Journal of Nanoscience and Nanotechnology*, vol. 6, no. 1, pp. 3–13, 2010.
- [69] V. Heinrich, B. Božič, S. Svetina, and B. Žekš, "Vesicle deformation by an axial load: from elongated shapes to tethered vesicles," *Biophysical journal*, vol. 76, no. 4, pp. 2056–2071, 1999.
- [70] C. Tardi, M. Drechsler, K. Bauer, and M. Brandl, "Steam sterilisation of vesicular phospholipid gels," *International journal of pharmaceuticals*, vol. 217, no. 1, pp. 161–172, 2001.
- [71] A. M. Krieg, "From bugs to drugs: therapeutic immunomodulation with oligodeoxynucleotides containing cpg sequences from bacterial dna," *Antisense and Nucleic Acid Drug Development*, vol. 11, no. 3, pp. 181–188, 2001.
- [72] J. M. Metselaar, P. Bruin, L. W. de Boer, T. de Vringer, C. Snel, C. Oussoren, M. H. Wauben, D. J. Crommelin, G. Storm, and W. E. Hennink, "A novel family of l-amino acid-based biodegradable polymer-lipid conjugates for the development of long-circulating liposomes with effective drug-targeting capacity," *Bioconjugate chemistry*, vol. 14, no. 6, pp. 1156–1164, 2003.
- [73] M. Riaz, "Liposomes preparation methods," *Pak J Pharm Sci*, vol. 9, no. 1, pp. 65–77, 1996.
- [74] H. Anwekar, S. Patel, and A. Singhai, "International journal of pharmacy & life sciences," *Int. J. of Pharm. & Life Sci.(IJPLS)*, vol. 2, no. 7, pp. 945–951, 2011.
- [75] K. A. Edwards and A. J. Baeumner, "Analysis of liposomes," *Talanta*, vol. 68, no. 5, pp. 1432–1441, 2006.
- [76] B. A. Korgel, J. H. van Zanten, and H. G. Monbouquette, "Vesicle size distributions measured by flow field-flow fractionation coupled with multiangle light scattering," *Biophysical journal*, vol. 74, no. 6, pp. 3264–3272, 1998.
- [77] B. Sun and D. T. Chiu, "Determination of the encapsulation efficiency of individual vesicles using single-vesicle photolysis and confocal single-molecule detection," *Analytical chemistry*, vol. 77, no. 9, pp. 2770–2776, 2005.

- [78] Q. Chaudhry, M. Scotter, J. Blackburn, B. Ross, A. Boxall, L. Castle, R. Aitken, and R. Watkins, "Applications and implications of nanotechnologies for the food sector," *Food additives and contaminants*, vol. 25, no. 3, pp. 241–258, 2008.
- [79] J.-C. Colas, W. Shi, V. M. Rao, A. Omri, M. R. Mozafari, and H. Singh, "Microscopical investigations of nisin-loaded nanoliposomes prepared by mozafari method and their bacterial targeting," *Micron*, vol. 38, no. 8, pp. 841–847, 2007.
- [80] E. Magee and N. Olson, "Microencapsulation of cheese ripening systems: Stability of microcapsules," *Journal of Dairy Science*, vol. 64, no. 4, pp. 611–615, 1981.
- [81] M. Choi and H. Maibach, "Liposomes and niosomes as topical drug delivery systems," *Skin pharmacology and physiology*, vol. 18, no. 5, pp. 209–219, 2005.
- [82] M. B. Pierre, A. C. Tedesco, J. M. Marchetti, and M. V. L. Bentley, "Stratum corneum lipids liposomes for the topical delivery of 5-aminolevulinic acid in photodynamic therapy of skin cancer: preparation and in vitro permeation study," *BMC dermatology*, vol. 1, no. 1, p. 5, 2001.
- [83] D. Yarosh, L. G. Alas, V. Yee, A. Oberyszyn, J. T. Kibitel, D. Mitchell, R. Rosenstein, A. Spinowitz, and M. Citron, "Pyrimidine dimer removal enhanced by dna repair liposomes reduces the incidence of uv skin cancer in mice," *Cancer research*, vol. 52, no. 15, pp. 4227–4231, 1992.
- [84] P. Basnet, H. Hussain, I. Tho, and N. Skalko-Basnet, "Liposomal delivery system enhances anti-inflammatory properties of curcumin," *Journal of pharmaceutical sciences*, vol. 101, no. 2, pp. 598–609, 2012.
- [85] R. Banerjee, "Liposomes: applications in medicine," *Journal of Biomaterials applications*, vol. 16, no. 1, pp. 3–21, 2001.
- [86] S. E. SELTZER, R. G. SWENSSON, P. F. JUDY, and R. D. NAWFEL, "Size discrimination in computed tomographic images effects of feature contrast and display window." *Investigative radiology*, vol. 23, no. 6, pp. 455–462, 1988.
- [87] I. K. Adzamlı, S. E. SELTZER, M. SLIFKIN, M. BLAU, and D. F. ADAMS, "Production and characterization of improved liposomes containing radiographic contrast media." *Investigative radiology*, vol. 25, no. 11, pp. 1217–1223, 1990.
- [88] R. Schiffelers, G. Storm, and I. Bakker-Woudenberg, "Liposome-encapsulated aminoglycosides in pre-clinical and clinical studies," *Journal of Antimicrobial Chemotherapy*, vol. 48, no. 3, pp. 333–344, 2001.

- [89] J. A. Leff, J. W. Baer, J. M. Kirkman, M. E. Bodman, P. F. Shanley, O. J. Cho, M. J. Ostro, and J. E. Repine, "Liposome-entrapped pge1 posttreatment decreases il-1 alpha-induced neutrophil accumulation and lung leak in rats," *Journal of Applied Physiology*, vol. 76, no. 1, pp. 151–157, 1994.
- [90] B. Uziely, S. Jeffers, R. Isacson, K. Kutsch, D. Wei-Tsao, Z. Yehoshua, E. Libson, F. M. Muggia, and A. Gabizon, "Liposomal doxorubicin: antitumor activity and unique toxicities during two complementary phase i studies." *Journal of Clinical Oncology*, vol. 13, no. 7, pp. 1777–1785, 1995.
- [91] F. M. Muggia, J. D. Hainsworth, S. Jeffers, P. Miller, S. Groshen, M. Tan, L. Roman, B. Uziely, L. Muderspach, A. Garcia *et al.*, "Phase ii study of liposomal doxorubicin in refractory ovarian cancer: antitumor activity and toxicity modification by liposomal encapsulation." *Journal of Clinical Oncology*, vol. 15, no. 3, pp. 987–993, 1997.
- [92] A. Gabizon, D. Goren, R. Cohen, and Y. Barenholz, "Development of liposomal anthracyclines: from basics to clinical applications," *Journal of controlled release*, vol. 53, no. 1, pp. 275–279, 1998.
- [93] A. Akbarzadeh, M. Samiei, and S. Davaran, "Magnetic nanoparticles: preparation, physical properties, and applications in biomedicine," *Nanoscale research letters*, vol. 7, no. 1, pp. 1–13, 2012.
- [94] J. R. Lakowicz, *Principles of fluorescence spectroscopy*. Springer Science & Business Media, 2013.
- [95] A. Jablonski, "Uber den mechanisms des photolumineszenz von farbstoffphosphores," *Z phys*, 1935.
- [96] M. Kasha, "Characterization of electronic transitions in complex molecules," *Discussions of the Faraday society*, vol. 9, pp. 14–19, 1950.
- [97] E. Sezgin and P. Schwille, "Fluorescence techniques to study lipid dynamics," *Cold Spring Harbor perspectives in biology*, vol. 3, no. 11, p. a009803, 2011.
- [98] T. Baumgart, G. Hunt, E. R. Farkas, W. W. Webb, and G. W. Feigenson, "Fluorescence probe partitioning between l/o/d phases in lipid membranes," *Biochimica et Biophysica Acta (BBA)-Biomembranes*, vol. 1768, no. 9, pp. 2182–2194, 2007.
- [99] R. B Mythri and M. M Srinivas Bharath, "Curcumin: a potential neuroprotective agent in parkinson's disease," *Current pharmaceutical design*, vol. 18, no. 1, pp. 91–99, 2012.



- [100] S. Mishra and K. Palanivelu, "The effect of curcumin (turmeric) on alzheimer's disease: An overview," *Annals of Indian Academy of Neurology*, vol. 11, no. 1, p. 13, 2008.
- [101] E. D. El Khoury and D. Patra, "Ionic liquid expedites partition of curcumin into solid gel phase but discourages partition into liquid crystalline phase of 1, 2-dimyristoyl-sn-glycero-3-phosphocholine liposomes," *The Journal of Physical Chemistry B*, vol. 117, no. 33, pp. 9699–9708, 2013.
- [102] M. Mouslmani, K. H. Bouhadir, and D. Patra, "Poly (9-(2-diallylaminoethyl) adenine hcl-co-sulfur dioxide) deposited on silica nanoparticles constructs hierarchically ordered nanocapsules: Curcumin conjugated nanocapsules as a novel strategy to amplify guanine selectivity among nucleobases," *Biosensors and Bioelectronics*, vol. 68, pp. 181–188, 2015.
- [103] M. Chebl, M. G. Abiad, Z. Moussa, and D. Patra, "Two modes of associations of curcumin with pre-and nano-aggregated chitosan oligosaccharide lactate: Ionic strength and hydrophobic bile salt modulate partition of drug and self-assembly process," *The Journal of Physical Chemistry C*, 2016.
- [104] E. El Khoury, M. Abiad, Z. G. Kassaiy, and D. Patra, "Green synthesis of curcumin conjugated nanosilver for the applications in nucleic acid sensing and anti-bacterial activity," *Colloids and Surfaces B: Biointerfaces*, vol. 127, pp. 274–280, 2015.
- [105] H. H. Tønnesen, M. Másson, and T. Loftsson, "Studies of curcumin and curcuminoids. xxvii. cyclodextrin complexation: solubility, chemical and photochemical stability," *International Journal of Pharmaceutics*, vol. 244, no. 1, pp. 127–135, 2002.
- [106] K. Maiti, K. Mukherjee, A. Gantait, B. P. Saha, and P. K. Mukherjee, "Curcumin–phospholipid complex: preparation, therapeutic evaluation and pharmacokinetic study in rats," *International journal of pharmaceutics*, vol. 330, no. 1, pp. 155–163, 2007.
- [107] Z. Moussa, M. Hmadeh, M. G. Abiad, O. H. Dib, and D. Patra, "Encapsulation of curcumin in cyclodextrin-metal organic frameworks: dissociation of loaded cd-mofs enhances stability of curcumin," *Food Chemistry*, 2016.
- [108] S. Bisht, G. Feldmann, S. Soni, R. Ravi, C. Karikar, A. Maitra, and A. Maitra, "Polymeric nanoparticle-encapsulated curcumin ("nanocurcumi"): a novel strategy for human cancer therapy," *J Nanobiotechnology*, vol. 5, no. 3, pp. 1–18, 2007.
- [109] C. S. Mangolim, C. Moriwaki, A. C. Nogueira, F. Sato, M. L. Baesso, A. M. Neto, and G. Matioli, "Curcumin– $\beta$ -cyclodextrin inclusion complex: Stability,

- solubility, characterisation by ft-ir, ft-raman, x-ray diffraction and photoacoustic spectroscopy, and food application,” *Food chemistry*, vol. 153, pp. 361–370, 2014.
- [110] M. H. Leung, H. Colangelo, and T. W. Kee, “Encapsulation of curcumin in cationic micelles suppresses alkaline hydrolysis,” *Langmuir*, vol. 24, no. 11, pp. 5672–5675, 2008.
- [111] H. H. Tønnesen, “Solubility, chemical and photochemical stability of curcumin in surfactant solutions. studies of curcumin and curcuminoids, xxviii.” *Die Pharmazie*, vol. 57, no. 12, pp. 820–824, 2002.
- [112] E. M. Bruzell, E. Morisbak, and H. H. Tønnesen, “Studies on curcumin and curcuminoids. xxix. photoinduced cytotoxicity of curcumin in selected aqueous preparations,” *Photochemical & photobiological sciences*, vol. 4, no. 7, pp. 523–530, 2005.
- [113] F. Zsila, Z. Bikádi, and M. Simonyi, “Molecular basis of the cotton effects induced by the binding of curcumin to human serum albumin,” *Tetrahedron: Asymmetry*, vol. 14, no. 16, pp. 2433–2444, 2003.
- [114] V. Galasso, B. Kovac, A. Modelli, M. Ottaviani, and F. Pichierri, “Spectroscopic and theoretical study of the electronic structure of curcumin and related fragment molecules,” *The Journal of Physical Chemistry A*, vol. 112, no. 11, pp. 2331–2338, 2008.
- [115] Y. Manolova, V. Deneva, L. Antonov, E. Drakalska, D. Momekova, and N. Lambov, “The effect of the water on the curcumin tautomerism: a quantitative approach,” *Spectrochimica Acta Part A: Molecular and Biomolecular Spectroscopy*, vol. 132, pp. 815–820, 2014.
- [116] D. Patra and C. Barakat, “Unique role of ionic liquid [bmin][bf 4] during curcumin–surfactant association and micellization of cationic, anionic and non-ionic surfactant solutions,” *Spectrochimica Acta Part A: Molecular and Biomolecular Spectroscopy*, vol. 79, no. 5, pp. 1823–1828, 2011.
- [117] T. D. Renfro, W. Xie, G. Yang, and G. Chen, “Rhamnolipid surface thermodynamic properties and transport in agricultural soil,” *Colloids and Surfaces B: Biointerfaces*, vol. 115, pp. 317–322, 2014.
- [118] M. Nitschke, S. G. Costa, R. Haddad, G. Gonçalves, A. Lireny, M. N. Eberlin, and J. Contiero, “Oil wastes as unconventional substrates for rhamnolipid biosurfactant production by *pseudomonas aeruginosa* lbi,” *Biotechnology progress*, vol. 21, no. 5, pp. 1562–1566, 2005.

- [119] P. K. Rahman, G. Pasirayi, V. Auger, and Z. Ali, "Production of rhamnolipid biosurfactants by *Pseudomonas aeruginosa* ds10-129 in a microfluidic bioreactor," *Biotechnology and applied biochemistry*, vol. 55, no. 1, pp. 45–52, 2010.
- [120] M. J. Rosen, J. H. Mathias, and L. Davenport, "Aberrant aggregation behavior in cationic gemini surfactants investigated by surface tension, interfacial tension, and fluorescence methods," *Langmuir*, vol. 15, no. 21, pp. 7340–7346, 1999.
- [121] M. Bernabé-Pineda, M. T. Ramírez-Silva, M. Romero-Romo, E. González-Vergara, and A. Rojas-Hernández, "Determination of acidity constants of curcumin in aqueous solution and apparent rate constant of its decomposition," *Spectrochimica Acta Part A: Molecular and Biomolecular Spectroscopy*, vol. 60, no. 5, pp. 1091–1097, 2004.
- [122] R. Adhikary, P. Mukherjee, T. W. Kee, and J. W. Petrich, "Excited-state intramolecular hydrogen atom transfer and solvation dynamics of the medicinal pigment curcumin," *The Journal of Physical Chemistry B*, vol. 113, no. 15, pp. 5255–5261, 2009.
- [123] L. Shen and H.-F. Ji, "Theoretical study on physicochemical properties of curcumin," *Spectrochimica Acta Part A: Molecular and Biomolecular Spectroscopy*, vol. 67, no. 3, pp. 619–623, 2007.
- [124] D. Palit, A. Sapre, and J. Mittal, "Picosecond studies on the electron transfer from pyrene and perylene excited singlet states to n-hexadecyl pyridinium chloride," *Chemical physics letters*, vol. 269, no. 3, pp. 286–292, 1997.
- [125] L. Shen and H.-F. Ji, "The pharmacology of curcumin: is it the degradation products?" *Trends in molecular medicine*, vol. 18, no. 3, pp. 138–144, 2012.
- [126] Y.-R. Chen and T.-H. Tan, "Inhibition of the c-jun n-terminal kinase (jnk) signaling pathway by curcumin." *Oncogene*, vol. 17, no. 2, 1998.
- [127] P. Khajehdehi, B. Zanjanejad, E. Aflaki, M. Nazarinia, F. Azad, L. Malekmakan, and G.-R. Dehghanzadeh, "Oral supplementation of turmeric decreases proteinuria, hematuria, and systolic blood pressure in patients suffering from relapsing or refractory lupus nephritis: a randomized and placebo-controlled study," *Journal of Renal Nutrition*, vol. 22, no. 1, pp. 50–57, 2012.
- [128] M. Heng, M. Song, J. Harker, and M. Heng, "Drug-induced suppression of phosphorylase kinase activity correlates with resolution of psoriasis as assessed by clinical, histological and immunohistochemical parameters," *British Journal of Dermatology*, vol. 143, no. 5, pp. 937–949, 2000.
- [129] J. Chen, W. Da, D. Zhang, Q. Liu, and J. Kang, "Water-soluble antioxidants improve the antioxidant and anticancer activity of low concentrations of curcumin

- in human leukemia cells,” *Die Pharmazie-An International Journal of Pharmaceutical Sciences*, vol. 60, no. 1, pp. 57–61, 2005.
- [130] C.-C. Su, G.-w. Chen, J.-G. Lin, L.-T. WU, and J.-G. CHUNG, “Curcumin inhibits cell migration of human colon cancer colo 205 cells through the inhibition of nuclear factor kappa b/p65 and down-regulates cyclooxygenase-2 and matrix metalloproteinase-2 expressions,” *Anticancer research*, vol. 26, no. 2A, pp. 1281–1288, 2006.
- [131] J. Fang, J. Lu, and A. Holmgren, “Thioredoxin reductase is irreversibly modified by curcumin a novel molecular mechanism for its anticancer activity,” *Journal of Biological Chemistry*, vol. 280, no. 26, pp. 25 284–25 290, 2005.
- [132] G. M. Cole, B. Teter, and S. A. Frautschy, “Neuroprotective effects of curcumin,” in *The molecular targets and therapeutic uses of curcumin in health and disease*. Springer, 2007, pp. 197–212.
- [133] R. N. Moussawi and D. Patra, “Synthesis of au nanorods through prereduction with curcumin: Preferential enhancement of au nanorod formation prepared from ctab-capped over citrate-capped au seeds,” *The Journal of Physical Chemistry C*, vol. 119, no. 33, pp. 19 458–19 468, 2015.
- [134] H. H. Tønnesen and J. Karlsen, “Studies on curcumin and curcuminoids,” *Zeitschrift für Lebensmittel-Untersuchung und Forschung*, vol. 180, no. 2, pp. 132–134, 1985.
- [135] Z. Wang, M. H. Leung, T. W. Kee, and D. S. English, “The role of charge in the surfactant-assisted stabilization of the natural product curcumin,” *Langmuir*, vol. 26, no. 8, pp. 5520–5526, 2009.
- [136] A. Safavy, K. P. Raisch, S. Mantena, L. L. Sanford, S. W. Sham, N. R. Krishna, and J. A. Bonner, “Design and development of water-soluble curcumin conjugates as potential anticancer agents#,” *Journal of medicinal chemistry*, vol. 50, no. 24, pp. 6284–6288, 2007.
- [137] M. J. Johnston, S. C. Semple, S. K. Klimuk, S. Ansell, N. Maurer, and P. R. Cullis, “Characterization of the drug retention and pharmacokinetic properties of liposomal nanoparticles containing dihydrosphingomyelin,” *Biochimica et Biophysica Acta (BBA)-Biomembranes*, vol. 1768, no. 5, pp. 1121–1127, 2007.
- [138] R. Banerjee, P. Tyagi, S. Li, and L. Huang, “Anisamide-targeted stealth liposomes: A potent carrier for targeting doxorubicin to human prostate cancer cells,” *International journal of cancer*, vol. 112, no. 4, pp. 693–700, 2004.
- [139] R. Parthasarathy, P. G. Sacks, D. Harris, H. Brock, and K. Mehta, “Interaction of liposome-associated all-trans-retinoic acid with squamous carcinoma cells,” *Cancer chemotherapy and pharmacology*, vol. 34, no. 6, pp. 527–534, 1994.

- [140] D. Komes, T. Lovrić, K. Kovačević Ganić, and L. Gracin, “Study of trehalose addition on aroma retention in dehydrated strawberry puree,” *Food Technology and Biotechnology*, vol. 41, no. 2, pp. 111–119, 2003.
- [141] A. M. Abdel-Mawgoud, M. M. Aboulwafa, and N. A.-H. Hassouna, “Characterization of rhamnolipid produced by pseudomonas aeruginosa isolate bs20,” *Applied biochemistry and biotechnology*, vol. 157, no. 2, pp. 329–345, 2009.
- [142] A. Abalos, A. Pinazo, M. Infante, M. Casals, F. Garcia, and A. Manresa, “Physicochemical and antimicrobial properties of new rhamnolipids produced by pseudomonas aeruginosa at 10 from soybean oil refinery wastes,” *Langmuir*, vol. 17, no. 5, pp. 1367–1371, 2001.
- [143] G. Chen, “Rhamnolipid biosurfactant behavior in solutions,” *Journal of Biomaterials Science, Polymer Edition*, vol. 15, no. 2, pp. 229–235, 2004.
- [144] R. Cohen and D. Exerowa, “Surface forces and properties of foam films from rhamnolipid biosurfactants,” *Advances in colloid and interface science*, vol. 134, pp. 24–34, 2007.
- [145] C. SGVAO, F. Lépine, S. Milot, E. Déziel, M. Nitschke, and J. Contiero, “Cassava wastewater as a substrate for the simultaneous production of rhamnolipids and polyhydroxyalkanoates by pseudomonas aeruginosa,” *J Ind Microbiol Biotechnol*, vol. 36, pp. 1063–1072, 2009.
- [146] F. Nomura, M. Nagata, T. Inaba, H. Hiramatsu, H. Hotani, and K. Takiguchi, “Capabilities of liposomes for topological transformation,” *Proceedings of the National Academy of Sciences*, vol. 98, no. 5, pp. 2340–2345, 2001.
- [147] N. Deo and P. Somasundaran, “Disintegration of liposomes by surfactants: mechanism of protein and cholesterol effects,” *Langmuir*, vol. 19, no. 6, pp. 2007–2012, 2003.
- [148] ———, “Effects of sodium dodecyl sulfate on mixed liposome solubilization,” *Langmuir*, vol. 19, no. 18, pp. 7271–7275, 2003.
- [149] A. M. Harmon, M. H. Lash, N. Tishbi, D. Lent, E. A. Mintzer, and K. E. Uhrich, “Thermodynamic and physical interactions between novel polymeric surfactants and lipids: Toward designing stable polymer–lipid complexes,” *Langmuir*, vol. 27, no. 15, pp. 9131–9138, 2011.
- [150] J. A. Castillo, A. Pinazo, J. Carilla, M. R. Infante, M. A. Alsina, I. Haro, and P. Clapés, “Interaction of antimicrobial arginine-based cationic surfactants with liposomes and lipid monolayers,” *Langmuir*, vol. 20, no. 8, pp. 3379–3387, 2004.

- [151] C. F. Chignell, P. Bilskj, K. J. Reszka, A. G. Motten, R. H. Sik, and T. A. Dahl, "Spectral and photochemical properties of curcumin," *Photochemistry and photobiology*, vol. 59, no. 3, pp. 295–302, 1994.
- [152] E. El Khoury and D. Patra, "Length of hydrocarbon chain influences location of curcumin in liposomes: Curcumin as a molecular probe to study ethanol induced interdigitation of liposomes," *Journal of Photochemistry and Photobiology B: Biology*, vol. 158, pp. 49–54, 2016.
- [153] D. Patra, E. El Khoury, D. Ahmadieh, S. Darwish, and R. M. Tafech, "Effect of curcumin on liposome: Curcumin as a molecular probe for monitoring interaction of ionic liquids with 1, 2-dipalmitoyl-sn-glycero-3-phosphocholine liposome," *Photochemistry and photobiology*, vol. 88, no. 2, pp. 317–327, 2012.
- [154] J. Sujatha and A. Mishra, "Phase transitions in phospholipid vesicles: Excited state prototropism of 1-naphthol as a novel probe concept," *Langmuir*, vol. 14, no. 9, pp. 2256–2262, 1998.
- [155] C. Schneider, O. N. Gordon, R. L. Edwards, and P. B. Luis, "Degradation of curcumin: From mechanism to biological implications," *Journal of agricultural and food chemistry*, vol. 63, no. 35, pp. 7606–7614, 2015.
- [156] D. Ke, Y. Wu, and X. Wang, "Shift of acid–base equilibrium of curcumin in its complexes with gemini surfactant hexamethylene-1, 6-bis-(dodecyl dimethyl ammonium bromide)," *Colloids and Surfaces A: Physicochemical and Engineering Aspects*, vol. 443, pp. 481–487, 2014.
- [157] G. Began, E. Sudharshan, K. Udaya Sankar, and A. Appu Rao, "Interaction of curcumin with phosphatidylcholine: a spectrofluorometric study," *Journal of agricultural and food chemistry*, vol. 47, no. 12, pp. 4992–4997, 1999.
- [158] Z. Huang and R. P. Haugland, "Partition coefficients of fluorescent probes with phospholipid membranes," *Biochemical and biophysical research communications*, vol. 181, no. 1, pp. 166–171, 1991.
- [159] S. Mabrey and J. M. Sturtevant, "Investigation of phase transitions of lipids and lipid mixtures by sensitivity differential scanning calorimetry," *Proceedings of the National Academy of Sciences*, vol. 73, no. 11, pp. 3862–3866, 1976.
- [160] W.-C. Hung, F.-Y. Chen, C.-C. Lee, Y. Sun, M.-T. Lee, and H. W. Huang, "Membrane-thinning effect of curcumin," *Biophysical journal*, vol. 94, no. 11, pp. 4331–4338, 2008.
- [161] S.-J. Marrink and H. J. Berendsen, "Simulation of water transport through a lipid membrane," *The Journal of Physical Chemistry*, vol. 98, no. 15, pp. 4155–4168, 1994.

- [162] M. T. Jonker and A. A. Koelmans, "Sorption of polycyclic aromatic hydrocarbons and polychlorinated biphenyls to soot and soot-like materials in the aqueous environment: mechanistic considerations," *Environmental Science & Technology*, vol. 36, no. 17, pp. 3725–3734, 2002.
- [163] B. Hoff, E. Strandberg, A. S. Ulrich, D. P. Tieleman, and C. Posten, "2 h-nmr study and molecular dynamics simulation of the location, alignment, and mobility of pyrene in popc bilayers," *Biophysical journal*, vol. 88, no. 3, pp. 1818–1827, 2005.
- [164] H. Abbasi, K. A. Noghabi, and A. Ortiz, "Interaction of a bacterial monorhamnolipid secreted by pseudomonas aeruginosa ma01 with phosphatidylcholine model membranes," *Chemistry and physics of lipids*, vol. 165, no. 7, pp. 745–752, 2012.
- [165] Y. Murakami, H. Ishii, N. Takada, S. Tanaka, M. MACHINO, S. Ito, and S. Fujisawa, "Comparative anti-inflammatory activities of curcumin and tetrahydrocurcumin based on the phenolic oh bond dissociation enthalpy, ionization potential and quantum chemical descriptor," *Anticancer research*, vol. 28, no. 2A, pp. 699–707, 2008.
- [166] M. Heger, R. F. van Golen, M. Broekgaarden, and M. C. Michel, "The molecular basis for the pharmacokinetics and pharmacodynamics of curcumin and its metabolites in relation to cancer," *Pharmacological reviews*, vol. 66, no. 1, pp. 222–307, 2014.
- [167] S. Singh and B. B. Aggarwal, "Activation of transcription factor nf- $\kappa$ b is suppressed by curcumin (diferuloylmethane)," *Journal of Biological Chemistry*, vol. 270, no. 42, pp. 24 995–25 000, 1995.
- [168] K. I. Priyadarsini, "Photophysics, photochemistry and photobiology of curcumin: Studies from organic solutions, bio-mimetics and living cells," *Journal of Photochemistry and Photobiology C: Photochemistry Reviews*, vol. 10, no. 2, pp. 81–95, 2009.
- [169] D. Patra, R. Aridi, and K. Bouhadir, "Fluorometric sensing of dna using curcumin encapsulated in nanoparticle-assembled microcapsules prepared from poly (diallylammonium chloride-co-sulfur dioxide)," *Microchimica Acta*, vol. 180, no. 1-2, pp. 59–64, 2013.
- [170] B. Zebib, Z. Mouloungui, and V. Noirot, "Stabilization of curcumin by complexation with divalent cations in glycerol/water system," *Bioinorganic chemistry and applications*, vol. 2010, 2010.
- [171] C. G. Silva, A. Corma, and H. García, "Metal–organic frameworks as semiconductors," *Journal of Materials Chemistry*, vol. 20, no. 16, pp. 3141–3156, 2010.

- [172] O. S. Bushuyev, G. R. Peterson, P. Brown, A. Maiti, R. H. Gee, B. L. Weeks, and L. J. Hope-Weeks, "Metal-organic frameworks (mofs) as safer, structurally reinforced energetics," *Chemistry-A European Journal*, vol. 19, no. 5, pp. 1706-1711, 2013.
- [173] H. Furukawa, K. E. Cordova, M. O'Keeffe, and O. M. Yaghi, "The chemistry and applications of metal-organic frameworks," *Science*, vol. 341, no. 6149, p. 1230444, 2013.
- [174] H. Furukawa, N. Ko, Y. B. Go, N. Aratani, S. B. Choi, E. Choi, A. Ö. Yazaydin, R. Q. Snurr, M. O'Keeffe, J. Kim *et al.*, "Ultrahigh porosity in metal-organic frameworks," *Science*, vol. 329, no. 5990, pp. 424-428, 2010.
- [175] K. Schlichte, T. Kratzke, and S. Kaskel, "Improved synthesis, thermal stability and catalytic properties of the metal-organic framework compound cu 3 (btc) 2," *Microporous and Mesoporous Materials*, vol. 73, no. 1, pp. 81-88, 2004.
- [176] H. Deng, S. Grunder, K. E. Cordova, C. Valente, H. Furukawa, M. Hmadeh, F. Gándara, A. C. Whalley, Z. Liu, S. Asahina *et al.*, "Large-pore apertures in a series of metal-organic frameworks," *science*, vol. 336, no. 6084, pp. 1018-1023, 2012.
- [177] M. Hmadeh, Z. Lu, Z. Liu, F. Gándara, H. Furukawa, S. Wan, V. Augustyn, R. Chang, L. Liao, F. Zhou *et al.*, "New porous crystals of extended metal-catecholates," *Chemistry of Materials*, vol. 24, no. 18, pp. 3511-3513, 2012.
- [178] K. M. Choi, H. M. Jeong, J. H. Park, Y.-B. Zhang, J. K. Kang, and O. M. Yaghi, "Supercapacitors of nanocrystalline metal-organic frameworks," *Acs Nano*, vol. 8, no. 7, pp. 7451-7457, 2014.
- [179] R. A. Smaldone, R. S. Forgan, H. Furukawa, J. J. Gassensmith, A. M. Slawin, O. M. Yaghi, and J. F. Stoddart, "Metal-organic frameworks from edible natural products," *Angewandte Chemie International Edition*, vol. 49, no. 46, pp. 8630-8634, 2010.
- [180] D. Wu, J. J. Gassensmith, D. Gouvea, S. Ushakov, J. F. Stoddart, and A. Navrotsky, "Direct calorimetric measurement of enthalpy of adsorption of carbon dioxide on cd-mof-2, a green metal-organic framework," *Journal of the American Chemical Society*, vol. 135, no. 18, pp. 6790-6793, 2013.
- [181] B. Gogoi and N. Sen Sarma, "Curcumin-cysteine and curcumin-tryptophan conjugate as fluorescence turn on sensors for picric acid in aqueous media," *ACS applied materials & interfaces*, vol. 7, no. 21, pp. 11 195-11 202, 2015.
- [182] D. Patra and F. Sleem, "A new method for ph triggered curcumin release by applying poly (l-lysine) mediated nanoparticle-congregation," *Analytica chimica acta*, vol. 795, pp. 60-68, 2013.



- [183] S. Ghosh and S. Mondal, "Spectroscopic study on the interaction of medicinal pigment, curcumin with various surfactants: An overview," *J. Surf. Sci. Technol.*, vol. 28, pp. 179–195, 2012.
- [184] P. K. Mohan, G. Sreelakshmi, C. Muraleedharan, and R. Joseph, "Water soluble complexes of curcumin with cyclodextrins: Characterization by ft-raman spectroscopy," *Vibrational Spectroscopy*, vol. 62, pp. 77–84, 2012.
- [185] L. Szente, K. Mikuni, H. Hashimoto, and J. Szejtli, "Stabilization and solubilization of lipophilic natural colorants with cyclodextrins," *Journal of inclusion phenomena and molecular recognition in chemistry*, vol. 32, no. 1, pp. 81–89, 1998.
- [186] B. Tang, L. Ma, H.-y. Wang, and G.-y. Zhang, "Study on the supramolecular interaction of curcumin and  $\beta$ -cyclodextrin by spectrophotometry and its analytical application," *Journal of agricultural and food chemistry*, vol. 50, no. 6, pp. 1355–1361, 2002.
- [187] P. M. Mareeswaran, E. Babu, V. Sathish, B. Kim, S. I. Woo, and S. Rajagopal, "p-sulfonatocalix [4] arene as a carrier for curcumin," *New Journal of Chemistry*, vol. 38, no. 3, pp. 1336–1345, 2014.
- [188] T. Harada, D.-T. Pham, M. H. Leung, H. T. Ngo, S. F. Lincoln, C. J. Easton, and T. W. Kee, "Cooperative binding and stabilization of the medicinal pigment curcumin by diamide linked  $\gamma$ -cyclodextrin dimers: a spectroscopic characterization," *The Journal of Physical Chemistry B*, vol. 115, no. 5, pp. 1268–1274, 2010.